THE ROLE OF THE *RHODOBACTER CAPSULATUS* INTEGRAL MEMBRANE PROTEIN, ORF1696, IN LIGHT-HARVESTING I COMPLEX ASSEMBLY

by

CONAN S. YOUNG

A THESIS SUBMITTED IN PARTIAL FULFILLMENT OF THE REQUIREMENTS FOR THE DEGREE OF DOCTOR OF PHILOSOPHY

in

THE FACULTY OF GRADUATE STUDIES
Department of Microbiology and Immunology

We accept this thesis as conforming to the required standard

THE UNIVERSITY OF BRITISH COLUMBIA

December 1997

© Conan S. Young, 1997

In presenting this thesis in partial fulfilment of the requirements for an advanced degree at the University of British Columbia, I agree that the Library shall make it freely available for reference and study. I further agree that permission for extensive copying of this thesis for scholarly purposes may be granted by the head of my department or by his or her representatives. It is understood that copying or publication of this thesis for financial gain shall not be allowed without my written permission.

Department of Microbiology/Immunology

The University of British Columbia
Vancouver, Canada

Date Dec. 22, 1997

ABSTRACT

ORF1696 is included as part of the *bchFNBHLMORF1696puhA* superoperon found within the photosynthesis gene cluster on the chromosome of *Rhodobacter capsulatus* and mutation of *ORF1696* results in reduced levels of the light-harvesting I (LHI) complex in cells grown photosynthetically.

ORF1696 mutant strains were created by insertion of antibiotic resistance cartridges at different sites within the *ORF1696* gene in a strain that lacks the light-harvesting II (LHII) complex. All of the mutant strains were deficient in the LHI complex, including one (ΔNae) with a disruption located 13 codons before the 3' end of the gene. A 5'-proximal disruption after the 31st codon of *ORF1696* resulted in a mutant strain (ΔMun) with a novel absorption spectrum. The two more 3' mutant strains (ΔStu and ΔNae) were restored to levels close to the parental strain phenotype when *trans*-complemented with a plasmid expressing the *ORF1696* gene, but ΔMun was not. The absorption spectrum of ΔMun resembled that of a strain which had a polar mutation in *ORF1696.*

A comparison of LHI complex assembly kinetics showed that assembly occurred 2.8-fold faster in the parental strain compared to strain ΔStu. In contrast, LHI complex decay occurred 1.7-fold faster in the *ORF1696* parental strain than in ΔStu. These results indicate that the major activity of the ORF1696 protein is in LHI complex assembly.

A membrane topology model of the ORF1696 protein is proposed consisting of twelve membrane-spanning domains with both the N- and C-termini localized to the cytoplasmic side of the membrane similar to that predicted for the PucC protein of *R. capsulatus* which is required to maintain levels of the LHII complex. Suggestions for the function of the ORF1696 protein in LHI complex assembly are also proposed.

TABLE OF CONTENTS

LIST OF TABLES

LIST OF FIGURES

ABBREVIATIONS

Ap^r	ampicillin resistance
bchl	bacteriochlorophyll
Ble^r	bleomycin resistance
bp	base pairs
DNA	deoxyribonucleic acid
dNTP	deoxynucleotide triphosphate
ds	double-stranded
DTT	dithiothreitol
Gm^r	gentamycin resistance
GTA	gene transfer agent
h	hour
kb	kilobase
kDa	kiloDaltons
Km^r	kanamycine resistance
LH	light-harvesting
L-PCR	long polymerase chain reaction
pfu	plaque forming units
RC	reaction center
s	second
SDS	sodium dodecyl sulfate
ss	single-stranded
Tc^r	tetracycline resistance
Tp^r	trimethoprim resistance

ACKNOWLEDGEMENTS

I would like to thank my supervisor, Tom Beatty, for guiding and supporting me through all of the research that has culminated in the writing of this thesis. Tom's infectious enthusiasm for the careful scientific study of photosynthesis has been a great influence on me. I would also thank the members of my committee for their guidance and input into this project.

I thank Drs. C. Bauer and W. Hess for providing me with biological materials required for my experiments. I thank Dr. G. von Heijne for providing me with the TopPred II 1.1 computer program.

Members of the Beatty lab, both past and present, were indispensable for technical and theoretical discussions which contributed greatly to my graduate education. These people include Tim Lilburn, Heidi Leblanc, Danny Wong, Farahad Dastoor, Jorg Overmann, Nora Lem, Andrew Lang, Vladimir Yurkov, Xiao-yi Chen, and Andrea Harmer. Undergraduate students to whom I am indebted for their unfailing efforts include Jeff Kwan, Romina Reyes, and Victor Yih.

Finally, thank you Sharon for your friendship and support over the years.

DEDICATION

This thesis is dedicated to the memory of my grandparents, Lilias and Cecil Miller. I further dedicate this thesis to my parents, Rick and Pat Young, who have consistently supported me through my educational endeavors.xiiixiii

1 INTRODUCTION

1.1 PHOTOSYNTHESIS AND *RHODOBACTER CAPSULATUS*

In 1779, Jan Ingen-Housz reported that the production of "dephlogisticated air" (oxygen) by plants required light energy, and up until the late 19th century it was thought that photosynthesis always involved the evolution of oxygen and the use of CO_2 as a carbon source in the presence of light (51). T. Engelmann observed, in the 1880s, that illuminated purple phototrophic bacterial cells did not evolve detectable quantities of oxygen although they could grow in the presence of light with CO_2 as the carbon source. Experiments conducted by C. B. van Niel in the 1930s on purple and green sulfur bacteria led him to propose a general formula summarizing the reactions carried out during photosynthesis in both plants and bacteria (51):

$CO_2 + 2H_2A = CH_20 + H_20 + 2A$ (where H_2A is H_2 or an inorganic sulfur compound)

This equation failed to account for the observation of photoheterotrophic growth in purple non-sulfur bacteria made originally by H. Molisch in 1907 in which organic compounds are oxidized and CO_2, in some cases, is produced (51). H. Gest later suggested that a more general feature of photosynthesis is that light energy is transduced into chemical energy in the form of phosphodiester bonds (ATP) by a mechanism of light-driven cyclic electron transport (50, 51).

Rhodobacter capsulatus is a member of the α-subgroup of Proteobacteria based on its 16S rRNA sequence. It is Gram-negative and forms ovoid to rod-shaped cells which give rise to brown to red pigmented cultures due to the presence of bacteriochlorophyll *a* and carotenoids (61, 124). *R. capsulatus* is well adapted for growth under a wide range of conditions because of its ability to switch between different modes of metabolism. Under anaerobic conditions it grows by

photosynthesis in the light, but it can also carry out anaerobic respiration in the dark in the presence of compounds such as dimethyl sulfoxide or trimethylamine N-oxide, which act as terminal electron acceptors (162). *R. capsulatus* can also grow under aerobic conditions by respiration and this ability, along with the induction of the intracytoplasmic membrane (ICM) system which contains the photosynthetic apparatus at lowered oxygen tensions, makes this bacterium useful for studying photosynthesis because mutations that abolish photosynthetic function are not lethal (39).

It is possible to do gene replacement in *R. capsulatus* (9), and the chromosome has been physically mapped (49, 140). The DNA sequence of the chromosome is about two-thirds complete.

1.2 THE PHOTOSYNTHETIC APPARATUS OF *R. CAPSULATUS*

The ICM of *R. capsulatus* consists of vesicles derived from invaginations of the cytoplasmic membrane, and although the amount of ICM present in cells is greatest under conditions of low oxygen tension (<1 kPa) it is present in much lower amounts, but is not absent, under higher oxygen tensions (39). The pigment-protein complexes of the photosynthetic apparatus involved in absorbing light energy for photosynthesis are embedded within the ICM and include the reaction center (RC) complex and light-harvesting I (LHI) complex, which together comprise the "core" photosynthetic unit, and the accessory light-harvesting II (LHII) complex (39).

The photosynthetic apparatus can be thought of as a light-driven proton pump (see Fig. 1). Each of the above complexes binds bacteriochlorophyll (bchl) molecules which enable the mature holocomplexes to absorb light energy in the near infra-red (800 to 890 nm) range. Light energy is absorbed by the LH complexes and is passed along to the RC complex where a bchl dimer, referred to as the special pair, is oxidized and the electron released moves through the RC via a series of molecules (bacteriopheophytin and two ubiquinones), ultimately resulting in the

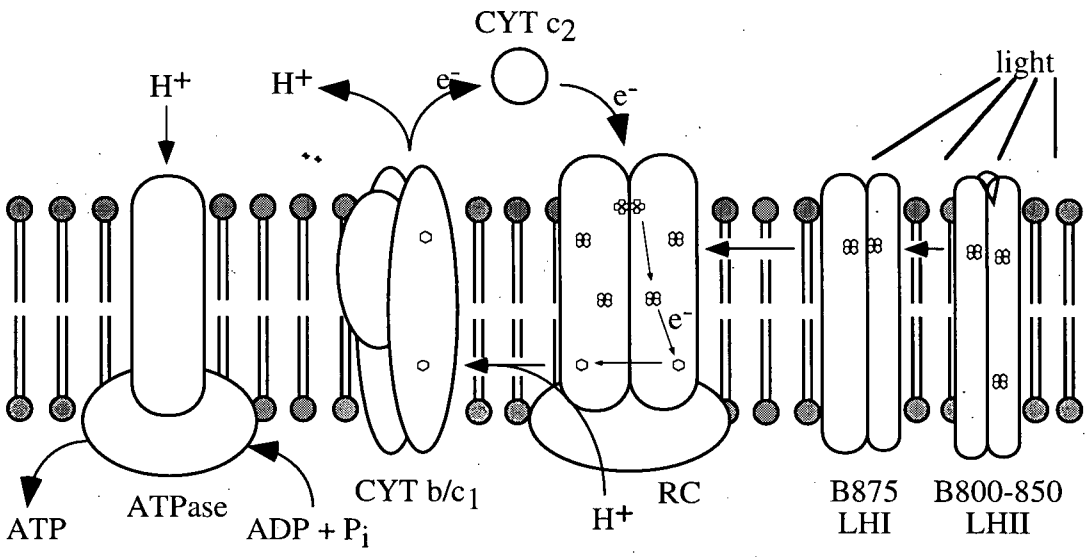

Figure 1. Schematic illustration of photosynthesis in *R. capsulatus*. Pill shapes represent polypeptides which either span the membrane or are soluble. Phospholipids of the intracytoplasmic membrane are represented by the ball-and-stick symbols. CYT = cytochrome, RC = reaction center, LH = light-harvesting, ATPase = ATP synthase, H^+ = proton, and e^- = electron. Hexagons symbolize quinone molecules and the pentagon clusters symbolize both bacteriochlorophyll and bacteriopheophytin molecules. See the Introduction text for an explanation of the diagram.

reduction of a ubiquinone to ubiquinol (after the uptake of two photons and the transfer of two electrons). The ubiquinol molecule diffuses from the RC to a nearby cytochrome b/c_1 complex, facilitated by the PufX protein (85), and is then oxidized back to ubiquinone resulting in the pumping of protons across the ICM from the cytoplasm to the periplasmic space (101). Cytochrome b/c_1 then reduces the periplasmically located cytochrome c_2 or the membrane-bound cytochrome c_y which, in turn, reduce the bchl special pair of the RC. In this way, a cyclic flow of electrons generates a proton concentration gradient across the ICM from the periplasm to the cytoplasm, where ATP is synthesized due to proton migration through a membrane-bound ATP synthase complex (55).

The RC complex of *R. capsulatus* consists of three subunit polypeptides, L, M and H, which have molecular masses of 31565, 34440, and 28534 Da, respectively (157). The cofactor molecules bound to the L and M subunits consist of four bacteriochlorophyll molecules, two bacteriopheophytin molecules, two ubiquinones, and one non-heme iron atom. The cofactors are arranged along two branches (the A- and B-branch) around an axis of two-fold symmetry, and only one of the branches (the A branch) is engaged in electron transfer reactions (79). A giant leap in the understanding of the RC complex and membrane protein structure in general, came with the determination of the structure of the RC from the purple non-sulfur bacteria, *Rhodopseudomonas viridis* (34) and *Rhodobacter sphaeroides* (4), by X-ray crystallography. These bacteria belong to the Proteobacteria and are, thus, closely related to *R. capsulatus* whose RC is highly homologous to that of both *Rs. viridis* and *R. sphaeroides* (48). The L and M subunit polypeptides act as the cofactor scaffolding and are integral membrane proteins which span the ICM with five transmembrane α-helices each (110). The H subunit has one transmembrane α-helix near its N-terminus which extends from the periplasm to the cytoplasm along the RC axis of symmetry between the L and M subunits. The H subunit seems to be

required for RC assembly and probably participates in the stabilization of the LHI antenna complex by protein-protein interactions (107, 138, 152). Furthermore, it has been suggested that the H subunit is involved in proton translocation from the cytoplasm to the Q_B binding site (ubiquinone binding site along the B-chain) due to the presence of potential water channels in the protein (45, 128).

The accessory LH complex of *R. capsulatus*, LHII (B800-850), consists of an oligomer of three polypeptides, α, β and γ which have molecular masses of 7322 Da, 4579 Da, and 14160 Da, respectively (129 ,130). In total, three bchl *a* molecules and one or two carotenoids are bound by each α and β polypeptide dimer. Two of the bchl molecules form a dimer and absorb light of the 850 nm wavelength whereas the remaining monomeric bchl molecule absorbs light at the 800 nm wavelength. The stoichiometry and role of the third polypeptide, γ, in LHII function is unknown. The γ protein does not bind pigments although it may participate peripherally in the stabilization of the 800 nm monomeric bchl molecule (46, 156). Decreases in light intensity or oxygen tension result in an increase in the size of the photosynthetic unit of the ICM, primarily due to the up-regulation of LHII formation (117, 118). Thus, the variation in the size of the photosynthetic unit in response to changing environmental conditions allows *R. capsulatus* to modulate and fine-tune the intake of light energy required for ATP synthesis. Although the crystallization of the *R. capsulatus* LHII complex has been achieved, the crystals were of insufficient quality for X-ray diffraction studies (149). However, the crystal structure of the LHII complex of the purple, non-sulfur bacterium, *Rhodopseudomonas acidophila,* has been reported revealing a nonameric ring with the β polypeptides forming an outer ring, the α polypeptides forming an inner ring, and the B850 bchl and carotenoid pigments sandwiched in between the two polypeptide rings (91). No ordered molecules were identified in the channel running down the middle of the structure. Two-dimensional crystals of the *R. capsulatus* LHII complex evaluated by electron

microscopy to 2.7 nm resolution recently suggested that, similar to the *R. acidophila* LHII structure, a nonameric arrangement of subunits exists (102).

The LHI (B816) antenna subunit consists of two polypeptides, α (molecular mass = 6594 Da) and β (molecular mass = 5466 Da), each spanning the ICM once due to a hydrophobic central region, (157). Each αβ pair binds two carotenoid pigment molecules and two bchl *a* molecules which form a dimer absorbing light of wavelength 816 nm (see Fig. 2A). The B816 form has only been found *in vitro* (87), and the subunits oligomerize to form a complex that absorbs at 870 nm. Under photosynthetic growth conditions, labeling of intact cells of *R. capsulatus* with $^{32}P[P_i]$ indicated that the LHI α polypeptide is phosphorylated at its Ser-2 residue and that phosphorylation occurs concomitantly or directly following membrane insertion of the protein (21, 31). Following or concurrent with *in vivo* assembly in the *R. capsulatus* ICM, the LHI complex closely associates with the reaction center (RC) complex and efficiently transfers light energy to the RC. Rapid energy (exciton) transfer between the various bchl molecules bound to the RC and LH photocomplexes occurs because they are buried at similar depths in the ICM and the contact made between the photocomplexes brings the pigment molecules into close proximity (30, 103). Chemical cross-linking experiments indicated a close association between the RC and LHI complexes in the ICM of *R. capsulatus* (106), and it is likely that the LHI complex forms a ring, consisting of 16 LHI (ab·2bchl·crt) subunits (B870) which absorb light having a wavelength of ~870 nm, and surrounds the RC (see Fig. 2B) (30, 143).

Figure 2. The LHI antenna complex of *R. capsulatus,* A. The LHI antenna B816 subunit. The amino acids comprising the α and β polypeptides are given in single letter code and membrane-spanning segments are enclosed in pill shapes. Ball-and-stick symbols are phospholipids and the pentagonal clusters with Mg^{2+} inside are bacteriochlorophyll molecules, B. The LHI-RC "core" complex. The outer ring ovals are the b polypeptides and the inner ring circles are the a polypeptides. The PufX protein is indicated as a hatched circle. Bold lines represent bchl molecules. The RC-L, -M, and -H subunit polypeptides are shown in the center of the LHI ring as shapes with dashed lines.

A

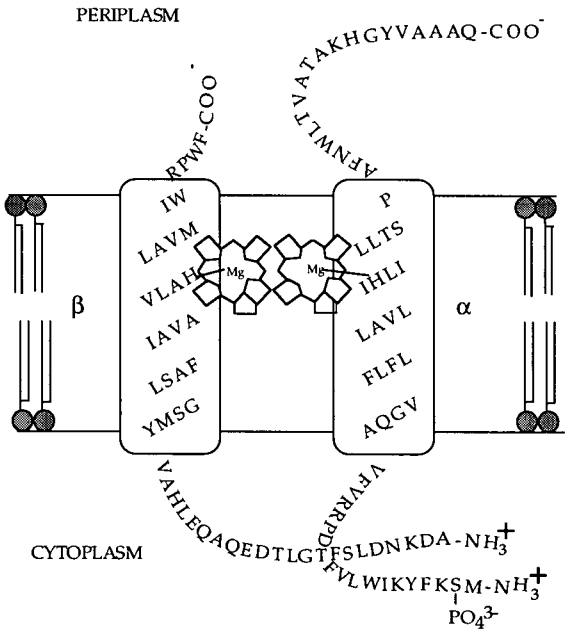
PERIPLASM
RPWF-COO
AFNWLL
VATAKHGYVAAAQ-COO
IW
LAVM
VLAH
IAVA
LSAF
YMSG
P
LLTS
IHLI
LAVL
FLFL
AQGV
Mg
Mg
β
α
VAHLEQAQEDTLGT
VFVRRPD
FSLDNKDA-NH3+
FVLWIKYFKSM-NH3+
PO4 3-
CYTOPLASM

B

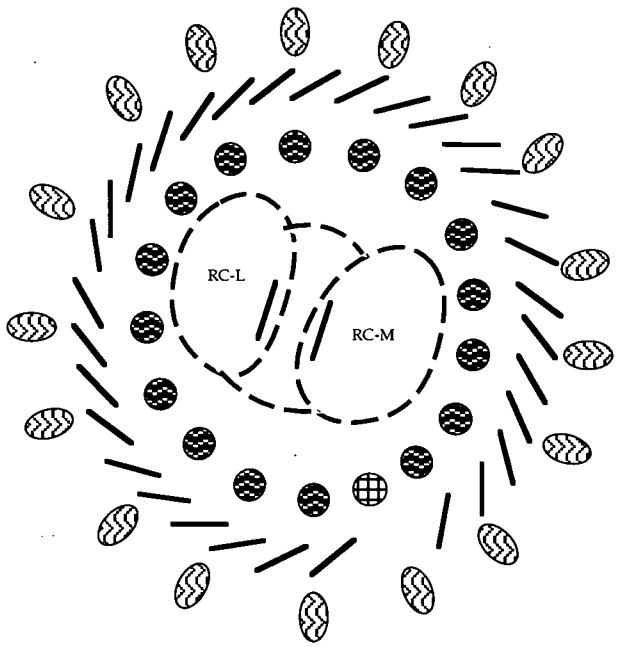
RC-L
RC-M

1.3 ORGANIZATION AND REGULATION OF PHOTOSYNTHESIS GENES IN *R. CAPSULATUS*

1.3.1 The Photosynthesis Gene Cluster

All of the genes in *R. capsulatus* known to be unique to and essential for photosynthesis are clustered in a 46 kb region of the chromosome (see Fig. 3). The *puf* and *puh* operons contain structural genes encoding polypeptides of the LHI and RC complexes, and are arranged at either end of a central cluster of genes required for synthesis of bchl (*bch*) and carotenoids (*crt*). The *puc* operon, which encodes the proteins of the LHII complex, is not located within this photosynthesis gene cluster (3, 158).

1.3.2 Regulation of the *puf* operon by oxygen and light

The *puf* operon consists of the genes *pufQBALMX* of which *pufQ* encodes a protein required for bchl biosynthesis, *pufBA* encode the β and α polypeptides of the LHI complex, *pufLM* encode the L and M subunit polypeptides of the RC, and *pufX* encodes a protein required to facilitate quinone/quinol exchange between the Q_B site of the RC and the cytochrome b/c_1 complex (8, 11, 85, 157). The coordinated expression and regulation of the *puf* operon (as well as the *puh* and *puc* operons) with that of the *bch* genes (which encode bchl biosynthetic enzymes) has been demonstrated to occur in response to decreased oxygen tension and light intensity (28, 163, 164). Regulation of photosynthesis gene expression has been demonstrated to occur at the level of mRNA transcription and also post-transcriptionally due to differential rates of mRNA decay (9, 69). The regulation of the assembly of the resulting polypeptides and pigment molecules into pigment-protein complexes adds an additional post-translational component of regulation (9, 71, 152).

Transcription of the *R. capsulatus puf* operon is initiated from three promoters which give rise to overlapping mRNA transcripts. These include an oxygen-regulated promoter upstream of the *pufQ* gene and two promoters

Figure 3. The photosynthesis gene cluster of *R. capsulatus*. Shaded boxes along the cluster represent *bch* genes which encode bacteriochlorophyll biosynthetic enzymes, cross-hatched boxes represent *crt* genes, which encode carotenoid biosynthetic enzymes, and genes that encode bacteriochlorophyll-binding structural polypeptides *puf* and *puh*,are shown as hatched boxes. The *puhA* gene encodes the H polypeptide of the RC. Genes whose functions are unknown are labelled "orf" and are shown as speckled boxes. The approximate length and direction of transcription of mRNA molecules is represented by the bent arrows. Only the operons flanking the photosynthesis gene cluster are shown in detail because they are relevant to this thesis.

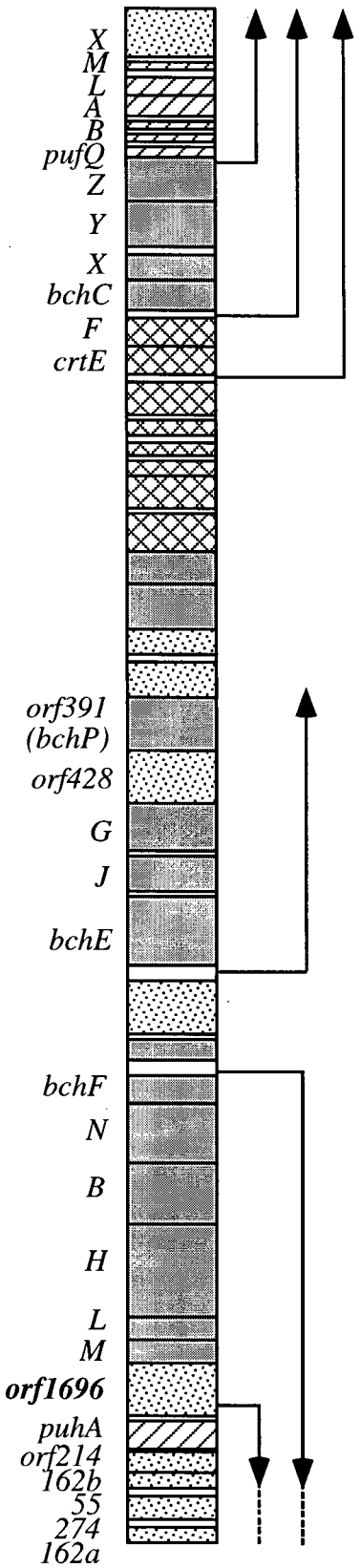
X
M
L
A
B
pufQ
Z
Y
X
bchC
F
crtE
orf391
(bchP)
orf428
G
J
bchE
bchF
N
B
H
L
M
orf1696
puhA
orf214
162b
55
274
162a

upstream of the *crtEF* and *bchCXYZ* pigment biosynthesis genes (see Fig. 3) (147, 148). Although the *bch* promoter contributes equally with the *puf* promoter in expression of the *puf* genes, oxygen regulation of *puf* operon expression is largely mediated by the *puf* promoter (148). It has been demonstrated that a DNA sequence upstream of the *R. capsulatus puf* promoter having dyad symmetry can form two distinct protein-DNA complexes under conditions of high oxygen tension and that a single base mutation in this region relieves oxygen- and light-dependent repression of *puf* operon transcription (67, 75, 99). A similar region of dyad symmetry exists upstream of the *puf* promoter in *R. sphaeroides* and has been shown to bind a single protein under high oxygen tension or high light intensity growth conditions (122).

Some of the *trans*- and *cis*-acting elements which control the expression of the *puf, puc,* and *puh* operons have been identified and the signal transduction mechanisms which, in turn, regulate their activity are becoming more clear. The *regA* gene product was the first *trans*-acting factor identified in the induction of photosynthetic structural gene expression at reduced oxygen tensions, as evaluated by the expression of *lacZ* in-frame translational fusions to photosynthesis genes in $regA^+$ and $regA^-$ strains. The RegA amino acid sequence resembles that of other response regulator proteins but not subclasses of these proteins that bind DNA (120). A second gene involved in activation of *puf, puc,* and *puh* gene expression under reduced oxygen tension, *regB*, has been identified and encodes a protein which acts as a membrane-bound sensor kinase capable of autophosphorylation and transferring a phosphate group to the RegA protein (62, 98). It is thought that the RegA and RegB proteins are part of a two-component oxygen-sensing regulatory cascade which includes the phosphorylation of RegA by RegB followed by the activation of photosynthesis structural gene expression in response to reduced levels of molecular oxygen (9, 98). An additional accessory factor in the activation of *puf* and *puh* expression in response to oxygen levels is SenC, although the

mechanism by which it affects photosynthesis gene regulation remains unknown (23). Homologs of the *R. capsulatus regA* and *regB* genes exist in *R. sphaeroides* and mutations in these genes affect transcription of the photosynthesis structural genes in an analogous fashion in that *R. sphaeroides regA* and *regB* mutants have reduced capacities for activating expression of the *puc, puf* and *puh* genes under conditions of reduced oxygen tension (43, 44, 108). The RegA/RegB sensory regulatory system of the purple, non-sulfur bacteria has been demonstrated to be involved globally in the activation of genes involved in nitrogen fixation and carbon dioxide assimilation under low oxygen conditions, as well as photosynthesis gene expression (65).

Another factor that modulates levels of photosynthetic complexes in the purple, non-sulfur bacteria is light intensity (9); it seems that blue light of 450 nm has the greatest inhibitory effect on the expression of the *puf* and *puc* operons (121). In response to dim light conditions (~40 $\mu E/m^2/s$), transcription of the *puf, puh* and *puc* operons is enhanced in *R. capsulatus* and contributes toward an increase in the size of the photosynthetic unit such that there is an increase in the amount of photosynthetic pigments for light energy absorption. The HvrA protein was shown to bind to the *puf* and *puh* operon promoters by DNA footprinting analysis and acts as a *trans*-acting activator of *puf* and *puh* operon expression under reduced light, but does not affect transcription of the *puc* or *bch* genes as indicated by studies with *lacZ* fusions (24). The SPB *trans*-acting repressor protein that binds to the *puf* promoter DNA of *R. sphaeroides* under aerobic or high light growth conditions possesses 53% identity to the HvrA protein of *R. capsulatus* (122, 123).

The exact nature of the photosensing mechanism by which cells of purple non-sulfur bacteria effect changes in the transcription of the photosynthesis genes remains unknown. However, there is evidence that the regulation of bchl levels in response to varying light intensities is independent of photosynthetic energy

transduction since bchl levels, manifested in the form of the LHII complex, varied significantly under low compared to high light in a strain of *R. capsulatus* lacking a functional RC (161). Regulation of bchl levels was not observed to be due to changes in the rates of *puc* operon transcription and translation and it was hypothesized that changes in light intensity might affect bchl biosynthetic enzyme activity.

Transcription of the *R. capsulatus puf* operon results in a 2.7 kb mRNA molecule which encodes the *pufQBALMX* genes and this transcript is processed to a ~2.3 kb *pufBALMX* molecule that in turn is processed to a 0.5 kb mRNA encoding only the *pufBA* genes. There is an increase in stability after each processing step (1). The differential stability of the *puf* messages is largely responsible for the ~15:1 ratios of LHI to RC polypeptides in photosynthetically growing cells, and thus constitutes a second level of regulation of *puf* gene expression (15, 118). The presence of a stem-loop structure in the intercistronic region between the *pufA* and *pufL* genes participates in terminating *puf* mRNA decay by the action of 3'-exoribonucleases and helps stabilize the 0.5 kb *pufBA* transcript following posttranscriptional processing of the full-length 2.7 kb mRNA (72). Recent evidence suggests that there are three stem-loop structures located between the *pufQ* and *pufB* genes which contribute toward the greater stability of the 0.5 kb *pufBA* mRNA and toward stabilizing the *pufBALMX* transcript (58). However, the intercistronic stem-loop structures are not entirely responsible for *puf* mRNA stability since endoribonucleolytic activity also contributes toward degradation of the 2.7 kb *puf* transcript (26). The *pufLM* DNA sequences contain at least three endoribonucleolytic cleavage sites and it is now clear that the degradation of the *puf* mRNA is dependent upon a combination of one or more exoribonucleases, endoribonucleases, and several mRNA decay-impeding hairpin structures (74). Endoribonucleolytic degradation of the 2.7 kb *puf* mRNA is accelerated in cells grown under high oxygen tension compared to low oxygen tension, adding an

additional level of complexity to the oxygen-dependent regulation of the *puf* operon (68). Studies of *puf* mRNA decay in *E. coli* suggest that an RNase E-type activity in *R. capsulatus* is responsible for the endonucleolytic digestion of the *pufLM* region (70).

1.4 ASSEMBLY OF THE LHI COMPLEX

1.4.1 Reconstitution of the LHI Complex *In Vitro*

The B870 form of the LHI complex can be converted to and separated from the RC complex as the B820 subunit, which is significantly reduced in size compared to the holocomplex, by using the detergent β-octyl glucoside in a purification procedure (96). Reconstituted subunit (αβ·2 bchl *a*) LHI complexes can also be obtained *in vitro* by combining purified α and β polypeptides with bchl molecules in β-octyl glucoside emulsions, although the *R. capsulatus* (B8i6) complex is about 4-fold less stable than similar complexes from *R. sphaeroides* (B825) and *R. rubrum* (B820) (59, 86). Site-directed mutagenesis of the *R. sphaeroides* β polypeptide indicated that the +4-Tyr (+4 means four residues C-terminal from the His bchl ligand), which is a Met residue in an alignment with the *R. capsulatus* β polypeptide, provides an additional hydrogen bond and accounts for the difference in B820 subunit stabilities between *R. capsulatus* and *R. sphaeroides*, despite 79% amino acid identity between the two polypeptides (33). The β polypeptide alone with bchl is capable of forming B820 complexes *in vitro*, whereas the α polypeptide alone with bchl does not result in the appearance of this complex (86). LHI complex reconstitution experiments with bchl *a* analogues indicate that the binding site for bchl is very specific in that certain alterations to the bchl *a* molecule are sometimes tolerated yielding B820 complexes of reduced stability, or the changes to bchl *a* are not tolerated and no reconstitution of the LHI complex takes place (32, 104).

The oligomeric B870 form of the LHI complex can be obtained *in vitro* from isolated α and β polypeptides combined with bchl in β-octyl glucoside solutions followed by reduction of the detergent concentration (105). *In vitro* LHI assembly experiments have determined that N-terminal truncations up to the -16-Ile amino acid of the *Rhodospirillum rubrum* LHI β peptide, and C-terminal truncations up to the +13-Glu amino acid (numbers refer to the distance from the His that binds the bchl Mg^{2+} cation) of the LHI α peptide, are capable of binding bchl in the presence of the full-length α or β peptide, respectively, in a detergent micelle (93). Thus, a central core region of about 40 amino acids exists in each of these polypeptides which contains sufficient information necessary to form B820 and B870 complexes *in vitro*. C-terminal truncations of the *R. sphaeroides* LHI α polypeptide expressed *in vivo* resulted in reduced levels of the LHI complex and reduced ratios of LHI bchl per RC suggesting that, *in vivo*, the C-terminal α polypeptide residues are required to obtain the normal arrangement of LHI surrounding the RC (92).

1.4.2 *In Vivo* Assembly of the LHI Complex

It is not surprising that strains of *R. capsulatus* defective in bchl synthesis are incapable of photosynthetic growth, since binding of bchl is believed to be essential for the proper membrane insertion of photosynthetic pigment-binding proteins, and thus bchl plays a structural as well as functional role (73). Site-directed mutagenesis of LHI α or β resulted in several different effects, depending on the position and nature of the amino acid substitution. Amongst the effects reported were increases and decreases in the amounts of LHI carotenoid and bchl pigments, as well as the complete loss of the LHI and RC complexes. In general, the data implicated several (especially N-terminal) residues in appropriate pigment binding or LHI assembly, and indicated that loss of the LHI complex may affect the structure of the RC (5). Other experiments employing *in vivo* ^{35}S-methionine pulse-labeling of ICM proteins followed by SDS-PAGE and autoradiography, yielded additional

information regarding a subunit sequences required for assembly of the LHI complex (112). In particular, the LHI α polypeptide residue, αTrp-8, was proposed to play a role in the insertion of the α polypeptide into the ICM, whereas mutation of αPro-13 interfered with the stable insertion of the β polypeptide into the ICM (numbers refer to the distance from the N-terminus). On the basis of the effects of changes of charged amino acids in the N-terminal segments of the LHI proteins (αLys-3, αLys-6, αArg-14, αArg-15, βAsp-2, βAsp-5, βAsp-13, βGlu-14), a model was proposed in which electrostatic interaction between the negatively charged N-terminus of the β polypeptide and the positively charged N-terminus of the α polypeptide is a prerequisite for assembly of the LHI complex (111, 127, 131, 132). Although the β polypeptide became intimately associated with the ICM in the absence of the α polypeptide with the same kinetics as when the α protein was present, the β subunit appeared to be degraded rapidly. In contrast, only trace quantities of the α protein were detected in the ICM in the absence of the β protein (113).

1.4.3 Factors That May Affect LHI Complex Assembly

1.4.3.1 PuhA and the RC Complex

As described in section 1.2, our current understanding is that the LHI (B870) complex forms an oligomeric ring that surrounds and interacts with the RC complex by protein-protein interactions. In *R. capsulatus*, this arrangement results in the stabilization of the LHI complex since only small amounts of LHI form in the absence of the RC brought about by deletion of the *puhA* gene (152). These observations are supported by evidence of a close interaction between the LHI complex and the H subunit (PuhA) as indicated by chemical cross-linking experiments (107). Additionally, attempts to obtain an "LHI only" strain by expression of the *pufQBA* genes in a strain containing disruptions of the *puc* and *puf* operon yielded negative results (12). Among the purple non-sulfur bacteria

there seems to be variation with regard to the requirement for an LHI-RC H association, since the LHI complex of *R. sphaeroides* was reported to form in the absence of the RC (64).

1.4.3.2 *ORF214, ORF162b*, and downstream ORFs

ORF214 and *ORF162b* (along with *ORF55, ORF274*, and *ORF162a*) lie directly downstream of the *puhA* gene on the *R. capsulatus* chromosome and *puhA* is, in turn, present downstream of *ORF1696* and a series of *bch* genes (3) (Fig. 3). The deduced ORF214 protein consists of 214 amino acids and, based on hydropathy analyses, is likely to be an integral membrane protein. Directed mutational studies of *ORF214* indicated that a translational in-frame deletion results in reduced levels of both RC and LHI levels; this phenotype could be complemented in *trans* by expressing the *ORF214* gene from a plasmid (152). It is possible that the ORF214 protein plays a major role in maintaining levels of the RC, and that in the absence of ORF214 the reduction in RC results in a drop in LHI due to the close interaction of the two complexes in the ICM. Alternatively, ORF214 could directly participate in the assembly or stabilization of both the RC and LHI complexes although this explanation seems less likely.

The putative ORF162b protein has 162 amino acids, as deduced from the nucleotide sequence of the gene, and hydropathy analysis predicts that one transmembrane segment exists near the N-terminus. *ORF162b* has also been subjected to mutational analyses in *R. capsulatus* and appears to have a complex effect on photosynthetic complex levels (57). Similarly to ORF214, it plays a role in maintaining levels of RC, LHI, and LHII. The specific functions of ORF214 and ORF162b with regard to the appearance of the photocomplexes in the ICM are unknown.

1.4.3.3 PucC

The deduced amino acid sequence of the PucC protein is 462 amino acids in length. PucC is an integral membrane protein which was proposed to consist of twelve transmembrane segments, with a N-in/C-in membrane topological organization (see Fig. 30, Discussion) (84). The *pucC* gene is transcribed as part of the *pucBACDE* operon (which encodes the LHII α , β, and γ polypeptides) and mutations in *pucC* result in the complete loss of the LHII complex from *R. capsulatus* cells (83, 134). The deduced amino acid sequence of PucC exhibits 47% identity with ORF1696 and these proteins probably play analogous roles in posttranslational regulation of the amounts of LH complexes (10, this thesis). An investigation into whether *pucC* gene expression in *trans* in an *ORF1696* mutant (ΔStu) could restore levels of the LHI complex indicated that it did not have any significant effect. However, it was observed that combination of a *pucBAΔCDE* expression vector with others expressing short *pucC'::pho'A* fusions in a *puc* operon deletion strain seemed to reduce levels of LHI significantly (82). Thus, although the requirement for PucC for the formation of LHII is specific despite the strong sequence similarity between it and ORF1696, there seem to be secondary effects on the LHI complex in strains that contain *pucBADE* genes and truncated versions of the PucC protein.

1.4.3.4 *ORF428*

ORF428 is included as part of the *bchEJGORF428bchPORF176* operon located within the photosynthesis gene cluster of *R. capsulatus* (Fig. 3). ORF428 is relevant to this work because it has 24% amino acid sequence identity with both ORF1696 and PucC. However, it was reported that disruption of the chromosomal copy of this gene did not directly result in the reduction or loss of any of the photosynthetic complexes (19). Thus, it seems that ORF428 plays no major role in LH complex assembly or stabilization, although it was unclear whether the effects of the loss of the ORF428 protein were compensated by, for example, ORF1696, PucC, or ORF214.

1.4.3.5 DnaK and GroEL

Both DnaK (Hsp 70) and GroEL (Hsp 60) belong to a group of proteins known as chaperonins that are responsible for the proper folding and assembly of nascent polypeptides into their functional, three-dimensional conformations in the cytoplasm of cells (41). Both GroEL and DnaK from *R. capsulatus* have been partially purified, and a cell-free translation system was used to propose their involvement in the synthesis of the LHI α and β polypeptides (94). DnaK seemed to play a significant role in the translation of both of the LHI polypeptides whereas GroEL was required for the stable insertion of both of the polypeptides into membranes added to the *in vitro* translation system. A model was proposed in which DnaK and GroEL comprise part of a chaperonin-mediated pathway in *R. capsulatus*, which delivers the LHI polypeptides to the cytoplasmic or intracytoplasmic membrane for insertion by membrane-bound import proteins (80, 94). The *dnaK* gene from *R. capsulatus* was recently cloned and sequenced (100).

1.5 ORF1696

The presence of the "F1696" open reading frame (hereafter designated as *ORF1696*) was first detected by DNA sequencing of the *R. capsulatus* photosynthesis gene cluster. The putative ORF1696 protein consists of 477 amino acids and has a predicted molecular mass of 50 396 Da (157). Northern blot and *lacZ* fusion analysis later demonstrated that *ORF1696* is part of the *bchFNBHLMORF1696puhA* superoperon, and that its expression is regulated by oxygen due to transcription deriving from an upstream *bch* promoter (Fig. 4). A second oxygen-regulated promoter (P*puhA*), located within the coding sequence of *ORF1696*, contributes to transcription of the *puhA* gene (10). The *R. capsulatus ORF1696* gene was first

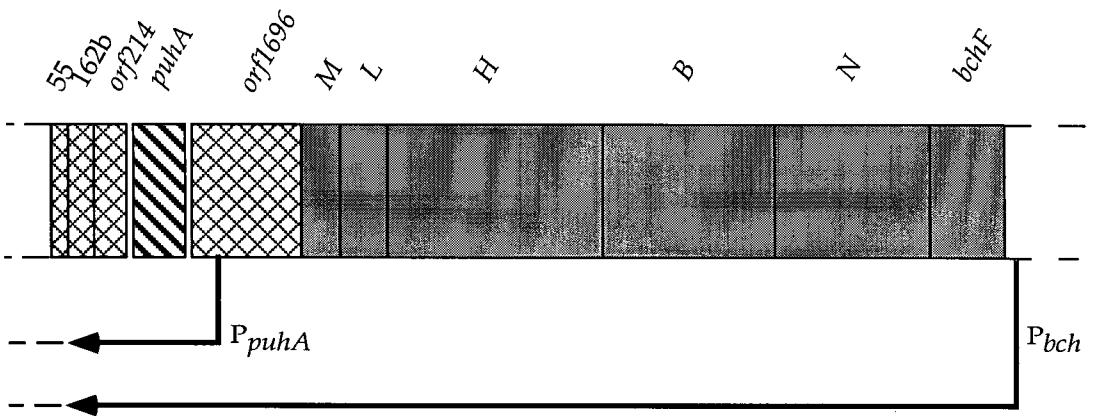

Figure 4. The *puhA* superoperon. See the Fig. 3 caption for an explanation of the symbols and abbreviations.

discovered to have a function in photosynthesis since insertion of transposon Tn5.7 into the chromosomal copy of the gene suggested that there was a reduction in the levels of the LHI and RC complexes (164). Insertion of a Km^r cartridge into the *ORF1696* gene had a similar effect in that a 60-70% decrease in LHI complex levels was observed as assessed by SDS-PAGE and spectral analyses of the mutants (10). These studies indicated that *ORF1696* plays a role in maintaining steady state levels of the LHI complex in *R. capsulatus* cells. *ORF1696* homologs have been discovered in other purple non-sulfur bacteria such as *R. sphaeroides, Rp. viridis,* and *Rs. rubrum* (16, 38, 150). In each case the *ORF1696* gene is located immediately upstream of the *puhA* gene, similar to the arrangement in *R. capsulatus,* but no investigation into the function of *ORF1696* has been done in these bacteria.

1.6 THESIS OBJECTIVES

My Ph. D thesis work focussed on expanding the understanding of the function of the ORF1696 protein and also to gain some insights into its structure. My thesis results are broken down into three components.

First, mutagenesis of *ORF1696* was performed to demonstrate structure-function relationships, and *trans*-complementation of the mutations was done to confirm that the ORF1696 protein acts to maintain levels of the LHI complex in *R. capsulatus* cells. Expression of a *pufB'::lac'Z* in-frame translational fusion in an *ORF1696*$^+$ strain compared to a strain containing an *ORF1696* disruption was done to confirm that *ORF1696* does not affect transcription and translation of the *puf* genes. Site-directed mutagenesis of the ORF1696 His-152 residue was done to determine if it played a role in the function of the ORF1696 protein in maintaining levels of LHI.

Second, kinetic analyses of LHI assembly and decay in an ORF1696$^+$ strain compared to a strain containing an ORF1696 disruption were done to determine the role played by the ORF1696 protein in maintaining LHI complex levels.

Third, a model of the membrane topology of ORF1696 was derived from a combination of hydropathy analyses, the "positive-inside" rule, and analyses of *ORF1696*'::*pho'A* and *ORF1696*'::*lac'Z* fusions.

2 MATERIALS AND METHODS

2.1 BACTERIAL STRAINS AND GROWTH CONDITIONS

The *E. coli* strains utilized have been previously described. Subcloning was performed in *E. coli* DH5αF' (56), an *hsdR* derivative of C600 (17), and RB404 (22), and SM10 (125) and HB101(pRK2013) (37) were used for the conjugal transfer of plasmids into *R. capsulatus* strains. The *phoA* deletion strain CC118 was used to express *ORF1696'::pho'A* fusions (90), the *lacZ* deletion strain DH5αF' (56), was used to express *ORF1696'::lac'Z* fusions, and the *phoR* strain CC149 was used as a control for PhoA production. *E. coli* was grown in Luria-Bertani medium (Sambrook, *et al.*, 1989) or M63 medium (97) (lacking L-methionine) at 30° C or 37° C. Antibiotics were added as required at the following concentrations (μg ml^{-1}): ampicillin, 200, kanamycin sulfate, 50, tetracycline-HCl, 10, trimethoprim, 40, spectinomycin-2HCl, 50, and gentamycin-sulfate, 25.

R. capsulatus strains used in this study are listed in Table 1. The *R. capsulatus* strains ΔLHII (83), a derivative of SB1003 (154)with the *puc* operon deleted, and the *pucC* point mutant (12) MW442 (119), were used as parental backgrounds to create chromosomal disruptions of the *ORF1696* gene with antibiotic resistance cartridges. Strain ZY1 (10), SB1003 with an *ORF1696*::Km^r chromosomal disruption, was used to study *trans*-complementation of the disrupted *ORF1696* gene with an intact copy of *ORF1696* expressed from a plasmid. Strain DE442, a *crtD* derivative of Y262 which overproduces the gene transfer agent (GTA) (153), was used in GTA transduction experiments.

R. capsulatus was grown in RCV minimal medium (14) or YPS complex medium (144) at 34° C as described previously (83) with antibiotics added as required in the following concentrations (μg ml^{-1}): kanamycin sulfate, 10; tetracycline-HCl,

0.5; spectinomycin-2HCl, 10; gentamycin sulfate, 2. High aeration growth conditions employed an Erlenmeyer flask filled to 8% of its nominal capacity

Table 1. *R. capsulatus* strains

Strain	Genotype	Phenotype	Reference
DE442	*crtD*, derived from Y262	GTA overproducer	(153)
ΔLHII	Δ*pucBACDE*::Ω, *rif*-10	LHII$^-$, Sp^r	(83)
ΔLHII ΔORF428	*ORF428*::Gm^r at *Pvu* II site, Δ*pucBACDE*::Ω, *rif*-10	LHII$^-$, LHI$^+$, RC$^+$, Gm^r, Sp^r	This study
ΔMun	*ORF1696*::Km^r at *Mun* I site, Δ*pucBACDE*::Ω, *rif*-10	LHII$^-$, LHI$^-$, RC$^-$, Km^r, Sp^r	This study
ΔMun ΔORF428	*ORF428*::Gm^r at *Pvu* II site, *ORF1696*::Km^r, Δ*pucBACDE*::Ω, *rif*-10	LHII$^-$, LHI$^-$, RC (deficient), Gm^r, Km^r, Sp^r	This study
MW442	*pucC* point mutation, *rif*-10	LHII$^-$, LHI$^+$, RC$^+$	(119)
ΔNae	*ORF1696*::Km^r at *Nae* I site, Δ*pucBACDE*::Ω, *rif*-10	LHII$^-$, LHI$^-$, RC$^+$, Km^r, Sp^r	This study
SB1003	*rif*-10	LHII$^+$, LHI$^+$, RC$^+$	(154)
SB1003 ΔORF428	*ORF428*::Gm^r at *Pvu* II site, *rif*-10	LHII$^+$, LHI$^+$, RC$^+$, Gm^r	This study

Table 1 cont.

ΔStu	*ORF1696*::Km^r between *Stu* I sites, Δ*pucBACDE*::Ω, *rif*-10	LHII$^-$, LHI$^-$, RC$^+$, Km^r, Sp^r	This study
ΔStu ΔORF428	*ORF428*::Gm^r at Pvu II site, *ORF1696*::Km^r, Δ*pucBACDE*::Ω, *rif*-10	LHII$^-$, LHI$^-$, RC (deficient), Gm^r, Km^r, Sp^r	This study
ΔStu::Ω	*ORF1696*::Ω between *Stu* I sites in MW442, *pucC* point mutation, *rif*-10	LHII$^-$, LHI$^-$, RC$^-$, Sp^r	This study
ZY1	*ORF1696*::Km^r between *Stu* I sites in SB1003, *rif*-10	LHII$^+$, LHI$^-$, RC$^+$, Km^r	(10)

Δ = deletion or disruption of DNA sequence, :: = 'disrupted by'

with liquid growth medium at 300 rpm on a gyrorotary water bath shaker (Model G76, New Brunswick Scientific Co., Inc., New Brunswick, NJ, USA). Low aeration growth condtions employed a 50 ml long-necked Erlenmeyer flask (No. 4442) filled to 80% of its nominal capacity with liquid growth medium at 150 rpm on a gyrorotary water bath shaker. Anaerobic, photosynthetic growth conditions employed screw-cap Pyrex (No. 9826) test tubes filled completely with liquid growth medium. Following inoculation, the test tubes were submerged in a water-filled aquarium illuminated with Lumiline 60 W incandescent, tungsten filament lamps. Water temperature and circulation in the aquarium were maintained using a Haake D3-V circulator (Haake Mess-Technik GmbH u. Co., Karlsruhe, Germany). Light

intensity was measured using a LI-COR LI-185B photometer (LI-COR, Inc., Lincoln, NE) equipped with a LI-190SB quantum sensor. A Klett-Summerson photometer (filter #66) was used to monitor growth by measuring culture turbidity.

2.2 *IN VITRO* DNA MANIPULATIONS

Restriction endonuclease digestion, DNA ligation, agarose gel electrophoresis, transformation of *E. coli* and other recombinant DNA procedures were carried out as described (115). Preparation of ds plasmid DNA for sequencing was done as described for the PRISM Ready Reaction DyeDeoxy Terminator Cycle Sequencing Kit (Perkin Elmer-ABI). Briefly, plasmid DNA was released from stationary phase *E. coli* cultures by alkaline lysis, RNase A was added to digest RNA molecules followed by extraction of the solution with chloroform. Plasmid DNA was precipitated with PEG 8000, re-extracted with chloroform then re-precipitated with ethanol. Double stranded plasmid DNA was prepared for other *in vitro* manipulations using the QIAGEN Plasmid Midi kit according to the manufacturer's instructions (Qiagen, Inc., Chatsworth, CA, USA).

2.3 PLASMID CONSTRUCTION

The construction of plasmids is described in detail below and brief descriptions of the plasmids are given in Table 2.

2.3.1 pCY42

Refer to Fig. 10 (Results) for the relative positions of genes and restriction sites in DNA fragments. Plasmid pCY42 was constructed by subcloning the 4.2 kb *ORF1696*::Ω fragment from pΔPUHA::Ω2 (152) as a *Bcl* I to *Pvu* II fragment into the *Bam*H I and *Pst* I (treated with T4 DNA polymerase) sites on the pJAJ9 expression vector (63), as illustrated in Fig. 5. This resulted in the cloning of the *ORF1696*::Ω

fragment into pJAJ9 in an orientation which placed *ORF1696* under the transcriptional control of the *puf* operon promoter present on pJAJ9. The Ω cartridge included downstream of *ORF1696* provided a *rho*-independent transcriptional terminator that should protect the 3' end of the *ORF1696* message from exonucleolytic degradation.

2.3.2 pCY34 and pCY1800

Construction of these plasmids is illustrated in Fig. 6. Plasmid pCY34 was constructed by subcloning the 3.4 kb *Bam*H I to *Xho* I DNA fragment, which includes sequences encoding the *bch'HLMORF1696puhA'* genes, from pUC13::EcoF (151) into pUC13 (95) previously digested with *Bam*H I and *Sal* I.

Plasmid pCY1800 was constructed by subcloning the 1.8 kb *Pst* I DNA fragment, which includes sequences encoding the *bch'MORF1696puhA'* genes, from pCY34 into pUC13 previously digested with *Pst* I. The *bch'MORF1696puhA'* DNA insert was screened for orientation by restriction analysis.

2.3.3 pCYNAE and pCYMUN

Plasmids pCYNAE and pCYMUN were constructed as illustrated in Fig. 6. Plasmid pCY34 was separately digested with the restriction endonuclease *Nae* I or *Mun* I. Following digestion with *Mun* I, the 5'-overhanging end of the plasmid DNA was made blunt using T4 DNA polymerase. The pUC4KIXX plasmid (Pharmacia Biotech Inc., Baie d'Urfe, Que.) was digested with *Sma* I to generate a 1.2 kb blunt-ended DNA fragment encoding Km^r and a 5' segment of the Ble^r gene. The Km^r cassette was separated from plasmid DNA by agarose gel electrophoresis, purified, separately ligated into either the *Nae* I or *Mun* I (end made blunt) linearized pCY34 plasmid, and transformed into *E. coli* .

Figure 5. Construction of the *ORF1696* expression plasmid pCY42. See section 2.3.1 of Materials and Methods for details. The positions of sites for restriction enzymes used is indicated. Thin shaded boxes represent vector DNA, thick darkly shaded boxes represent *bch* genes, thick lightly shaded boxes represent Km^r cartridge DNA, black boxes represent *puhA* sequences and open boxes represent *ORF1696* sequences. The bent arrows indicate the location and direction of transcription originating from the *puf* promoter.

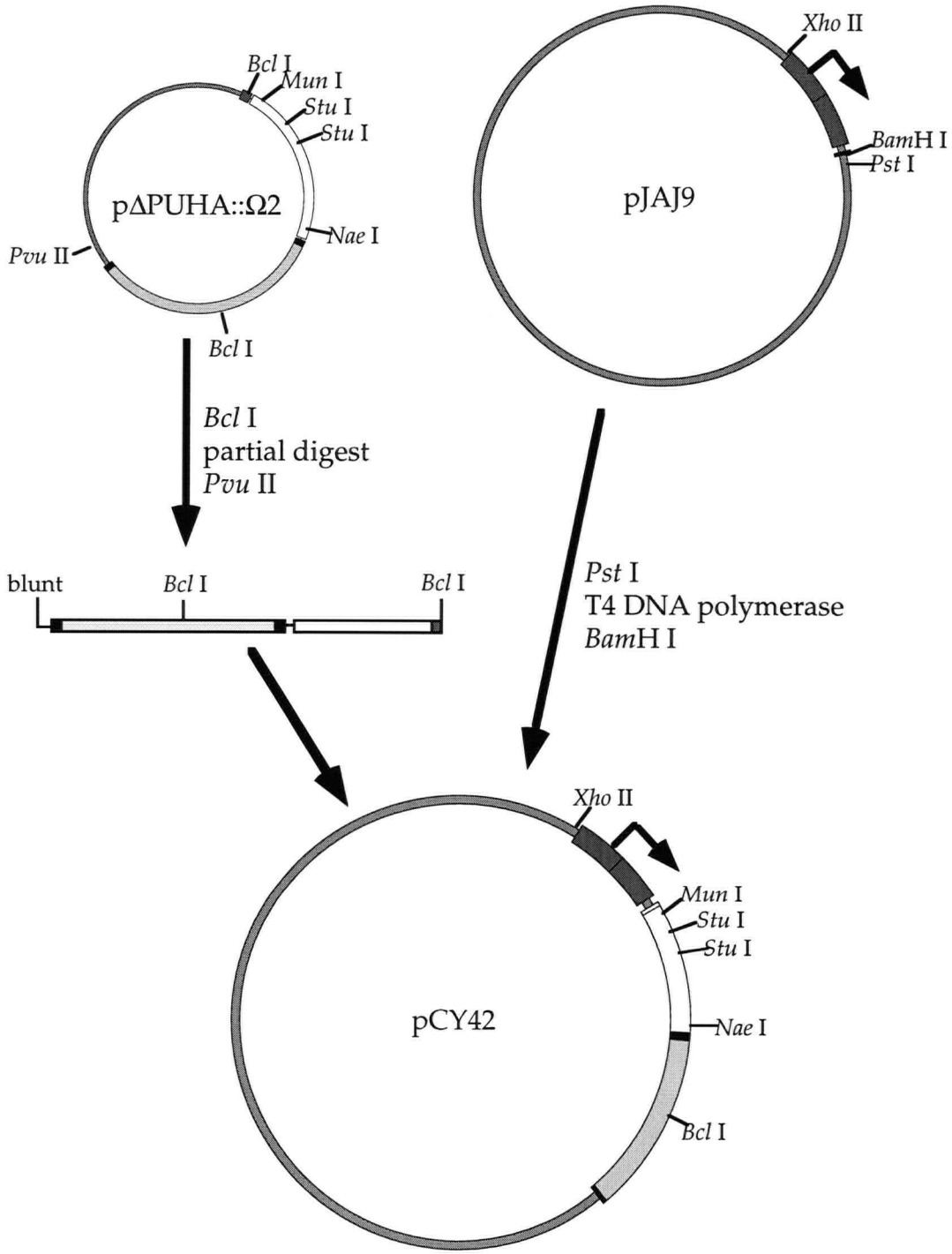
Bcl I
Mun I
Stu I
Stu I
pΔPUHA::Ω2
Nae I
Pvu II
Bcl I
Xho II
BamH I
Pst I
pJAJ9
Bcl I
partial digest
Pvu II
blunt
Bcl I
Bcl I
Pst I
T4 DNA polymerase
BamH I
Xho II
Mun I
Stu I
Stu I
pCY42
Nae I
Bcl I

Figure 6. Construction of plasmids pCY34, pCY1800, pCYMUN, pCYNAE and pRR3. For details see sections 2.3.2, 2.3.3, and 2.3.5 of Materials and Methods. The sites of restriction enzymes are indicated. The thin shaded lines represent pUC13 vector DNA, the thick darkly shaded boxes represent *bch* genes, the black boxes represent *puhA* DNA sequences, the thick lightly shaded boxes represent antibiotic resistance cartridge DNA and the unshaded boxes represent *ORF1696* (largest unshaded box), *ORF214* and *ORF162b*.

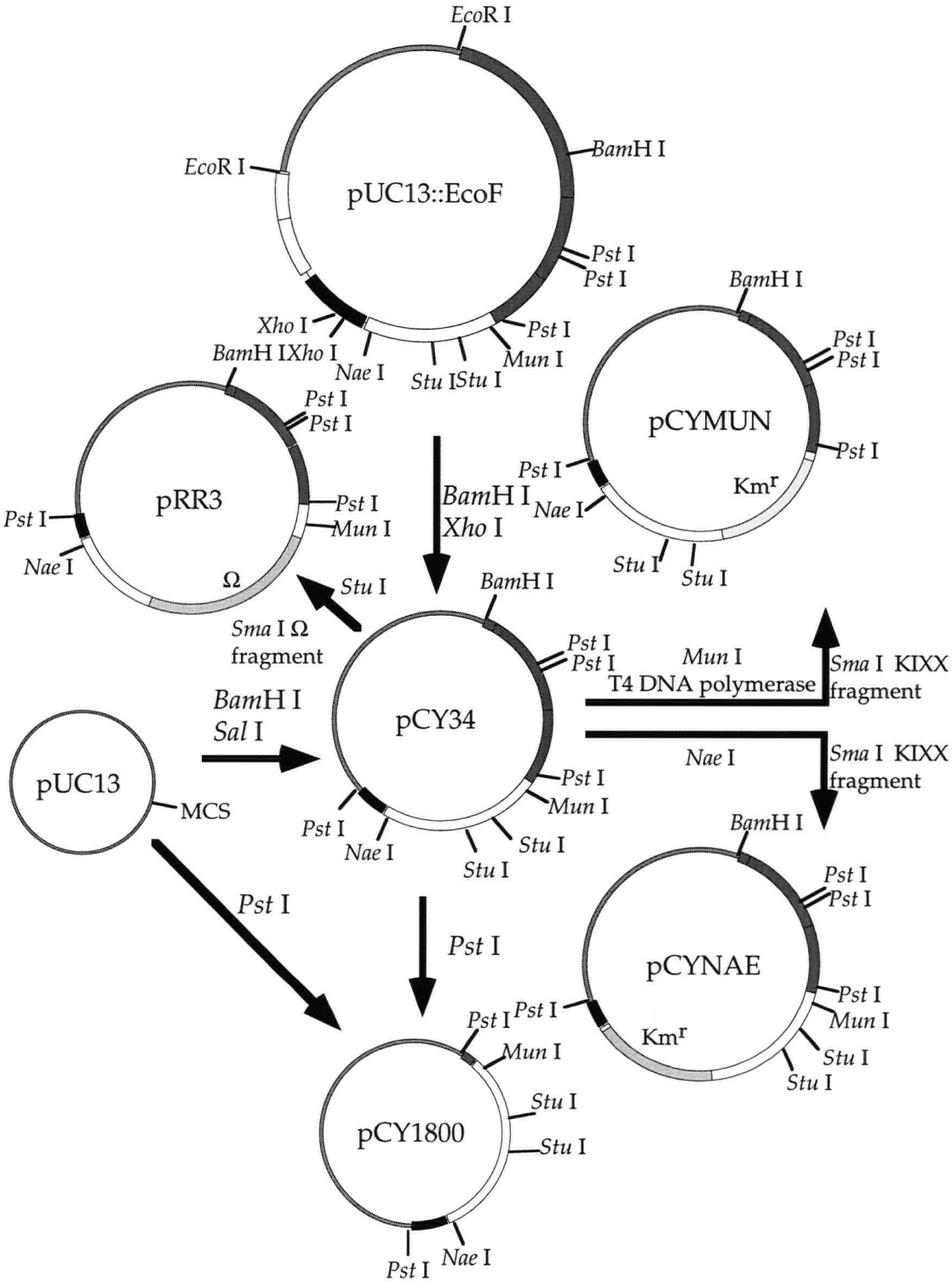
EcoR I
BamH I
pUC13::EcoF
EcoR I
Pst I
Pst I
Xho I
Pst I
BamH I
Xho I
Mun I
Nae I
Stu I
Stu I
BamH I
Pst I
Pst I
pCYMUN
Pst I
Pst I
Km^r
Pst I
Nae I
Stu I
Stu I
Pst I
Pst I
pRR3
Pst I
Mun I
Pst I
Nae I
Ω
BamH I
Xho I
Stu I
BamH I
Sma I Ω
fragment
Pst I
Pst I
Mun I
T4 DNA polymerase
Sma I KIXX
fragment
BamH I
Sal I
pCY34
Nae I
Sma I KIXX
fragment
pUC13
MCS
Pst I
Mun I
Pst I
Nae I
Stu I
Stu I
BamH I
Pst I
Pst I
Pst I
pCYNAE
Pst I
Mun I
Pst I
Km^r
Stu I
Stu I
Pst I
Pst I
Mun I
Stu I
pCY1800
Stu I
Pst I
Nae I

Table 2. Plasmids

Plasmid	Description	Reference
pCY1800	pUC13 with 1.8 kb *Pst* I subclone encoding *bch'MORF1696puhA'* from pCY34, Ap^r	This study
pCY42	pJAJ9 with 4.2 kb *Bcl* I/*Pvu* II subclone from pΔPUHA::Ω2, Tc^r, Sp^r	This study
pCY34	pUC13 with 3.4 kb *BamH* I/*Xho* I Bam F subclone, Ap^r	This study
pCYMUN	pCY34 with *ORF1696*::Km^r, insertion at *Mun* I site	This study
pCYNAE	pCY34 with *ORF1696*::Km^r, insertion at *Nae* I site	This study
pDPT51	mobilizing vector, Ap^r, Tp^r	(133)
pHP45Ω	pHP45 Ω interposon, Ap^r, Sp^r	(109)
pJAJ9	expression vector, Tc^r	(63)
pPUFP	expression vector, Km^r, Str^r	(19)
pΔ*puhA*::Ω2	pUC13 with 2.4 kb *Mlu* I-*Bam*H I Δ*puhA*::Ω insert and 1.3 kb *Pst* I/*Mlu* I *ORF1696* insert, Ap^r, Sp^r	(152)
pRK2013	mobilizing vector, Km^r	(37)
pRKPUHA2	pRKPUHA1 minus 1.0kb *Hind* III fragment, Tc^r	This study
pRR3	pCY34 with 2.0 kb Ω cartridge replacing DNA between *Stu* I sites, Ap^r, Sp^r	This study
pRR4	pTB12 with *ORF428*::Gm^r, insertion at *Pvu* II site	This study
pRR5	pPUFP with 2.2 kb *Eco*R I-*Bgl* II insert encoding *bch'HLMORF1696'*KIXX', Km^r, Gm^r, Str^r	This study
pRR5C	pRR5 minus 3.2 kb *Sma* I fragment encoding *bch'MORF1696'*KIXX, Gm^r, Str^r	This study

Table 2 cont.

pRR6	pPUFP with 1.9 kb *Eco*R I to *Stu* I *bch'MORF1696*KIXX insert and 2.6 kb *Hin*d III Gm^r cartridge from pWKR440, Km^r, Gm^r, Str^r	This study
pRRMun+	pCY1800 with 1.2 kb *Sma* I KIXX cartridge inserted at blunted *Mun* I site in *ORF1696*, Ap^r, Km^r	This study
pSP72::lacZ	pSP72 with truncated *lacZ* allele, Ap^r	(84)
pTB12	*Acc* I- *Xho* I 0.9 kb fragment encoding *ORF'304ORF428'* inserted into *Cla* I-*Xho* I digested pSP72, Ap^r	(19)
pUC4 KIXX	pUC4 Km^r cassette, Km^r, Ap^r	(6)
pUC13	*lacZ*α, cloning vector, Ap^r	(95)
pUC19::phoA	pUC19 with truncated *phoA* allele and inverted repeat (IR) from Tn*phoA*, Ap^r	(18)
pUI310	pUC19 with truncated *phoA* allele, Ap^r	(139)
pUI320	pUC19 with truncated *phoA* allele, Ap^r	(139)
pVYASN	pJAJ9 with 1.8 kb *Bcl* I/ *Pst* I *ORF1696* His-152 -> Asn allele cloned into *Bam*H I/ *Pst* I sites, Tc^r	This study
pVYHIS	pJAJ9 with 1.8 kb *Bcl* I/ *Pst* I *ORF1696* wild type allele cloned into *Bam*H I/ *Pst* I sites, Tc^r	This study
pVYPHE	pJAJ9 with 1.8 kb *Bcl* I/ *Pst* I *ORF1696* His-152 -> Phe allele cloned into *Bam*H I/ *Pst* I sites, Tc^r	This study
pWKR440	pACYC184 with Gm^r cassette, Gm^r	gift from W. Klipp
pXCA6::935	*pufQpufB'::lac'Z* translational fusion vector, transcription driven by the *puf* promoter, Tc^r	(1)

2.3.4 pRKPUHA2

Plasmid pRKPUHA2 was made by digesting pRKPUHA1 (152) with *Hind* III, to remove a 1.0 kb DNA fragment encoding the translational start codon and 5' sequences of the *ORF1696* gene, but leaving the P_{puhA} promoter sequences intact on the remaining vector DNA. The 11.9 kb vector DNA was gel purified and self-ligated to yield pRKPUHA2.

2.3.5 pRR3

Plasmid pRR3 was created by digesting pCY34 with *Stu* I followed by gel purification of the linear blunt-ended plasmid DNA (see Fig. 6). The plasmid pHP45Ω (109) was digested with *Sma* I to generate a blunt-ended DNA fragment encoding spectinomycin resistance. The Ω cartridge was separated from plasmid DNA by agarose gel electrophoresis, purified, ligated into the *Stu* I linearized pCY34 DNA and transformed into *E. coli* . Gene transfer agent (GTA) was used to transduce (152) the insertion of Ω between the *Stu* I sites in *ORF1696* into the *R. capsulatus* strain MW442, resulting in a mutation differing from that of the ΔStu KIXX cartridge insertion in that Ω was shown to terminate transcription in *R. capsulatus* (146).

2.3.6 pRR4

Plasmid pRR4 was constructed by digesting pTB12 (19) with *Pvu* II followed by gel purification of the linear blunt-ended plasmid DNA. The plasmid pWKR440 (gift from W. Klipp) was digested with *Hin* dIII and *Sal* I to yield the 2.6 kb Gm^r cartridge which was separated from plasmid DNA by gel electrophoresis, purified, and treated with T4 DNA polymerase to make the ends blunt. The Gm^r cartridge was ligated into the *Pvu* II linearized pTB12 and transformed into *E. coli.* GTA was used to transduce (152) the Gm^r cartridge inserted into the *Pvu* II site of *ORF428* in the *R. capsulatus* strains SB1003, ΔLHII, ΔStu, and ΔMun, resulting in mutations which differed from that of the TB428 KIXX mutation (19) in that the Gm^r cartridge

was used to disrupt *ORF428* instead of the KIXX cartridge and, besides the SB1003 strain, the parental strain backgrounds had mutations in one or both of the *ORF1696* and *pucC* genes.

2.3.7 pRR5, pRR5C, pRRMun+, and pRR6

The construction of these plasmids is shown in Fig. 7. Plasmid pRR5 was constructed by subcloning the 2.2 kb *bch'HLMORF1696'*KIXX' DNA fragment, obtained from pCYMUN digested with *Eco*R I and *Bgl* II, into the 9.9 kb expression plasmid pPUFP1 cut with the same enzymes (separated from a 1.2 kb DNA fragment and purified). The gentamicin resistance (Gm^r) cartridge from plasmid pWKR440 was subcloned as a 2.6 kb *Hind* III DNA fragment into plasmid pRR5, digested with *Hind* III, to allow for selection of this plasmid with gentamicin. Plasmid pRR5C was constructed by digesting pRR5 with *Sma* I to release a 3.2 kb DNA fragment encoding the *bchH'LMORF1696'*KIXX sequences and an 11.5 kb linear vector fragment. The 11.5 kb vector DNA was purified by agarose gel electrophoresis and recircularized in a ligation reaction to yield pRR5C. Plasmid pRRMun+ was constructed by digesting pCY1800 with *Mun* I, treated with Klenow fragment to generate blunt ends, then subcloning the 1.2 kb *Sma* I KIXX cartridge DNA fragment from pUC4KIXX into the blunt-ended pCY1800 DNA.

Plasmid pRRMun+ was digested with *Eco*R I and *Stu* I to give a 1.9 kb linear DNA segment encoding a 3'-segment of *bchM*, and including 90 nucleotides from the 5' end of *ORF1696* followed by the KIXX fragment sequences. This 1.9 kb fragment was purified and ligated into pRR5C DNA linearized by digestion with *Eco*R I and *Sma* I. The resulting 13.5 kb plasmid, pRR6, places the *ORF1696* sequences under the transcriptional control of the *puf* promoter, originating from the pPUFP1 expression plasmid (19), and is Km^r and Gm^r.

Figure 7. Construction of plasmids pRR5, pRR5C and pRR6. See section 2.3.7 of Materials and Methods for details. The sites of restriction enzymes and the type of antibiotic resistance is indicated. Thin boxes represent vector DNA, thick darkly shaded boxes represent bchl biosynthesis genes, thick lightly shaded boxes represent antibiotic resistance cartridges, black boxes represent *puhA* sequences and unshaded boxes represent *ORF1696* sequences. The bent arrow indicates the location and direction of trancription originating from the *puf* promoter.

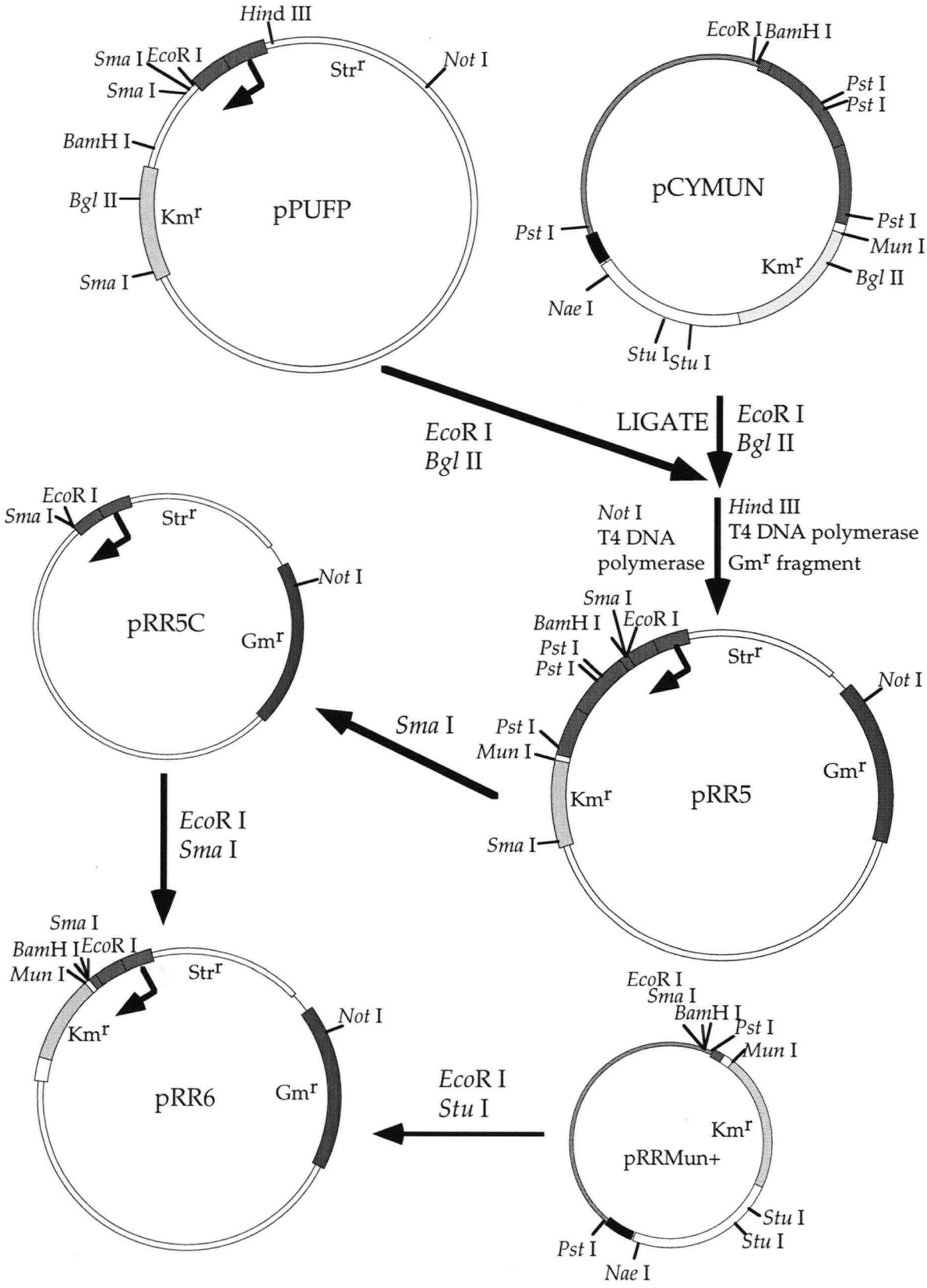
Hind III
Sma I
EcoR I
Sma I
Str^r
Not I
BamH I
Bgl II
Km^r
pPUFP
Sma I
EcoR I BamH I
Pst I
Pst I
pCYMUN
Pst I
Pst I
Mun I
Km^r
Bgl II
Nae I
Stu I
Stu I
EcoR I
Bgl II
LIGATE
EcoR I
Bgl II
Not I
T4 DNA
polymerase
Hind III
T4 DNA polymerase
Gm^r fragment
EcoR I
Sma I
Str^r
Not I
pRR5C
Gm^r
Sma I
BamH I
EcoR I
Pst I
Pst I
Str^r
Not I
Sma I
Pst I
Mun I
Km^r
pRR5
Gm^r
Sma I
EcoR I
Sma I
Sma I
BamH I
EcoR I
Mun I
Str^r
Km^r
Not I
pRR6
Gm^r
EcoR I
Stu I
EcoR I
Sma I
BamH I
Pst I
Mun I
Km^r
pRRMun+
Stu I
Stu I
Pst I
Nae I

2.4 CONJUGATION

Conjugal transfer of plasmids from *E. coli* to *R. capsulatus* was performed in diparental matings using the mobilizing *E. coli* strain, SM10 (125), or in triparental matings using the *E. coli* helper strain, HB101(pRK2013) (37). 200 µl of overnight stationary phase donor and recipient cultures were mixed, pelleted in a microcentrifuge then resuspended in 200 µl of antibiotic-free YPS medium. 10 µl aliquots of the mixed cultures were deposited on YPS agar plates and incubated overnight at 37° C, after which cells from each spot were streaked onto selective RCV agar medium to purify *R. capsulatus* transconjugants.

2.5 SPECTRAL ANALYSIS

Photosynthetic or low oxygen cultures of *R. capsulatus* strains were grown to stationary phase or 100 Klett units (Ku), respectively, then harvested (~1.8 x 10^9 cells) for spectral analysis. Cell pellets were resuspended in 1.0 ml of 22.5% bovine serum albumin (BSA) in RCV medium, added to a 1 cm light path quartz cuvette, and scanned for light absorption over light wavelengths ranging from 350 nm to 1000 nm using a Hitachi U-2000 spectrophotometer. Data collection was done using the SpectraCalc software package and analysis of spectra with the Grams 386 software package (Galactic Industries Corp.).

2.6 GENE TRANSFER AGENT (GTA) TRANSDUCTION

Plasmids were mobilized by conjugation from *E. coli* into the *R. capsulatus* GTA overproducer strain DE442 (153) by use of the mobilizing vector pDPT51, present in the *E. coli* strain Tec5 (133). DE442 transconjugants were grown photosynthetically in selective YPS medium to stationary phase (~350-400 Ku) and then ~5 ml of the culture was passed through a 0.45 µm Gelman Supor membrane filter to remove bacterial cells yielding a filtrate of GTA particles. Equal volumes

(0.1 ml) of GTA filtrate and stationary phase recipient cells were incubated together for 1 h at 34° C in 0.4 ml of filter sterilized 1x GTA buffer (1.0 mM Tris-HCl, pH 7.8, 1.0 mM $MgCl_2$, 1.0 mM $CaCl_2$, 1.0 mM NaCl, and 500 μg/ml BSA (Fraction V)) after which the cells were pelleted by centrifugation, resuspended in fresh RCV medium and incubated at 34° C for 4 h. Cells were pelleted, resuspended in fresh RCV medium and inoculated onto selective RCV agar. Transductants were isolated as single, antibiotic resistant colonies after 48 h incubation at 37° C.

2.7 CONSTRUCTION OF *R. CAPSULATUS* STRAINS ΔMUN, ΔSTU, ΔSTU::Ω AND ΔNAE

The *ORF1696*::Km^r insertions in plasmids pCYNAE and pCYMUN were obtained in the *R. capsulatus puc* operon deletion strain, ΔLHII (83), by GTA-mediated transduction. A suspension of GTA particles containing the ORF1696::Km^r insertion between the *Stu* I sites was a gift from C. Bauer. The *ORF1696*::Ω insertion in plasmid pRR3 was introduced into the *R. capsulatus pucC* mutant strain, MW442 (83, 119) by GTA-mediated transduction. The *ORF1696* mutants of ΔLHII were named according to the site(s) at which the Km^r (or Ω) cassette was inserted in the *ORF1696* gene, *i.e.*, ΔNae, ΔStu, ΔStu::Ω and ΔMun. Thus, the Km^r cartridge was inserted 1392 nt, 411 nt and 87 nt downstream of the putative ATG start codon for *ORF1696* in strains ΔNae, ΔStu and ΔMun, respectively. The ΔMun and ΔStu insertions are upstream of the reported *puhA* promoter, P_{puhA} (10), and the Ble^r gene segment is translationally out-of-frame with the 3' segments of *ORF1696*. The ΔNae insertion is downstream of P_{puhA}, and creates a translational in-frame fusion between the remaining 60 nt of *ORF1696* and a 5'-segment of the Ble^r gene on the *Sma* I fragment of the KIXX Km^r cartridge (6).

2.8 SITE-DIRECTED MUTAGENESIS OF ORF1696 HIS-152

Plasmid pTZ1800 was constructed by digesting pTZ18U and pCY1800 with *Pst* I followed by separation and purification of the 1.8 kb *Pst* I *ORF1696* fragment derived from pCY1800. The linearized pTZ18U vector DNA and ORF1696 *Pst* I fragment were ligated and transformed into *E.coli* strain RZ1032 which is *dut*$^-$*ung*$^-$ and which synthesizes DNA containing uridine (76). Single-stranded pTZ1800 template DNA was obtained by infecting 10 ml of exponential growth phase RZ1032(pTZ1800) cells with ~1.8 x 10^{10} pfu of M13KO7 (Pharmacia) phage (35 µl of phage suspension) followed by shaking at 37° C for 1 hr at 300 rpm. 2 ml was transferred to 50 ml of LB broth containing 70 µg/ml kanamycin sulfate and shaken at 300 rpm overnight at 37° C in a 500 ml flask. The cells were pelleted by centrifugation and 0.25 volumes of 3.5 M ammonium acetate/ 20% PEG8000 added to the supernatant, mixed and placed on ice for 30 min. Precipitated phage were pelleted by centrifugation at 13000 rpm for 30 min and the pellet was resuspended in 400 µl of TE buffer.

The phage suspension was extracted twice with phenol/chloroform and twice with chloroform and acidified by adding 0.1 volumes of 3 M sodium acetate, pH 5.2. The single-stranded DNA was precipitated by adding two volumes of absolute ethanol, mixing, and placing the solution on ice for 30 min followed by pelleting of the DNA by centrifugation (13000 rpm, 10 min) and washed with 70% ethanol. The DNA pellet was dried under vacuum then dissolved in 100 µl of TE buffer. The A_{260}/A_{280} ratio determined for the pTZ1800 single-stranded template preparation was 1.9.

Primer annealing to the single-stranded template and second strand synthesis were carried out as described by Sambrook *et al.* (1989). The oligonucleotide primers synthesized for the exchange of the ORF1696 His-152 residue for Asn and Phe were 5'-GGTCTGCGTCATGTTCATGCCGACGCCCGCCATCAGGAAG-3' and 5'-GGTCTGCGTCATGAACATGCCGACGCCCGCCATCAGGAAG-3', respectively, and

the altered codons are underlined. 10 pmol of each primer were combined with 1 μg of single stranded pTZ1800 DNA template in 1x PE1 buffer (20 mM Tris-HCl, pH 7.5, 10 mM $MgCl_2$, 50 mM NaCl, and 1 mM dithiothreitol) and heated to 98° C for 5 min after which the temperature was allowed to gradually return to 37° C to allow for primer annealing to the template DNA. Second strand synthesis was performed with the annealed primer/template solutions in 1x PE2 buffer (20 mM Tris-HCl, pH 7.5, 10 mM $MgCl_2$, 10 mM dithiothreitol) and 10 mM ATP with 5 units of T4 DNA ligase and 13 units of Sequenase 2.0 (USB Biochemicals) at 37° C for 2 h. The product was used to transform *E. coli* DH5αF' cells and plasmid DNA isolated from the transformants was screened by restriction analysis with *Sph* I for the presence of the mutated codons. There is an *Sph* I restriction site, which overlaps the codon for His-152, located at nucleotides 448 to 454 of *ORF1696* and this restriction site was eliminated in pTZ1800 containing the mutated codons. pTZ1800 lacking the *Sph* I site was sequenced to confirm the presence of Asn and Phe codons in place of the His in the ORF1696 protein.

Plasmids pVYASN, pVYPHE, and pVYHIS (Table 2) were introduced into the *R. capsulatus* strain ΔStu by conjugal transfer (section 2.4) and spectral analysis (section 2.5) of the resulting strains grown with low aeration was performed.

2.9 DETERMINATION OF BACTERIOCHLOROPHYLL (BCHL)

Five ml samples of *R. capsulatus* culture were pelleted by centrifugation and extracted in 2 ml of 99.5% acetone in the dark on ice overnight. Cells and cell debris were pelleted and 1 ml of the supernatant containing the bchl was scanned for absorption over light wavelengths of 700 nm to 900 nm using a Hitachi U-2000 spectrophotometer. The light absorption maximum for bchl at 770 nm and a baseline absorption value at 850 nm were used in the following equation to calculate [bchl] using an extinction coefficient (Σ_{bchl}) of 92.3 $ml \cdot mg^{-1} \cdot cm^{-1}$ (126):

$$[bchl]\ (\mu g/ml) = (A_{770} - A_{850})(V_{extract} / V_{sample} \times d \times \Sigma bchl)$$

where V = volume in ml and d = the light path distance (1 cm).

2.10 MEASUREMENT OF LHI COMPLEX DECAY KINETICS

R. capsulatus ΔLHII and ΔStu were grown to early stationary phase (A_{650} = 1.5-2.0) in RCV medium under anaerobic, photosynthetic conditions in 900 ml Roux bottles. Zero hour 5 ml samples were removed from these cultures, the cells pelleted by centrifugation and stored at -80° C for later analysis. Five hundred ml were used to inoculate 9.5 l of RCV medium in a 20 l Chemap series 3000 fermenter. Aeration, monitored using a steam sterilizable Ingold oxygen electrode (Westech Industrial Ltd.), was maintained at or near 20% pO_2 by sparging with air at a constant rate of 3 l/min as well as by automatic adjustment of the impeller rpm. Five hundred ml samples were removed every 2 h, the cells pelleted by centrifugation, and stored at -80° C prior to analysis. After thawing, cells were resuspended in 22.5% BSA in RCV medium and analyzed for LHI complex levels by absorption spectroscopy (section 2.5) (83). The cellular bchl content was determined for each sample (section 2.9). LHI complex levels were determined as the integrated area under the absorption peak at 875 nm in absorption spectra, and normalized to the light-scattering absorption at 650 nm, using the SpectraCalc and GRAMS 386 software packages. The ratios were plotted graphically as a function of time of incubation under high aeration, and the slopes were calculated.

2.11 MEASUREMENT OF LHI COMPLEX ASSEMBLY KINETICS

These experiments were done conversely to the LHI decay experiments described above. *R. capsulatus* ΔLHII and ΔStu were grown under highly aerated conditions in 100 ml of RCV medium in a 1 l Erlenmeyer flask incubated with shaking at 300 rpm, to an optical density of 2.0 to 2.5 OD_{650} units (zero hour sample

(5.0 ml) removed). Following removal of the zero hour sample from these highly aerated cultures, the remaining portion (95 ml) of the cultures was used to inoculate 700 ml of fresh RCV medium in two separate 1 l flasks, and the flasks were incubated at 150 rpm in a gyrorotary shaker. Samples of 10 ml were removed from these low aeration cultures every 30 min, the cells pelleted and stored at -80°C, and absorption spectroscopy was carried out for each sample as described above. The accumulation of the LHI complex was monitored by determination of the area under the LHI absorption peak at 875 nm, which was normalized to light scattering at 650 nm and the data plotted as described in section 2.10.

2.12 HYDROPATHY ANALYSIS

Hydropathy profiles were predicted for the ORF1696 protein using the computer program TopPred II 1.1 (29) (gift from G. von Heijne) with the hydropathy scales GES (42), Kyte and Doolittle (77) and a modified GES scale called GvH1 (143). The default sliding window value of 21 amino acid residues and the "core" value of 11 residues were used to predict "certain" or "putative" transmembrane segments of the protein. All conceivable topologies are generated by the TopPred program taking into consideration the most hydrophobic predicted transmembrane domains; those topologies with the largest positive charge bias toward the cytoplasmic side of the membrane are displayed, in accordance with the "positive-inside" rule (141). The highest ranked topologies predicted by each hydropathy scale mentioned above were compared to prepare a theoretical topological model of the ORF1696 protein.

2.13 CONSTRUCTION AND SCREENING OF *ORF1696'::PHO'A* FUSIONS

2.13.1 Shotgun cloning of *ORF1696* DNA fragments generated by BAL 31 nuclease digestion

A modification of the protocol described by Sambrook et al. (1989) for making nested deletions in DNA using the double stranded exonuclease activity of *Bal* 31 nuclease (145) was followed; a schematic representation is given in Fig. 8. The restriction endonucleases *Nae* I, *Bst*X I and *Bsa*A I, which have unique cleavage sites 1392, 787, and 534 nt downstream of the ATG start codon of the *ORF1696* gene, respectively, were chosen as C-terminal and central locations from which to begin digestion with *Bal* 31 nuclease in plasmid pCY1800. pCY1800 was separately digested and linearized with the above three restriction endonucleases. Appropriate amounts of 5 M NaCl, 1 M $CaCl_2$ and 1 M $MgCl_2$ were added to bring the concentration of the restriction digestion solution to 0.6 M NaCl, 12 mM $CaCl_2$, and 12 mM $MgCl_2$, and 9 units of *Bal* 31 nuclease were added (0.02 units per µl of reaction solution) to begin the reaction (this was calculated to be enough enzyme to remove ~32 bp/min/terminus of double-stranded DNA). Samples were removed from the *Nae* I/*Bal* 31 and *Bst*X I/*Bal* 31 reaction solutions at 5 min intervals over a 30 min total incubation period, and from the *Bsa*A I/*Bal* 31 reaction solution 1 min, 2 min, 5 min, 10 min and 20 min following addition of the *Bal* 31 nuclease. Samples were mixed with 0.1 volume of 0.5 M ethylene glycol-bis(β-aminoethyl ether)-N,N,N',N'-tetraacetic acid (EGTA) and incubated at 65° C for 10 min to stop the reaction, and the DNA ethanol precipitated. Due to the fact that *Bal* 31 nuclease

Figure 8. Construction of *ORF1696'::pho'A* fusions using *Bal* 31 nuclease. See section 2.13.1 of Materials and Methods for details. The sites of restriction enzymes used are indicated. The thin boxes are pUC vector DNA, thick shaded boxes represent *bch* gene sequences, the black boxes represent *puhA* sequences, the unshaded boxes represent *ORF1696* sequences, and the checkered box represents the *pho'A* allele. The bent arrow indicates the location and direction of transcription originating from the *lac* promoter.

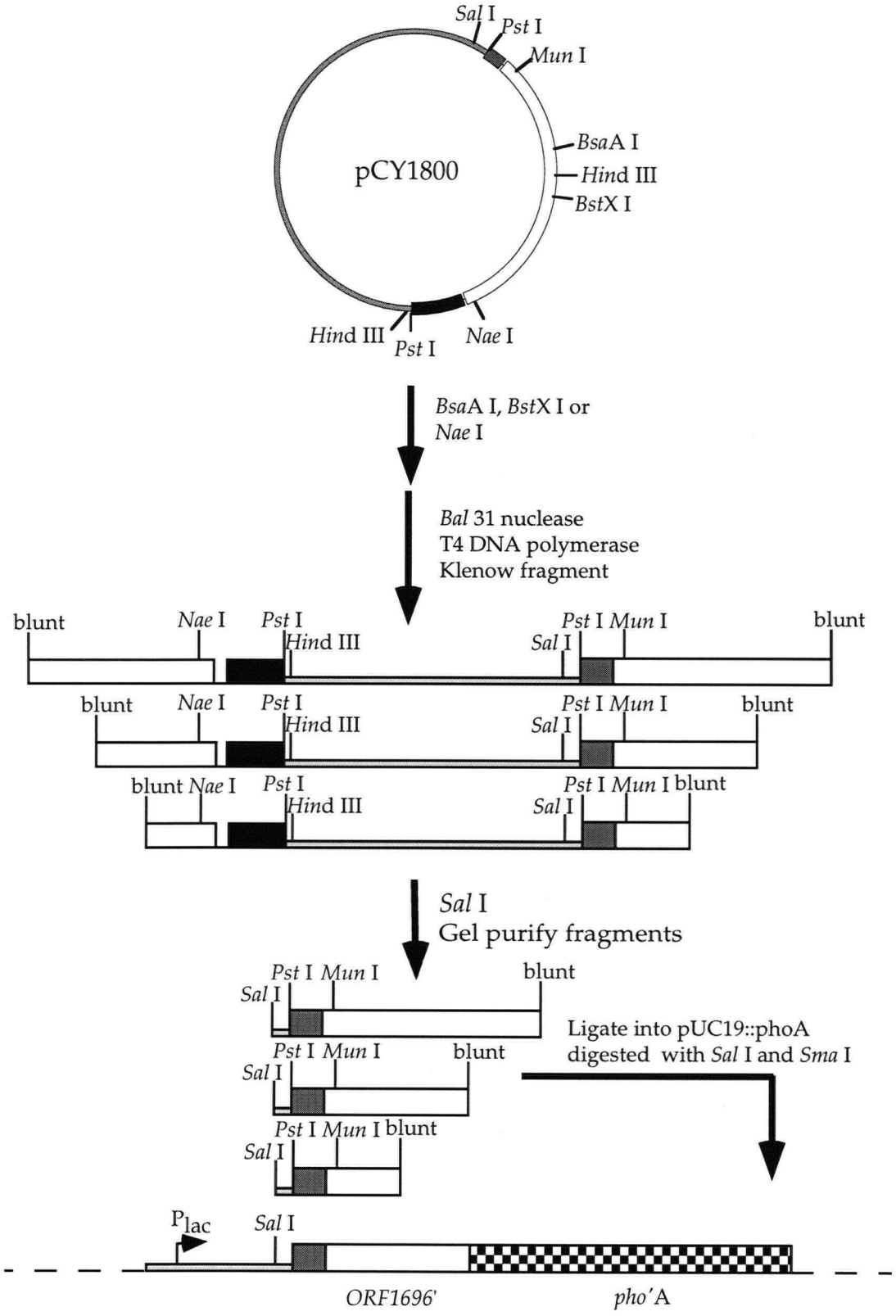
Sal I
Pst I
Mun I
BsaA I
Hind III
BstX I
pCY1800
Hind III
Pst I
Nae I
BsaA I, BstX I or
Nae I
Bal 31 nuclease
T4 DNA polymerase
Klenow fragment
blunt
Nae I
Pst I
Hind III
Pst I Mun I
Sal I
blunt
Sal I
Gel purify fragments
Ligate into pUC19::phoA
digested with Sal I and Sma I
Plac
ORF1696'
pho'A

possesses both a 5' and a 3'-exonucleolytic activity when the substrate is linear ds DNA (145), both 5' and 3' overhanging ends are generated among the products of a *Bal* 31 nuclease reaction. For this reason, each sample of *Bal* 31 degraded DNA was treated with T4 DNA polymerase and Klenow fragment consecutively to create blunt ends (115). The DNA samples were then digested with *Sal* I to release families of sticky/blunt-ended DNA fragments varying in size over a 200-300 bp range, which were separated from vector DNA by agarose gel electrophoresis and then purified from low-melting point agarose or by electroelution onto DEAE paper (115). The purified products were cloned into the *pho'A* fusion plasmid, pUC19::*phoA* (18) which had been digested with *Sal* I and *Sma* I. The ligated products were introduced into the *E. coli* CC118 *phoA*$^-$ strain by $CaCl_2$ transformation and the cells were spread on LB/Amp/XPho (5-bromo-4-chloro-3-indolyl phosphate *p*-toluidine salt, 40 μg/ml) agar plates. Both blue and white colored colonies were screened by isolating DNA and checking for inserted *ORF1696*' DNA by restriction analysis. Plasmids which had inserts were sequenced across the fusion joint by the dideoxy chain termination method using the primer, CYPHOA1 (5'-GCAAAACGGGAAAGGTT-3') to confirm that the *ORF1696* and *phoA* sequences were translationally in-frame.

2.13.2 Construction of pMun0.2, pHin1.0, and pNae1.5

Plasmid pMun0.2 was constructed to generate a short N-terminal ORF1696 fusion with PhoA. Plasmid pCY34 (Fig. 5) was digested with *Mun* I and treated with T4 DNA polymerase. The 6.1 kb linear pCY34 DNA was then digested with *Hin*d III to yield a 230 bp DNA fragment which was separated from vector DNA by gel electrophoresis and purified. The *phoA* fusion vector, pUI320 (139), was digested with *Pst* I and treated with T4 DNA polymerase. The 4.2 kb linear pUI320 DNA was then digested with *Hin*d III and ligated with the 230 bp *Hin*d III/blunt *ORF1696*' fragment to yield the 4.4 kb plasmid, pMun0.2. The first 93 nucleotides of *ORF1696* are fused to the *pho'A* allele in plasmid pMun0.2.

Plasmid pHin1.0 was constructed to yield a fusion of the central region of *ORF1696* with *phoA*. Plasmid pCY1800 was digested with *Hin*d III to yield a 1.0 kb DNA fragment, encoding 3' sequences of *ORF1696* and 5' *puhA* sequences, and a 3.5 kb linear vector DNA fragment. The DNA was treated with T4 DNA polymerase and digested with *Pst* I to yield a 0.8 kb DNA fragment encoding the 5' sequences of *ORF1696,* which was separated from contaminating DNA molecules by gel electrophoresis and purified. Plasmid pUI320 was digested with *Xba* I and treated with T4 DNA polymerase. The linear pUI320 DNA was then digested with *Pst* I and ligated with the *Pst* I/blunt 0.8 kb *ORF1696'* DNA fragment to yield the 5.0 kb plasmid, pHin1.0. The first 734 nucleotides of *ORF1696* were fused in-frame with the *pho'A* allele in pHin1.0.

Plasmid pNae1.5 was constructed in order to obtain a fusion of the C-terminal domain of ORF1696 and PhoA. Plasmid pCY1800 was digested with *Nae* I and *Pst* I to yield a 1.5 kb *ORF1696'* DNA fragment which was separated from vector DNA by gel electrophoresis and then purified. Plasmid pUI310 (139) was digested with *Bam* HI and treated with T4 DNA polymerase. The 4.2 kb linear pUI310 DNA was then digested with *Pst* I and ligated with the *Pst* I/blunt 1.5 kb *ORF1696'* DNA fragment to yield the 5.7 kb plasmid, pNae1.5. The first 1394 nucleotides of *ORF1696* are fused in-frame with the *pho'A* allele in pNae1.5.

2.13.3 Construction of pCY165 by the long polymerase chain reaction (L-PCR)

The L-PCR protocol used to synthesize pCY165 was based upon a modification of the method described by Cheng *et al.* (27) and designed to conform with the manufacturer's instructions for use of *Tth* DNA polymerase (114) in PCR reactions (Boehringer Mannheim GmBH, Germany). This method allows for the amplification of relatively large (10 to 40 kb) DNA molecules (including entire plasmids and cosmids) and can be used to generate site-specific deletions.

The pUC19::phoA derived *ORF1696'::pho'A* fusion plasmid, pN10-2, was digested with *Kpn* I, which has a unique cleavage site located at the fusion joint between the *ORF1696* and *phoA* sequences, to linearize the plasmid. Linear pN10-2 template DNA (100 ng) was combined with 10 pmol each of the tailed primers CYPHOA2 (5'-TTACACGGTACCTGACTCTTATACACAA-3'), which specifies a *Kpn* I site and anneals to the fusion joint region of pN10-2, and CY165 (5'-TCTAGCGGTACCATCACCCGGTTGAGCGTGCCCA-3'), which also specifies a *Kpn* I site and is complementary to the *ORF1696* sequences between nt 143 to 165 downstream of the *ORF1696* ATG start codon. A mixture of dATP, dTTP, dCTP and dGTP (each dNTP 10 mM) was added to give a final concentration of 200 μM of each, and $MgCl_2$ was titrated over a range of 2.5 mM to 4.5 mM in separate reactions. 2 units of *Tth* DNA polymerase along with the supplied 10xPCR buffer (100 mM Tris-HCl, pH 8.9, 1 M KCl, 15 mM $MgCl_2$, 500 μg/ml BSA, 0.5% (v/v) Tween 20) were added to each reaction as a mix diluted appropriately in double distilled water to give a total reaction volume of 50 μl. The L-PCR reactions were performed using a Perkin Elmer GeneAmp PCR System 2400 thermal cycler (Perkin Elmer, Mississauga, Ontario) and thin-walled 0.2 ml snap-cap PCR tubes (Island Scientific, Bainbridge Island, WA, USA). The following thermal cycling regimen (Table 3) was determined to be optimal for yielding large quantities of the desired 5 kb PCR product from the above reactions. The second round of cycles includes incremental increases in the time of elongation to allow *Tth* DNA polymerase to finish synthesizing L-PCR products.

Table 3. Thermal cycling regimen for L-PCR reactions.

T_{den}	95° C	3 min	1 cycle
T_{den}	95° C	15 s	
T_{ann}	55° C	45 s	20 cycles
T_{elong}	70° C	4 min	
T_{den}	95° C	15 s	
T_{ann}	55° C	45 s	20 cycles
T_{elong}	70° C	4 min + 20 s/cycle	
T_{elong}	70° C	7 min	1 cycle
hold	4° C		

T_{den} = denaturing temperature, T_{ann} = annealing temperature, T_{elong} = elongation temperature.

A 5 kb PCR product was separated from smaller DNA products by gel electrophoresis, purified and digested with *Kpn* I. The PCR product was circularized in a dilute ligation reaction, transformed into *E. coli* CC118 and plated on LB/Amp/XPho agar medium. A dark blue colony growing on this medium yielded plasmid pCY165 which was sequenced and confirmed to have the correct *ORF1696* sequence as well as an in-frame fusion of the *ORF1696'* sequences with the *pho'A* sequences.

2.14 CONSTRUCTION AND SCREENING OF *ORF1696'::LAC'Z* FUSIONS

ORF1696'::pho'A fusions made in the pUC19::phoA plasmid background underwent the process of fusion switching (89) to *ORF1696'::lac'Z* fusions due to the availability of restriction sites on these plasmids for substituting the *lac'Z* allele in place of the *pho'A* allele. Plasmid pSP72::lacZ (84) was digested with *Hin*d III, treated with the Klenow fragment of DNA polymerase I, and digested with *Kpn* I to yield a 3 kb DNA fragment encoding the *lac'Z* allele which lacks the sequences

encoding the N-terminus of β-galactosidase (β-gal). *ORF1696'::pho'A* fusion plasmids were cut with *Eco*R I, treated with Klenow fragment and *Kpn* I, and vector DNA, including 5' sequences of *ORF1696*, was separated and purified from DNA encoding *phoA* and ligated with the *Kpn* I/blunt ended *lac'Z* DNA. The *ORF1696'::lac'Z* fusion plasmids were transformed into *E. coli* DH5αF', and spread on LB/Amp/Xgal (5-bromo-4-chloro-3-indolyl-β-D-galactoside, 40 μg/ml) agar. Plasmid preparations from blue colonies were screened by restriction analysis for the presence of *lac'Z* DNA and strains containing the *ORF1696'::lac'Z* fusion plasmids were assayed for β-gal activity as described in section 2.16.

2.15 ALKALINE PHOSPHATASE ASSAYS

The procedure outlined by Manoil (89) for assaying alkaline phosphatase activity in SDS/chloroform permeabilized *E. coli* cells was followed. Briefly, 2.5-5.0 x 10^8 exponential phase cells were pelleted by centrifugation, washed and resuspended in 1 ml of cold 1 M Tris-HCl, pH 8.0. 0.1 ml of washed cells were combined with 0.9 ml 1 M Tris-HCl, pH 8.0, 0.1 mM $ZnCl_2$ and permeabilized by treatment with 50 μl 0.1% SDS and 50 μl chloroform. Alkaline phosphatase assays were started by adding 0.4% *p*-nitrophenol phosphate (PNPP) (in 1 M Tris-HCl, pH 8.0), the start time was noted and incubation at 37° C was continued until a yellow color was observed. The reactions were halted by the addition of 120 μl 0.5 M EDTA, 1 M KH_2PO_4, pH 8.0 solution, the stop time was noted and the reactions placed in an ice bath. All determinations of alkaline phosphatase activity in *ORF1696'::pho'A* fusion strains were performed in duplicate and units of alkaline phosphatase activity were defined as $\Delta OD_{420} \cdot min^{-1} \cdot 10^6$ cells^{-1}.

2.16 β-GALACTOSIDASE ASSAYS

The procedure outline by Miller (97) was followed for assaying β-galactosidase activity in SDS/chloroform permeabilized *E. coli* cells. Briefly, ~1.2 x 10^8 cells were added to 0.5 ml of Z buffer, pH 7.0 (60 mM $Na_2HPO_4.7H_2O$, 40 mM $NaH_2PO_4.H_2O$, 10 mM KCl, 1 mM $MgSO_4.7H_2O$, 50 mM β-mercaptoethanol) and then were permeabilized by adding 50 µl of 0.1% SDS and 50 µl of chloroform. The reactions were started by adding 200 µl of 4 mg/ml ONPG (o-nitrophenol-β-D-galactoside), the start time was noted and incubation at room temperature was continued until a yellow color developed. The reactions were stopped by adding 500 µl of 1 M Na_2CO_3 solution, the stop time was noted and the reactions placed in an ice bath. All β-galactosidase assays were performed in duplicate and units of β-galactosidase activity are defined as the $\Delta OD_{420} \cdot min^{-1} \cdot 10^6$ $cells^{-1}$.

2.17 WESTERN BLOT ANALYSIS

The detection of ORF1696'::Pho'A fusion proteins was performed by Western blot chemiluminescence analysis using ECL detection reagents (Amersham International plc, England), according to the manufacturer's instructions.

E. coli CC149 *phoR* cell extracts were prepared by pelleting ~2.5 x 10^8 cells grown to an OD_{650} of 0.5 and boiled with 50 µl 2xSDS-PAGE loading buffer (1 M Tris-HCl, pH 6.8, 1 M DTT in sodium acetate, 10% SDS, 0.2% bromophenol blue, 20% glycerol, 10 µl per 100 µl of culture centrifuged). 20 µl aliquots of the CC149 cell extract were loaded onto a 4% stacking/12% separating SDS polyacrylamide gel, the proteins separated by electrophoresis and blotted onto a nitrocellulose membrane as described below. 1:1000, 1:1500, 1:2000, and 1:2500 dilutions of a rabbit polyclonal antibody to bacterial alkaline phosphatase (5'-3', Inc., West Chester, PA, USA) were used with a 1:10000 dilution of a donkey anti-rabbit horseradish peroxidase conjugate (Amersham International) to perform chemiluminescence reactions on

the CC149 Western blots to determine the titer of the anti-alkaline phosphatase primary antibody. These experiments indicated that a 1:2500 dilution of the primary antibody and a 1:10000 dilution of the secondary antibody conjugate enabled detection of *E. coli* alkaline phosphatase protein without significant background.

Samples for SDS-PAGE were prepared as follows: approximately 2.5 x 10^8 exponential phase cells of each *ORF1696'::pho'A* fusion strain were pelleted by centrifugation and boiled in 2xSDS-PAGE loading buffer for 5 min or until the cell pellet dissolved completely. SDS-PAGE was performed using a 4% polyacrylamide stacking gel and 12% separating gel in a Laemmli buffer system (25.5 mM Tris-HCl, 182 mM glycine, 0.1% SDS, pH 8.3). Volumes of loading sample added to wells were normalized to cell number and typically amounted to ~2 µl, and 10 µl of pre-stained protein molecular mass standards (size range 217 kDa to 14.3 kDa) (Gibco BRL) were loaded in one well of each gel. Gels were run for about 2.5 h at 100 V until the 43 kDa marker had run 2/3 of the way down the gel.

Separated proteins were electro-blotted from the SDS-polyacrylamide gels onto Nitro ME nitrocellulose membranes (Micron Separations Inc., Westborough, MA, USA) pre-soaked in Towbin transfer buffer (25 mM Tris, 192 mM glycine, 20% methanol v/v, pH 8.3) (135) using a voltage set at 100V for 1 h, and cooling provided by an ice pack inserted in the transfer buffer reservoir. All wash steps were carried out in TBST (20 mM Tris-HCl, 137 mM NaCl, 0.1% Tween-20, pH 7.6). The nitrocellulose membranes were then blocked for 1 h at room temperature with a mixture of 5% skim milk powder (IGA) and 800 µl of an *E. coli* CC118 cell extract (prepared similarly to the loading samples described above) in TBST, and then washed once for 15 min and twice for 5 min at room temperature with TBST. A 1:2500 dilution of the primary antibody in 10 ml of TBST was applied to the blocked membranes for 1 h at room temperature, and then the membranes were washed with TBST as described above and exposed to a 1:10000 dilution of the secondary

antibody conjugate in 10 ml of TBST after which the membranes were washed with 10 ml of TBST once for 15 min and four times for 5 min at room temperature. The membranes were exposed to the ECL chemiluminescence reagents according to the manufacturer's recommendations, wrapped in Saranwrap, and X-ray film (X-OMAT-AR, Eastman Kodak Co., Rochester, NY, USA) was exposed to the membranes to detect chemiluminescent protein bands.

2.18 ^{35}S-METHIONINE PULSE-LABELING OF ORF1696'::PHO'A FUSION PROTEINS

The procedure used for the ^{35}S-methionine pulse-labeling experiments was a modification of the method described by Manoil (89). All steps of the labeling procedure were carried out in a fumehood. *ORF1696'::pho'A* fusion strains, along with *E. coli* CC118 and CC149 as negative and positive controls, respectively, were grown to exponential phase (OD_{650} = 0.5-0.7) in M63 medium (97), supplemented with thiamine-HCl and ampicillin. 10-15 μCi of ^{35}S-methionine (>1000 mCi/mmol, Amersham International plc, England) was added to 0.5 ml of culture (~7-8 x 10^7 cells) and they were incubated at 37° C for 2 min. The radiolabeled cell suspension was incubated on ice for 15 min in the presence of 5% trichloroacetic acid and the insoluble debris was pelleted by centrifugation. The pellets were washed twice by vortexing in 1 ml of acetone and allowed to air dry for 30 min. The pellets were resuspended in 50 μl of Lysis buffer (10 mM Tris-HCl, pH 8.0, 1% SDS, 1 mM EDTA, 5% β-mercaptoethanol, 1 mM phenylmethylsulfonyl fluoride (PMSF), 10 μg/ml leupeptin, 1 μg/ml aprotinin, 10 μg/ml soybean trypsin inhibitor (STI)) boiled for 5 min, until the lysis suspension became clear. The protein preparations were cooled on ice for 1 min and mixed with 450 μl of cold RIPA buffer (30 mM Tris-HCl, pH 7.4, 150 mM NaCl, 1% NP-40, 0.5% sodium deoxycholate, 0.1% SDS, 2 mM EDTA + protease inhibitors in the same concentrations as in Lysis buffer) and immediately used for immunoprecipitation (section 2.19).

2.19 IMMUNOPRECIPITATION

All steps of the immunoprecipitation procedure were carried out on ice or at 4-6° C.

Pre-clearing of the ^{35}S-methionine labeled cell lysates from section 2.18 with Protein A-Sepharose beads (Pharmacia Biotech) was performed to remove proteins that bind non-specifically to the beads. 40 µl of chilled 50% (w/v) Protein A-Sepharose bead (Pharmacia Biotech) suspension in RIPA buffer was washed three times in cold RIPA buffer then added to radiolabeled cell lysates. The mixture was rocked for 1 h in a 4° C cabinet and then the beads were pelleted by centrifugation and the pre-cleared cell lysates were transferred to new chilled 1.7 ml microcentrifuge tubes.

Immunoprecipitation was begun by adding a 1:100 dilution of the rabbit polyclonal anti-alkaline phosphatase antibody (5'-3', Inc.) in 0.5 ml of RIPA buffer to the pre-cleared cell lysate and the solution was rocked for 2 h in a 4° C cabinet. 30 µl of the washed 50% (w/v) Protein A-Sepharose bead suspension was combined with the immunoprecipitation reaction and rocked in a cold cabinet overnight to bind antigen-antibody complexes to protein A. The beads were pelleted by centrifugation in a microfuge for 1 min, washed three times in 1 ml of cold RIPA buffer and then pelleted again by centrifugation. The supernatant fluid was removed and the beads resuspended in 20 µl of 1xSDS-PAGE loading buffer and boiled for 5 min.

5 µl of loading sample was applied to a 1 cm^2 piece of Whatman No. 1 filter paper and immersed in 5 ml of Ecolite$^+$ liquid scintillation cocktail (ICN Biochemicals). The radioactivity (cpm) in each sample was measured using a Beckman LS6000TA scintillation counter. SDS-PAGE consisted of a 4% stacking gel and a 10% separating gel and the gels were run using the Laemmli buffer system at 200 V for about 45 min until the bromophenol blue tracking dye front ran off the bottom of the separating gel. The gels were fixed in 10% acetic acid for 30 min and

dried at 80° C for 2 h on a Bio-Rad Model 583 gel dryer with vacuum. The dried gels were used to expose a phosphor screen for 18-24 h. Phosphorimaging was performed using a Phosphorimager SI and the Scanner Control SI software (Molecular Dynamics), and quantitative analysis of the phosphorimages was performed using the ImageQuant version 1.1 software program (Molecular Dynamics). The ImageQuant program was used to determine the pixel density or "volume", normalized to background, of the 47 kDa and 40 kDa bands (see Results, Fig. 27) in the phosphorimages for each lane, and the pixel numbers of the bands were added. The sum of the pixels was applied to normalize the raw AP activities to the fusion having the highest AP activity, (*ie.*, N15-3, see Results, Table 7).

3 RESULTS

3.1 DISRUPTION/COMPLEMENTATION ANALYSIS OF *ORF1696*

3.1.1 *Trans* complementation of *R. capsulatus* strain ZY1

A *trans* complementation experiment was performed to see whether the phenotype of a previously prepared disruption of *ORF1696* (strain ZY1, (10)) was due to the loss of an *ORF1696* gene product. Plasmid pCY42 (which contains the *ORF1696* transcribed from the *puf* promoter of pJAJ9; see Fig. 5, Materials and Methods) was introduced into ZY1 and the absorption spectrum of intact cells, grown under low aeration conditions, was compared with those of strain ZY1(pJAJ9) and the parental strain SB1003(pJAJ9) grown under the same conditions. The LHI complex level in ZY1(pCY42), manifested as a shoulder on the long-wavelength slope of the 850 nm LHII absorption peak, was partially restored compared to that of the SB1003 control, whereas the presence of pJAJ9 in strain ZY1 had no effect (Fig. 9). This indicates that the *ORF1696* encodes a protein required to maintain a high level of the LHI complex in an $LHII^+$ background.

3.1.2 Chromosomal disruptions of the *ORF1696* gene in the *R. capsulatus* strain ΔLHII

Using gene disruption/complementation experiments, an attempt was made to identify regions of the ORF1696 protein that might be important for obtaining high levels of the LHI complex; the well-characterized $LHII^-$ strain ΔLHII (83) allowed quantitative measurements of the relative amounts of the LHI complex.

Chromosomal disruptions were made at three sites in *ORF1696*, initially using a Km^r cartridge which rarely results in a polar effect (19). Fig. 10B gives a schematic representation of the *ORF1696* gene and flanking regions, and the sites of insertion

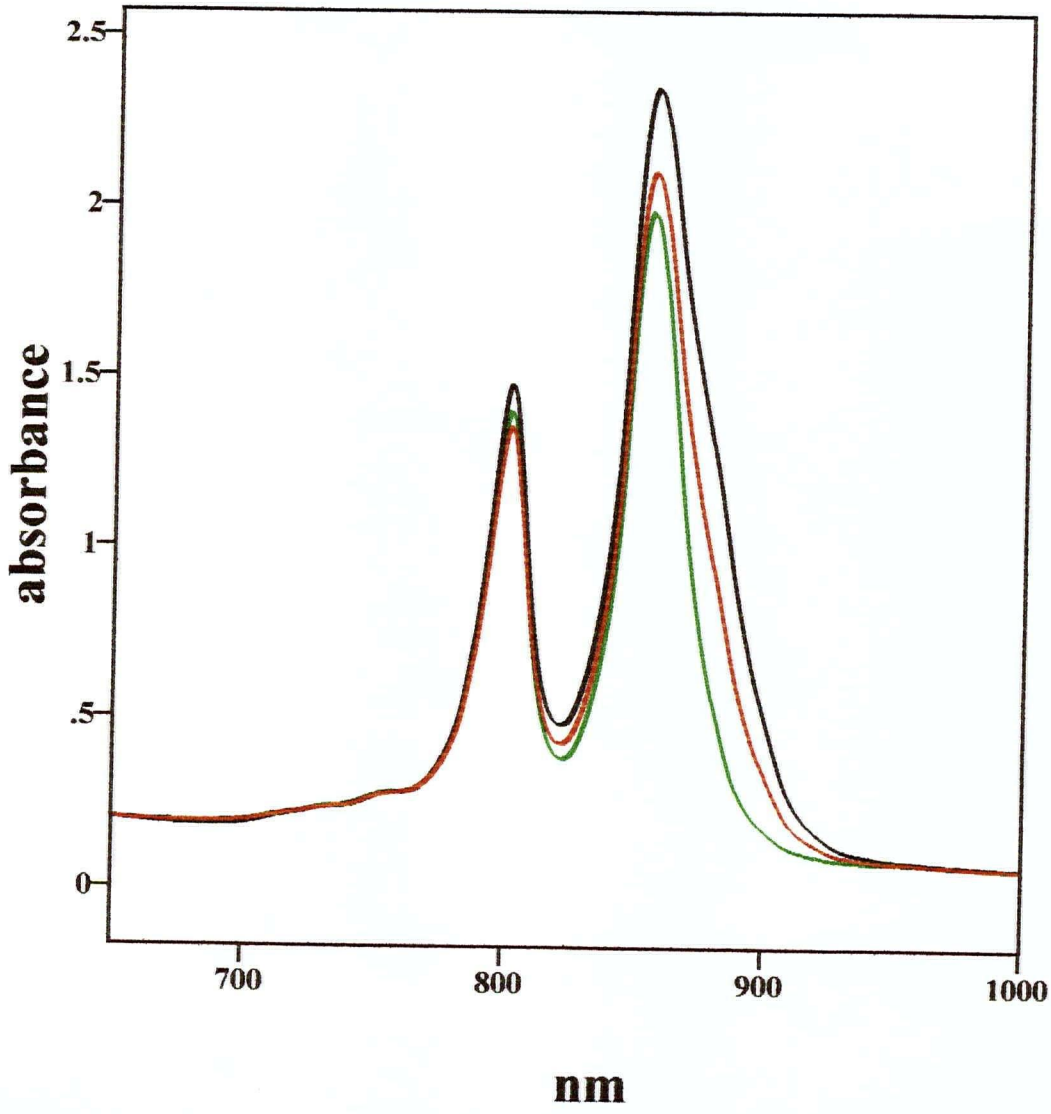

Figure 9. Absorption spectra of intact cells grown under low aeration conditions. Black = SB1003(pJAJ9), red = ZY1(pCY42), and green = ZY1(pJAJ9).

A

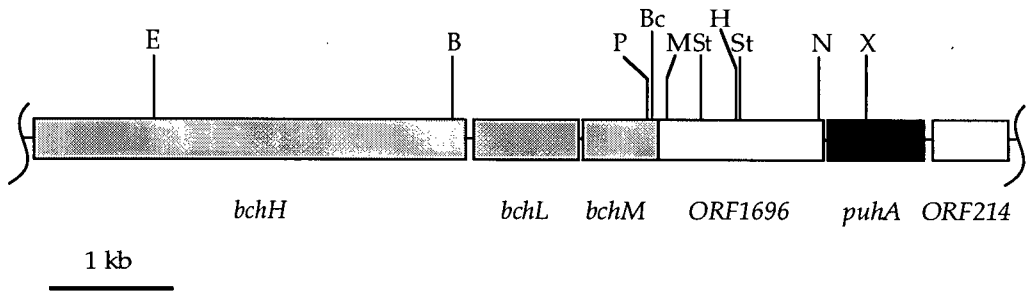

B

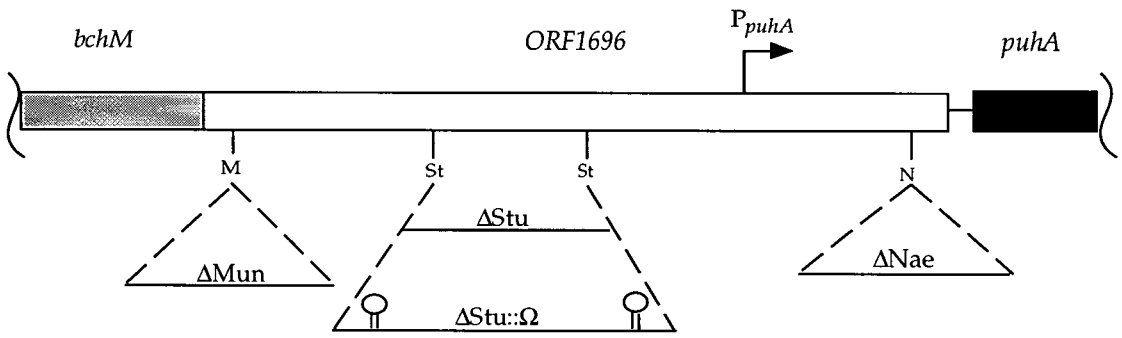

Figure 10. *ORF1696* and flanking genes. A. Restriction map of *ORF1696* and flanking genes in an 8 kb region of the photosynthesis gene cluster of the *R. capsulatus* genome. B= *Bam*H I, Bc= *Bcl* I, C= *Cla* I, E= *Eco*R I, H= *Hin*d III, M= *Mun* I, N= *Nae* I, P= *Pst* I, S= *Sac* I, Sa= *Sal* I, St= *Stu* I, X= *Xho* I. B. Schematic illustration of *ORF1696* and flanking genes with sites of antibiotic resistance cartridge insertion. Solid lines below the genes represent antibiotic resistance cartridge DNA molecules. Stem-loop symbols represent *rho*-independent transcription terminators. Dashed lines indicate the site of cartridge insertion in *ORF1696*. The *puhA* promoter (P_{puhA}) and direction of transcription is indicated by the bent arrow.

of antibiotic resistance cartridges at the *Mun* I site (yielding strain ΔMun), between the *Stu* I sites (ΔStu, ΔStu::Ω) and at the *Nae* I site (ΔNae).

The effects that the Km^r disruptions had on LHI complex levels is shown in Figure 11A. Each strain gave rise to a spectrum containing a peak at 875 nm corresponding to LHI absorption, and a relatively small RC peak at 800 nm. The LHI peak area was reduced to 20% in ΔStu, 30% in ΔMun and 50% in ΔNae, compared to ΔLHII. These results imply that deletion of as few as 13 of the C-terminal amino acid residues of the ORF1696 protein (in ΔNae) impairs its function in maintaining the wild type steady state level of LHI.

3.1.3 Photosynthetic growth of the *ORF1696* disruption mutants

Since the LHII complex was absent and there were reductions in the levels of the LHI complex in each of the *ORF1696* disruption strains, it was of interest to investigate the competency of each strain for photosynthetic growth. Growth curves for each strain grown under photosynthetic conditions are shown in Fig. 12. The data for ΔStu and ΔNae are typical examples taken from three separate experiments whereas the data for ΔMun is the one example out of six experiments. Thus, ΔStu and ΔNae are capable of growing reproducibly under photosynthetic growth conditions at a light intensity of 130 μEinsteins/m^2/s whereas ΔMun is not. The generation times measured for the mutant strains ΔStu (5.0 +/- 0.1 h) and ΔNae (5.0 +/- 0.2 h) compared with the parental ΔLHII strain (ΔLHII = 5.6 +/- 0.8 h) were similar during the exponential phase of growth (Fig. 12). In general, the reductions in the LHI complex observed for ΔStu and ΔNae do not impair growth similarly to the parental strain, ΔLHII, under the photosynthetic growth conditions tested. However, the reduction in the LHI and RC complexes observed in ΔMun (see Fig. 11) appears to impair the ability of this strain to grow

Figure 11. Absorption spectra of intact cells grown under low aeration conditions. A, Parental strain ΔLHII (black) and the Km^r disruption mutants ΔNae (red), ΔStu (green), and ΔMun (blue) B, parental strain ΔLHII, and pCY42 complemented ΔNae, ΔStu, and ΔMun strains. Note that spectra have been deliberately offset.

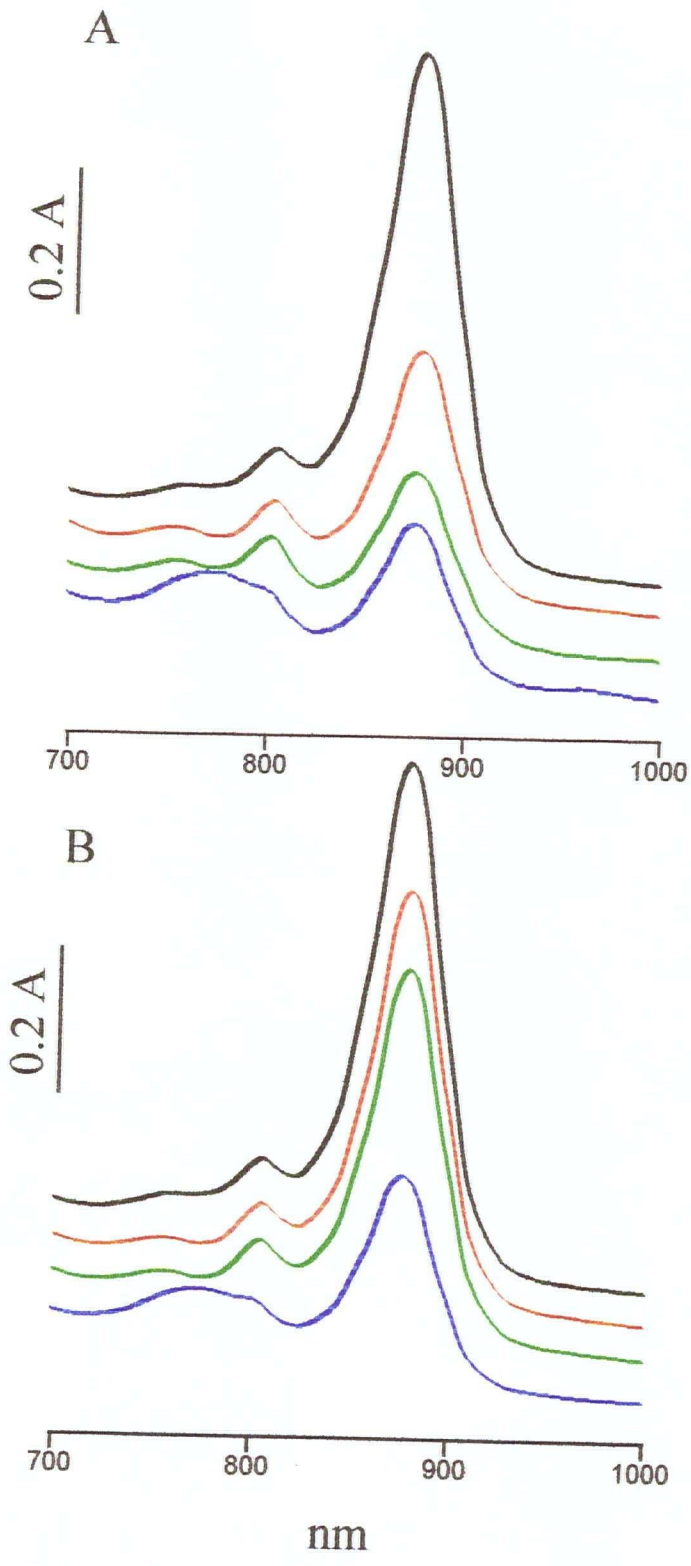
A
0.2 A
700
800
900
1000
B
0.2 A
700
800
900
1000
nm

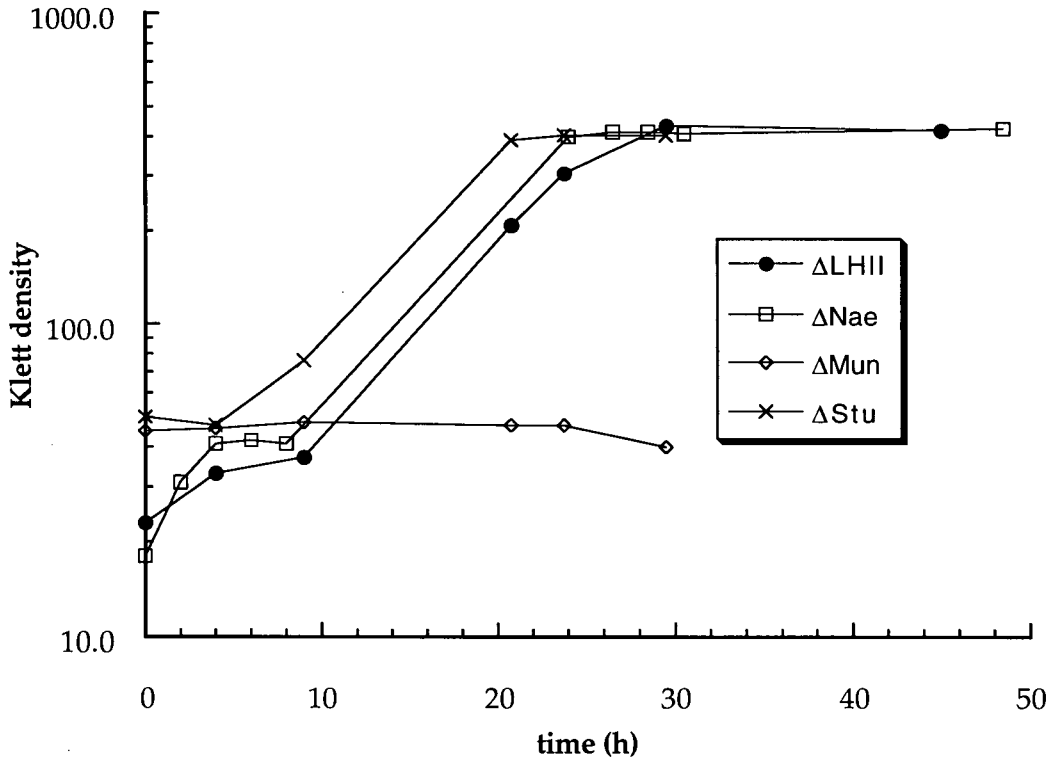

Figure 12. Growth curves for strains ΔLHII (parental strain), ΔNae, ΔStu and ΔMun grown photosynthetically at a light intensity of ~130 μEinsteins/m^2/s. Photosynthetic growth was not reproducible with the ΔMun strain.

consistently and at the same growth rate compared to the other strains under photosynthetic growth conditions.

3.1.4 *Trans* complementation of the *ORF1696* disruption mutants

Plasmid pCY42 was introduced into strains ΔStu and ΔNae; the *ORF1696* complemented strains were grown under low aeration conditions and spectral analysis carried out and compared to ΔLHII(pJAJ9). The area of the LHI complex peak was increased to 73% and 83%, respectively, of the ΔLHII(pJAJ9) area (Fig. 11B). Thus, there was nearly complete restoration of the level of LHI by complementation of ΔStu and ΔNae with the *ORF1696* gene, confirming the results obtained with the $LHII^+$ strain ZY1 (see above). (The presence of pJAJ9 in these strains had no effect on the spectral profiles.)

In the ΔMun mutant the reduction of LHI was accompanied by a decrease of the RC peak at 800 nm, with the appearance of a broad, heterogeneous area of absorption spanning from about 750 nm to 790 nm (Fig. 11A). This could be explained by: 1) the loss of amino acids encoded by *ORF1696* sequences between the *Mun* I and *Stu* I sites; 2) a toxic effect exerted by the 45 amino acid fusion peptide produced as a result of the ΔMun disruption; or 3) a polar effect exerted by the Km^r cassette on the expression of *puhA* and 3′ sequences (152).

Hypothesis 1) was tested by *trans* complementation of the ΔMun mutation with plasmid pCY42, which resulted in an increase of the LHI peak area from 30% to 41% of that of the ΔLHII parental strain (Fig. 11B). This slight LHI restoration was much less than seen with ΔStu(pCY42) (73%) and ΔNae (pCY42) (83%) (Fig. 11B). This relatively slight increase in LHI was interpreted as complementation of the direct effect of *ORF1696* disruption, whereas a polar effect of the ΔMun disruption was not complemented.

Hypothesis 2) was tested by *trans* expression of the 45 amino acid ΔMun ORF1696 fusion peptide from pRR6 in ΔLHII, ΔStu, ΔNae and ΔMun, but these

experiments indicated no change in the absorption spectra (see Fig. 13). Thus, the truncated ORF1696 protein of ΔMun does not seem to have a toxic effect that results in the ΔMun phenotype.

Hypothesis 3) was first tested by introduction of plasmid pRKPUHA2 (which expresses the *puhA* gene) into the ΔMun strain, which resulted in a slight decrease of the broad area of absorption from 750 to 790 nm (see Fig. 14A). This result indicates that the ΔMun disruption has a polar effect on expression of *puhA* and genes located 3′ of *puhA* (152). Because of the uncertainty of how many genes located 3' of *puhA* might be affected by a polar mutation in *ORF1696*, a different approach was adopted. The Ω cartridge contains translation and *rho*-independent transcription stop signals (109) and has been shown to have a strong polar effect in *R. capsulatus* (148, 152), whereas the KIXX Km^r cartridge rarely has a polar effect (19). To determine the phenotype of a genuinely polar mutation in *ORF1696*, which would reduce expression of all transcriptionally coupled genes located 3' of *ORF1696* , the Ω cartridge was inserted between the *Stu* I sites of the cloned *ORF1696* gene and recombined into the chromosome of the $LHII^-$ strain MW442. This Ω disruption is at the same position as the Km^r disruption of the ΔStu mutant. As shown in Fig. 14B, the ΔStu::Ω strain was found to exhibit a broad region of absorption from 750 to 790 nm. This ΔMun-like absorption spectrum of ΔStu::Ω indicates that insertion of the Km^r cartridge at the *Mun* I site in *ORF1696* exerts a polar effect on expression of downstream genes, whereas the absence of the 750 to 790 nm absorption in ΔStu and ΔNae indicates no polar effects in these strains (see the Discussion section).

Free bchl *a* in acetone solution possesses a light absorption peak maximum at 770 nm (81). Therefore, the possibility was tested that the broad region of absorption exhibited by ΔMun is solely due to bchl *a*,or might include degradation products or biosynthetic intermediates. The absorption spectra of the acetone-extracted bchl

Figure 13. Absorption spectra of intact cells grown under low aeration conditions. Control spectra of *R. capsulatus* strains ΔLHII, ΔNae, ΔStu, and ΔMun containing the vector pRR5C (left column) are compared with the same strains containing the ΔMun peptide expression plasmid, pRR6 (right column).

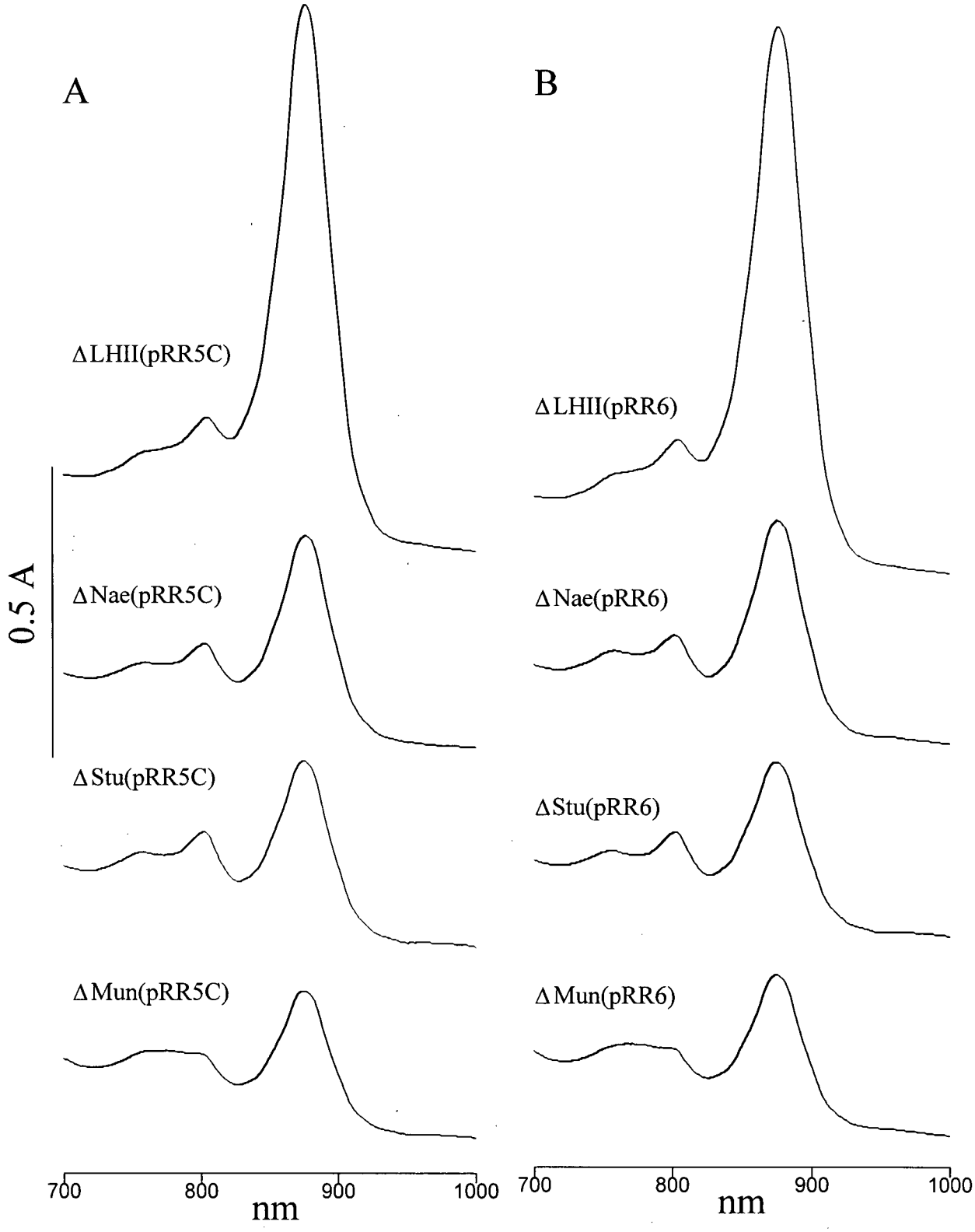
A
B
ΔLHII(pRR5C)
ΔNae(pRR5C)
ΔStu(pRR5C)
ΔMun(pRR5C)
ΔLHII(pRR6)
ΔNae(pRR6)
ΔStu(pRR6)
ΔMun(pRR6)
0.5 A
700
800
900
1000
nm
700
800
900
1000
nm

Figure 14. Absorption spectra of intact cells grown under low aeration conditions. A, Strain ΔMun (green) compared to ΔMun complemented in *trans* with *ORF1696* (pCY42) (black) and *puhA* (pRKPUHA2) (orange) B, Strains ΔMun (green) and ΔStu (blue) compared with ΔStu::Ω (black).

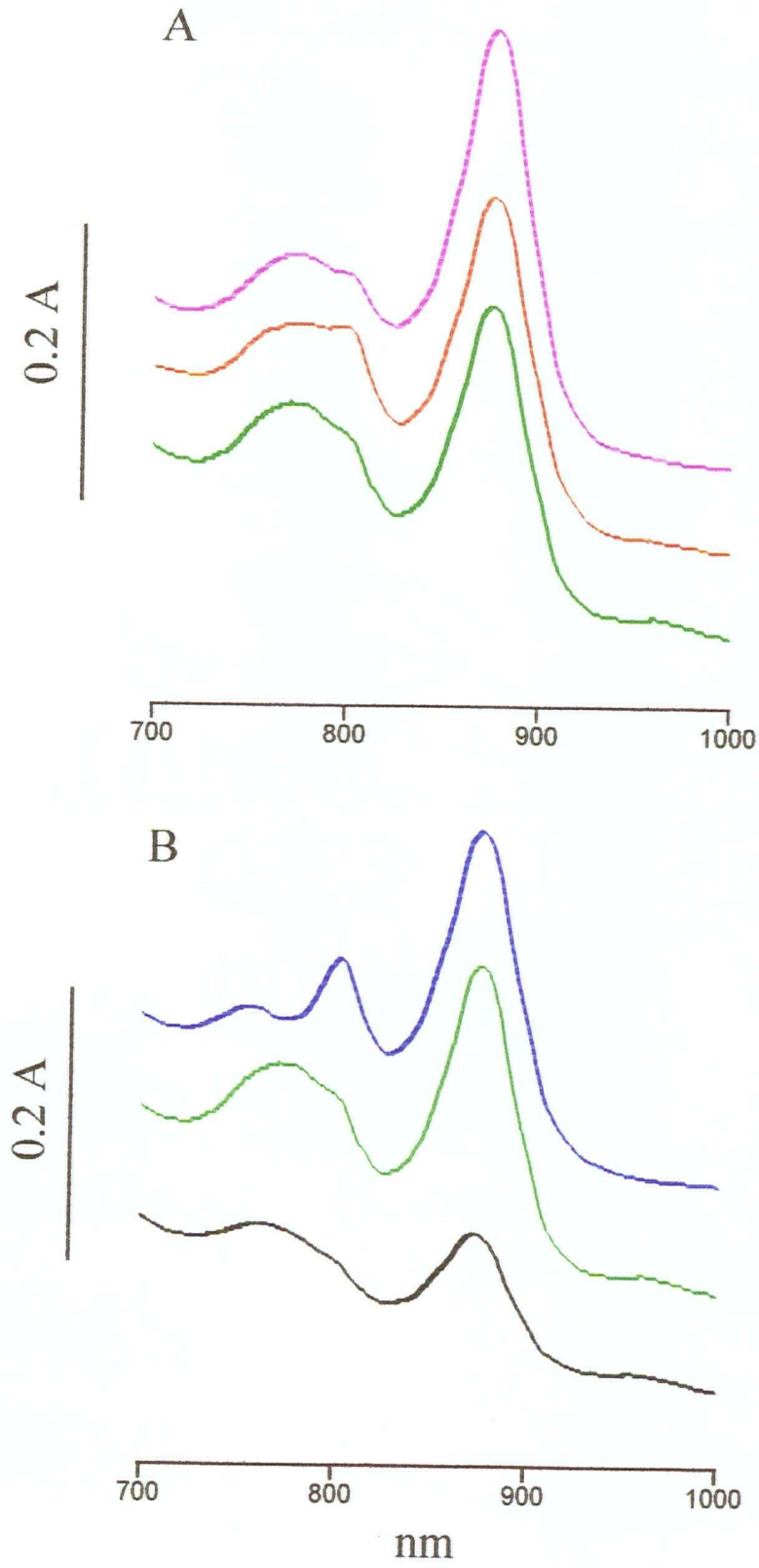
A
0.2 A
700
800
900
1000
B
0.2 A
700
800
900
1000
nm

pigments, shown in Fig. 15, reproducibly exhibited a bchl *a* peak at 770 nm which is superimposable for both ΔMun and ΔLHII. No additional peaks were observed in the ΔMun spectra when compared with the ΔLHII spectra in the 600 to 800 nm wavelength region. Thus, it does not appear that there are any bchl degradation products or biosynthetic intermediates in the ΔMun strain that account for the broad spectral peak observed in the ΔMun absorption spectra. Instead, it seems that the broad, heterogeneous region of absorption in the *in vivo* spectrum of ΔMun is due to bchl *a* that was free or bound incompletely to proteins.

3.1.5 Site-directed mutagenesis of ORF1696 His-152

Amino acid sequence comparisons between the *R. capsulatus* ORF1696 and PucC proteins, and homologues found in other purple non-sulfur bacteria reveal the presence of a conserved amino acid sequence, including an invariant histidine residue at position 152 of the *R. capsulatus* ORF1696, which could participate in binding of bchl (Fig. 16). The sequence Gly/Ala-X-X-X-His is conserved at bchl binding regions and is present in the LHI α and β polypeptides (159, 166). The Gly-X-X-X-His sequence is present in the *R. capsulatus* ORF1696 protein (as well as in the *ORF1696* and *pucC* homologues of other species), where the His residue is invariant as noted above. This motif is also present at the binding site for the accessory bchl molecules in *R. capsulatus* RC L and M polypeptides (Fig. 16), and *R. sphaeroides* and *R. viridis* homologues in which the α-helical nature of this sequence was shown by X-ray crystallography (48, 79). Perhaps this conserved sequence of amino acids in ORF1696 and PucC functions in transient binding of bchl for delivery to LH peptides. If this were an equilibrium-driven process, ORF1696 could remove bchl from the LHI complex in the absence of bchl synthesis, as suggested by the data summarized in Table 5.

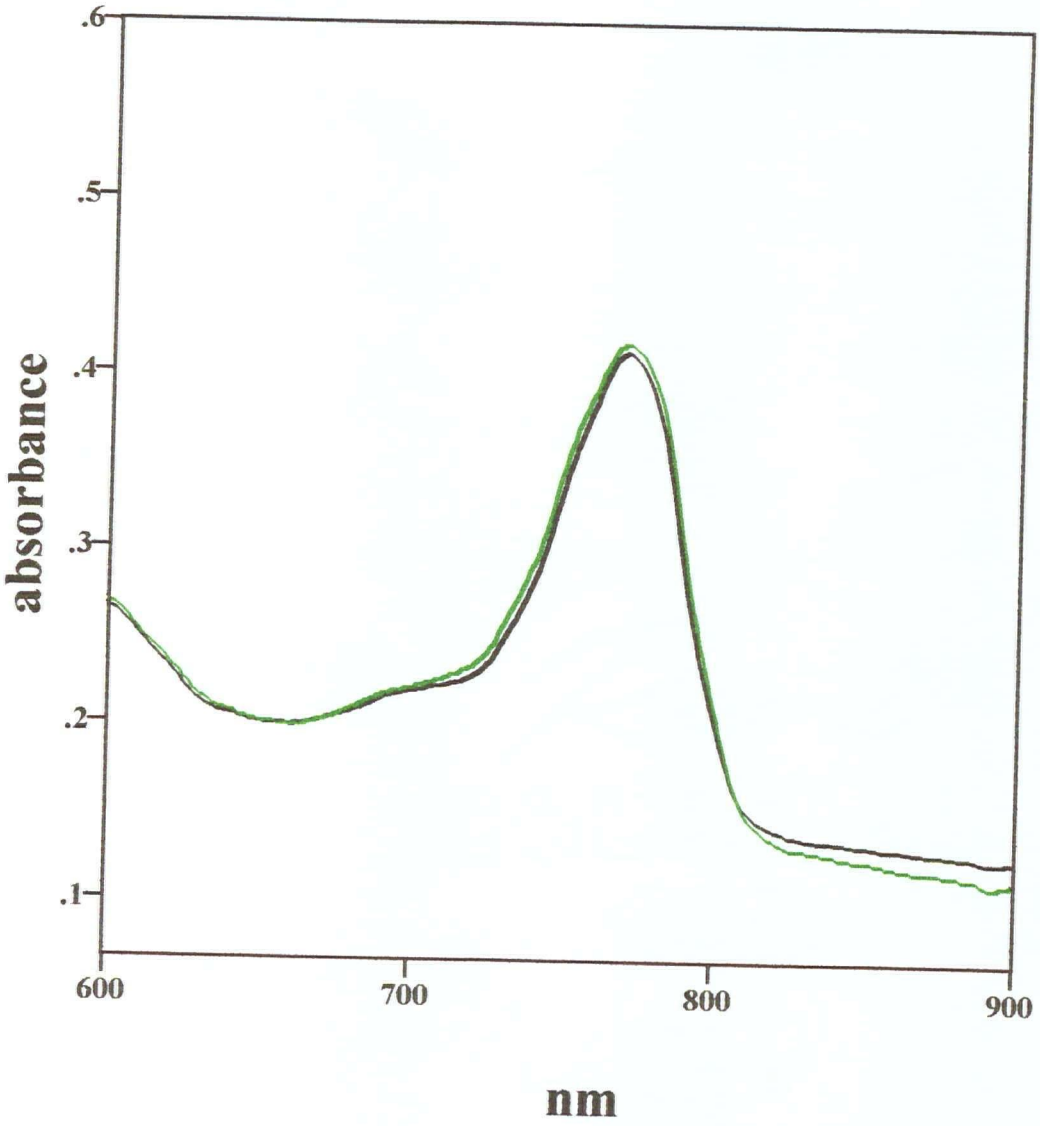

Figure 15. Absorption spectra of bchl pigments extracted in acetone from cells grown under low aeration conditions. ΔLHII is the black trace and ΔMun is the green trace. These experiments were performed in triplicate and the traces above represent average examples.

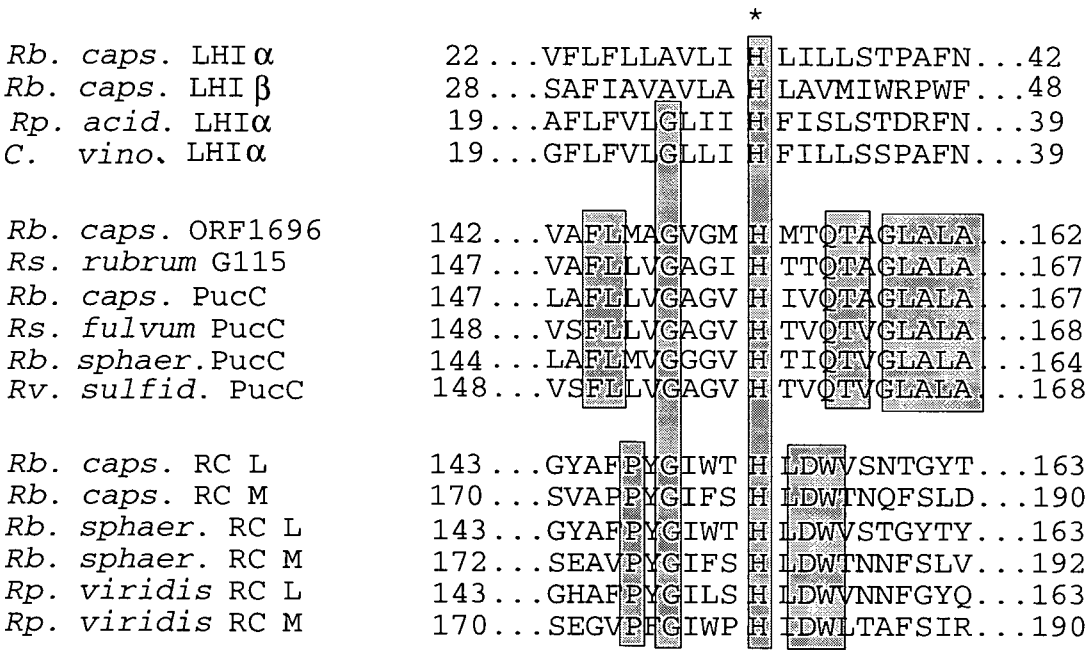

Figure 16. Alignment of amino acid sequences near a conserved histidine found in *R. capsulatus* ORF1696 (accesion no. Z11165) and homologues (accession nos. B61213, P23462, Q02443, U81968), the LHI α and β proteins (accession nos. K01184, P02948, P35092), and the RC L and M proteins (accession nos. B28771, A28771, P02954, P02953, A25102, B25102 (accession nos. are listed in order from top to bottom)). The conserved histidine residue is highlighted with an asterisk. Conserved Gly or Ala amino acids near the histidine residue are boxed. *Rb. caps* = *Rhodobacter capsulatus, Rs.= Rhodospirillum, Rb. sphaer.= Rhodobacter sphaeroides, Rp. acid. = Rhodopseudomonas acidophila, Rp. viridis = Rhodopseudomonas viridis, C. vino. = Chromatium vinosum., Rv. sulfid. = Rhodovulum sulfidophilum* The numbers indicate the position of the residues in the complete amino acid sequence of each protein.

Site-directed mutagenesis of His-152 of ORF1696 was done to investigate whether this amino acid plays an important part in the function of the ORF1696 protein as an LHI complex assembly factor. In particular, I was interested in addressing the question of whether His-152 participates in the transient binding of bchl *a* by the ORF1696 protein and whether this represented an aspect of ORF1696 function. Two amino acids, Phe and Asn, were chosen to replace the His-152 residue. The sidechain of Phe has a six-membered aromatic, planar ring structure while His has a five-membered aromatic ring. However, Phe lacks the N atom that in His is a ligand of the Mg^{2+} ion of bchl *a*. The Asn sidechain is not aromatic but it is planar and similar in size to the His sidechain. Thus, Asn and Phe satisfy some of the structural features of His which makes them reasonable choices for investigating the role of the His-152 residue in bchl binding by site-directed mutagenesis.

The wild type, His-> Phe, and His-> Asn *ORF1696* alleles were subcloned into the broad host range expression plasmid, pJAJ9, downstream of the *puf* promoter (pVYHIS, pVYPHE, and pVYASN, respectively) as described in Materials and Methods and then conjugated into the *R. capsulatus ORF1696* KIXX cartridge disruption strain ΔStu. Spectral analyses of cells grown with low aeration including ΔLHII(pJAJ9), ΔStu(pVYHIS), ΔStu(pVYASN), and ΔStu(pVYPHE) indicated that restoration of LHI complex levels occurs as a result of *trans* expression of the mutant ORF1696 proteins in the ΔStu ORF1696 mutant background (see Fig. 17). Compared to the pseudo-wild type ΔLHII(pJAJ9) strain (which has 100% levels of LHI), ΔStu(pVYASN) was restored to 95%, ΔStu(pVYPHE) was restored to 70%, and ΔStu(pVYHIS) was restored to 73%. The ΔStu(pJAJ9) control strain had only 25% of the LHI levels found in the pseudo-wild type strain. Thus, it appears that the ORF1696 His-152 residue does not play a role in the function of ORF1696 in LHI complex assembly.

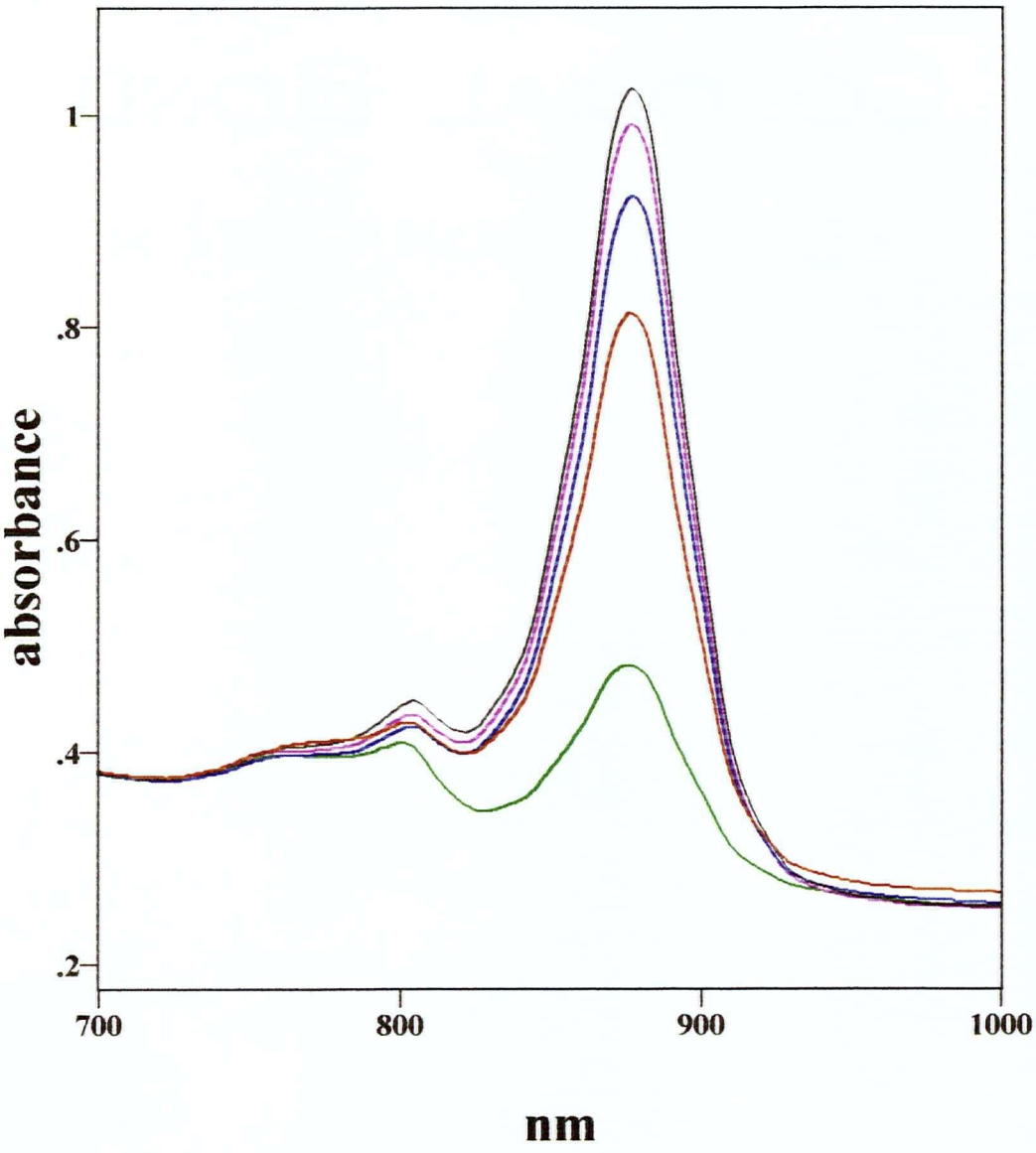

Figure 17. Absorption spectra of intact cells grown under low aeration conditions. The parental strain ΔLHII(pJAJ9) (black) and mutant strain ΔStu(pJAJ9) (green) are compared with strains ΔStu(pVYASN) (violet), ΔStu(pVYPHE) (red), and ΔStu(pVYHIS) (blue).

3.1.6 Chromosomal disruptions of the *ORF428* gene in SB1003, ΔLHII, ΔStu, and ΔMun

ORF428 is a gene located within the *R. capsulatus* photosynthesis gene cluster which shows 24% sequence identity in alignments with *ORF1696* and *pucC* (19), and was considered a possible factor in photocomplex assembly because of this similarity to the latter two genes, which are involved in LH complex assembly. However, a Km^r cartridge disruption of the *ORF428* gene in a wild type background suggested that it plays no role in the assembly of photosystem complexes although this disruption had a polar effect on the expression of *bchP* and *ORF176* genes, such that bchl *a* esterified with geranyl-geraniol (bchl a_{gg}) instead of phytol (bchl a_p) was synthesized (19). It was possible that an *ORF428* mutation might have subtle effects on the formation of the photocomplexes that were not obvious in the wild type background such that the presence of ORF1696 and PucC might compensate for the *ORF428* mutation. This was tested by inserting a Gm^r cartridge at the 14th codon of the *ORF428* gene on the chromosome in the wild type (SB1003), ΔLHII, ΔStu, and ΔMun backgrounds thus creating an *ORF428*::Gm^r single mutation, *ORF428*::Gm^r/*puc*::Ω double mutation, and two *ORF428*::Gm^r/*puc*::Ω/*ORF1696*::Km^r triple mutations.

Absorption spectra of the mutants compared with the parental strains revealed decreases in all of the peaks corresponding to the photosystem complexes (peaks at 800 nm (LHII and RC), 850 nm (LHII), and 875 nm (LHI) (Fig. 18) except for strain SB1003 *ORF428*::Gm^r where there does not appear to be a decrease in LHI (seen as a long wavelength shoulder in the SB1003 spectrum). However, the SB1003 *ORF428*::Gm^r far-red peak is shifted by 3 nm to the red.

Figure 18. Absorption spectra of intact cells grown under low aeration conditions. *ORF428*::Gm^r mutant spectral traces are red and the parental spectral traces are black.

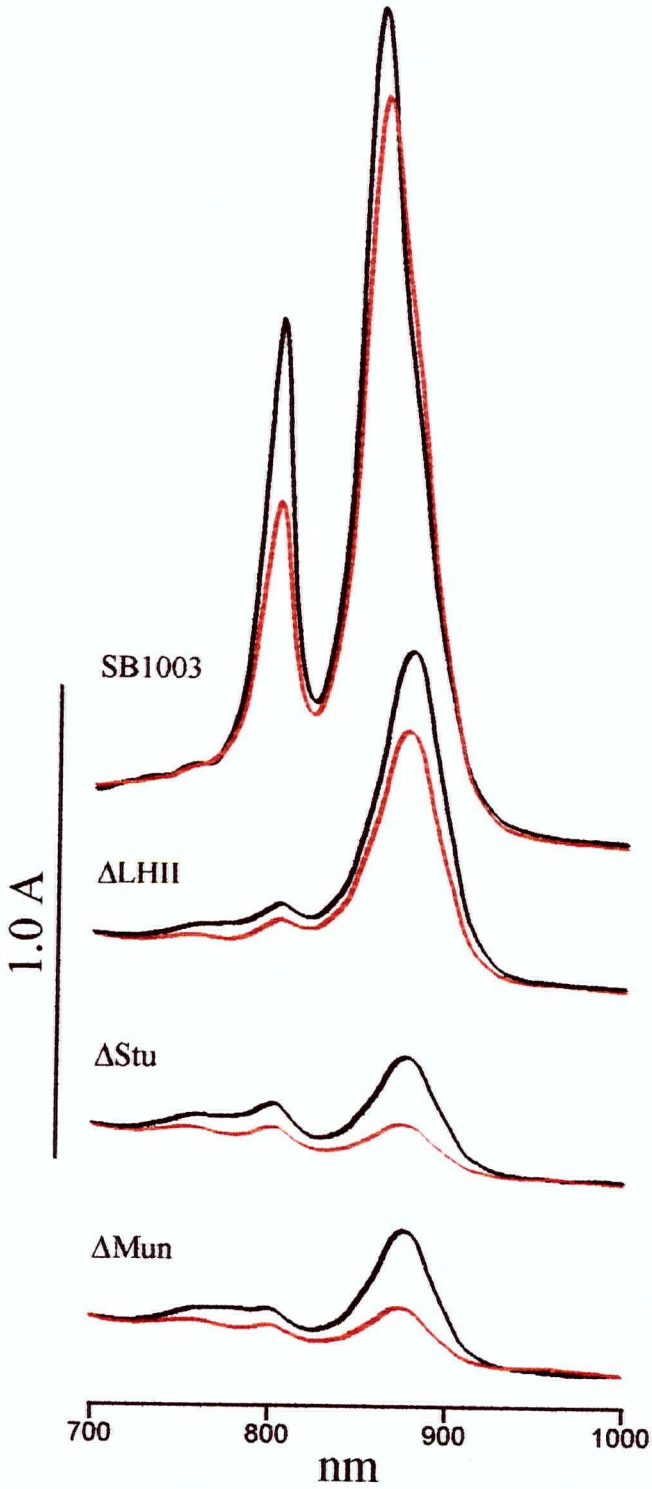
SB1003
ΔLHII
ΔStu
ΔMun
1.0 A
700
800
900
1000
nm

The results shown in Fig. 18 suggest that *ORF428* plays some minor role in maintaining photocomplex levels or that Gm^r cartridge insertions in *ORF428* have a partial polar effect on the expression of *bchP* that results in a mixture of bchl a_p and bchl a_{gg} which results in lower amounts of the RC, LHI, and LHII complexes. A combination of these effects might also be operative. However, it seems unlikely that ORF428 is functionally related to the ORF1696 and PucC proteins since the mutation of *ORF428* resulted in a reduction in the levels of all of the photocomplexes, and the effects of mutations in *ORF1696* and *pucC* have been shown to be specific for one type of LH complex (LHI and LHII, respectively) (this thesis, 10, 83). Bollivar *et al.* (1994) demonstrated by HPLC analysis of bchl extracted from *ORF428*::Km^r mutants that a mixture of bchl molecules esterified with phytol and the less reduced long chain alcohol geranyl-geraniol was present. They suggested that this was due to a partial polar effect of the Km^r cartridge insertion in *ORF428* on the expression of the *bchP* gene which is found directly downstream of *ORF428*. *bchP* was found to encode an enzyme that reduces the geranyl-geraniol covalently attached to bchl to phytol, and thus catalyzes the last step of bchl *a* biosynthesis (19). Nevertheless, it is possible that *ORF428* is required for some subtle photocomplex assembly or stabilization process. It would be interesting to study the *trans* complementation of SB1003 *ORF428*::Gm^r, ΔLHII *ORF428*::Gm^r, ΔStu *ORF428*::Gm^r, and ΔMun *ORF428*::Gm^r with the *ORF428* and *ORF391* genes to evaluate to what extent the phenotypes of these strains result from the disruption of expression of *ORF428* or *ORF391*.

3.1.7 Expression of a *pufQB'*::*lac'Z* translational fusion in ΔLHII and ΔStu

My results demonstrate that Km^r interposon mutations of the *ORF1696* gene in *R. capsulatus* strains ΔNae and ΔStu reduced the amount of the LHI complex, and were complemented in *trans* with a plasmid-borne copy of *ORF1696* (Fig. 11).

Northern blot analysis had earlier demonstrated that a *ORF1696* Km^r disruption mutation had no effect on the levels of *pufBA* (LHI a and b genes, respectively) mRNA, and so the ORF1696 protein should not modulate transcription of the *puf* operon (10). Therefore the possibility was tested that the ORF1696 protein regulates *pufB* gene expression at the level of transcription and/or translation by introducing a plasmid encoding a *pufB'::lac'Z* translational fusion into the strains ΔLHII and ΔStu, driven by the *puf* promoter (plasmid pXCA6::935, (1)). The β-galactosidase activities obtained with ΔLHII(pXCA6::935) were 754 units, and with ΔStu(pXCA6::935) were 677 units, confirming that the ORF1696 protein does not significantly affect transcription and indicating that it does not modulate translation of *puf* mRNA.

3.2 KINETIC ANALYSIS OF LHI COMPLEX ASSEMBLY AND DECAY

3.2.1 Kinetic comparison of LHI complex assembly in ΔLHII and ΔStu

The *trans* complementation studies of *ORF1696* disruptions in the ΔStu and ΔNae strains indicated that the ORF1696 protein is necessary to obtain high levels of the LHI antenna complex (section 3.1.4). In principle, the ORF1696 protein could function to stabilize (eg., protect from proteolysis) the otherwise assembled LHI complex in the ICM, or it could catalyze the assembly of the LHI complex from the α and β polypeptide subunits and pigment molecules. These two possibilities were differentiated by kinetic analyses of LHI complex formation and decay in the ΔLHII and ΔStu strains.

For evaluation of the role of the ORF1696 protein in LHI complex assembly, strains ΔStu and ΔLHII were grown with high aeration to repress expression of the photosynthetic apparatus. These LHI depleted cultures were used as inocula for low aeration cultures in which cells were induced to express photosynthesis genes and

assemble the LHI complex *de novo*. No significant differences in growth rates were detected (see Fig. 19 and Table 4). Thus, any differences in LHI assembly rates between these strains must be attributable to an effect of the *ORF1696* disruption in ΔStu on LHI accumulation.

Figure 19 and 20 illustrate the time course of an experiment comparing the rates of growth and LHI accumulation in cells of ΔStu and ΔLHII over a 5 h period after a shift to low aeration conditions. As summarized in Table 4, LHI accumulated in both strains (see Fig. 20), although more slowly in the ΔStu strain (average LHI accumulation slope of 1.4, see Table 4) as compared to the ΔLHII strain (average slope of 3.7, see Table 4). Comparison of the LHI accumulation in these two strains in three independent experiments revealed a range of 2.2 to 3.4 fold differences, with an average difference of 2.8 fold.

Table 4. Growth rates and LHI complex assembly rates expressed as the slopes taken from LHI assembly graphs for *R. capsulatus* ΔLHII and ΔStu grown under low aeration conditions in RCV medium

Strain	Generation time (h)	Slope of line from LHI assembly graph	Ratio of ΔLHII:ΔStu assembly slopes
ΔLHII	3.3	3.7	3.4
	3.2	3.6	2.8
	2.1	3.8	2.2
Average	2.9 +/- 0.7	3.7 +/- 0.1	2.8 +/- 0.6
ΔStu	3.2	1.1	
	3.5	1.3	
	2.6	1.7	
Average	3.1 +/- 0.5	1.4 +/- 0.3	

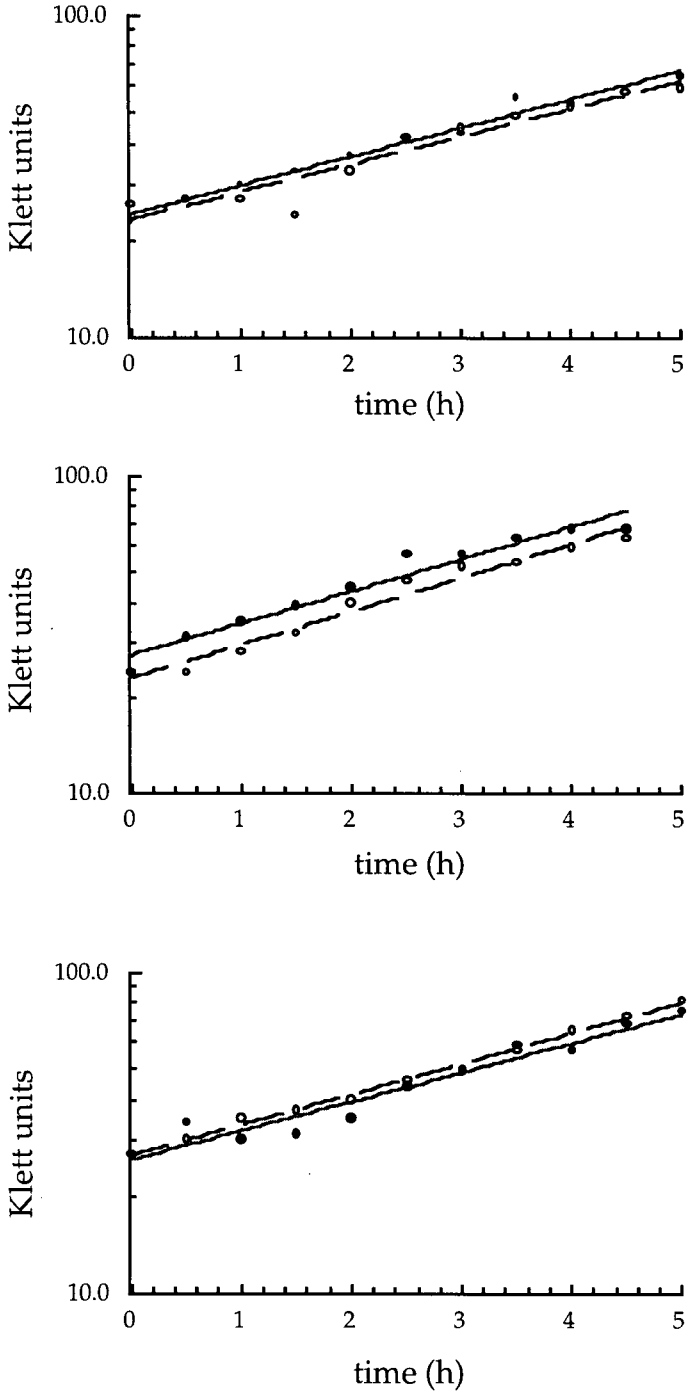

Figure 19. Growth curves for ΔLHII (solid line) and ΔStu (dashed line) over time for three replicate experiments. ΔStu and ΔLHII strains were grown under highly aerated conditions then transferred to growth conditions with reduced aeration to induce LHI synthesis.

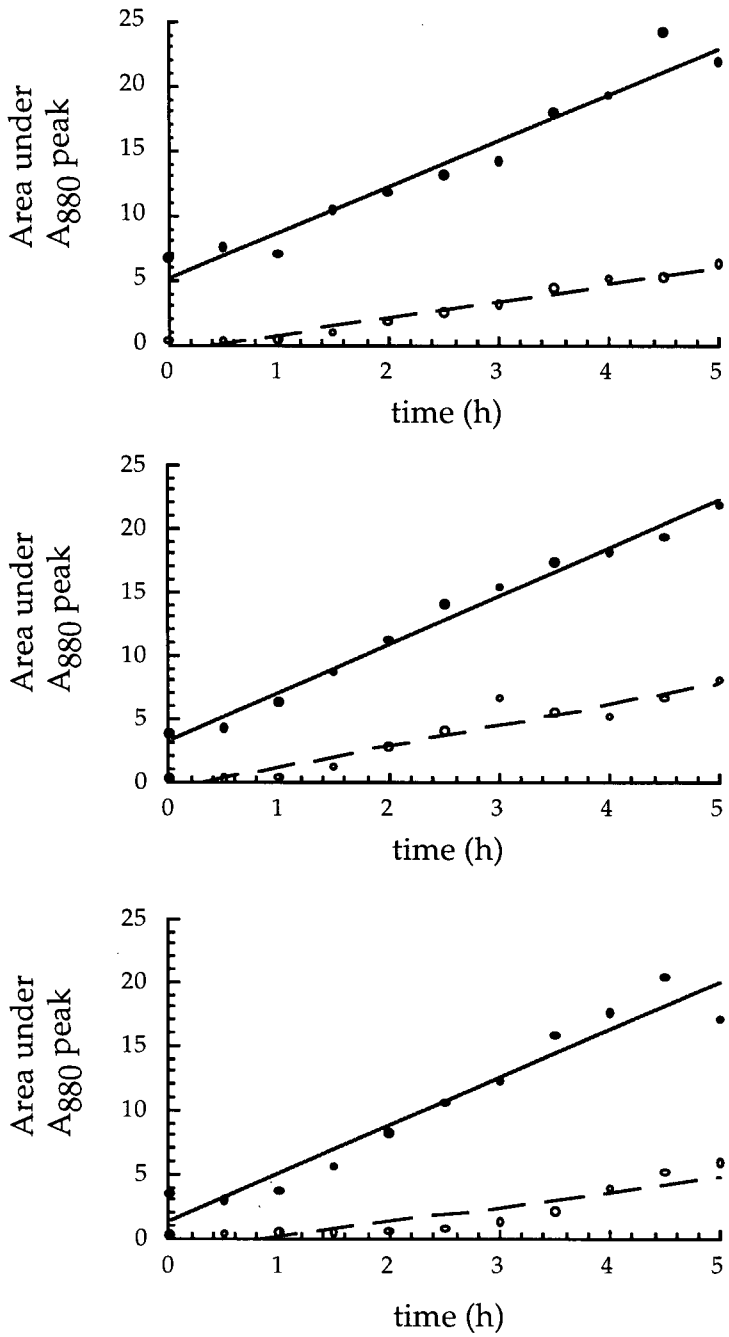

Figure 20. Assembly of LHI complexes in strains ΔLHII (solid line) and ΔStu (dashed line) over time. ΔStu and ΔLHII strains were grown under highly aerated conditions then transferred to growth conditions with reduced aeration to induce LHI synthesis.

3.2.2 Kinetic comparison of LHI complex decay in ΔLHII and ΔStu

The dissimilarity of the rates of accumulation of the LHI complex in the experiments described above (section 3.2.1) could be due to differences in efficiencies of assembly, differences in stability or a combination of these two processes. The logic underlying the LHI decay experiments was that LHI would be formed maximally during anaerobic, photosynthetic growth but would be synthesized at a reduced rate under aerobic growth, and so the rates of decay of 880 nm peak areas would approximate the relative stabilities of the LHI complex in these two strains. Therefore, I compared the rates of decay of the LHI complex in ΔLHII and ΔStu cultures that underwent a shift from anaerobic, photosynthetic to aerobic, respiratory conditions of growth.

The amounts of the LHI complex were determined by absorption spectra measurements of samples removed at intervals after a photosynthetic to aerobic culture shift, and the A_{880} peak area:A_{650} ratios were plotted graphically as a function of time. Figures 21, 22 and 23 show the results of three experiments comparing the growth rates, levels of bchl, and rates of LHI decay in ΔStu and ΔLHII, respectively. Cells of both strains contained reduced amounts of the LHI complex as the fermenter cultures grew aerobically. Surprisingly, the LHI complex was lost more rapidly from the ΔLHII cells compared to the ΔStu cells (see Fig. 23 and Table 5). Since the growth rates of these strains were very similar as shown in Table 5 (average generation times of 3.2 *vs.* 3.4 h for ΔLHII and ΔStu, respectively),

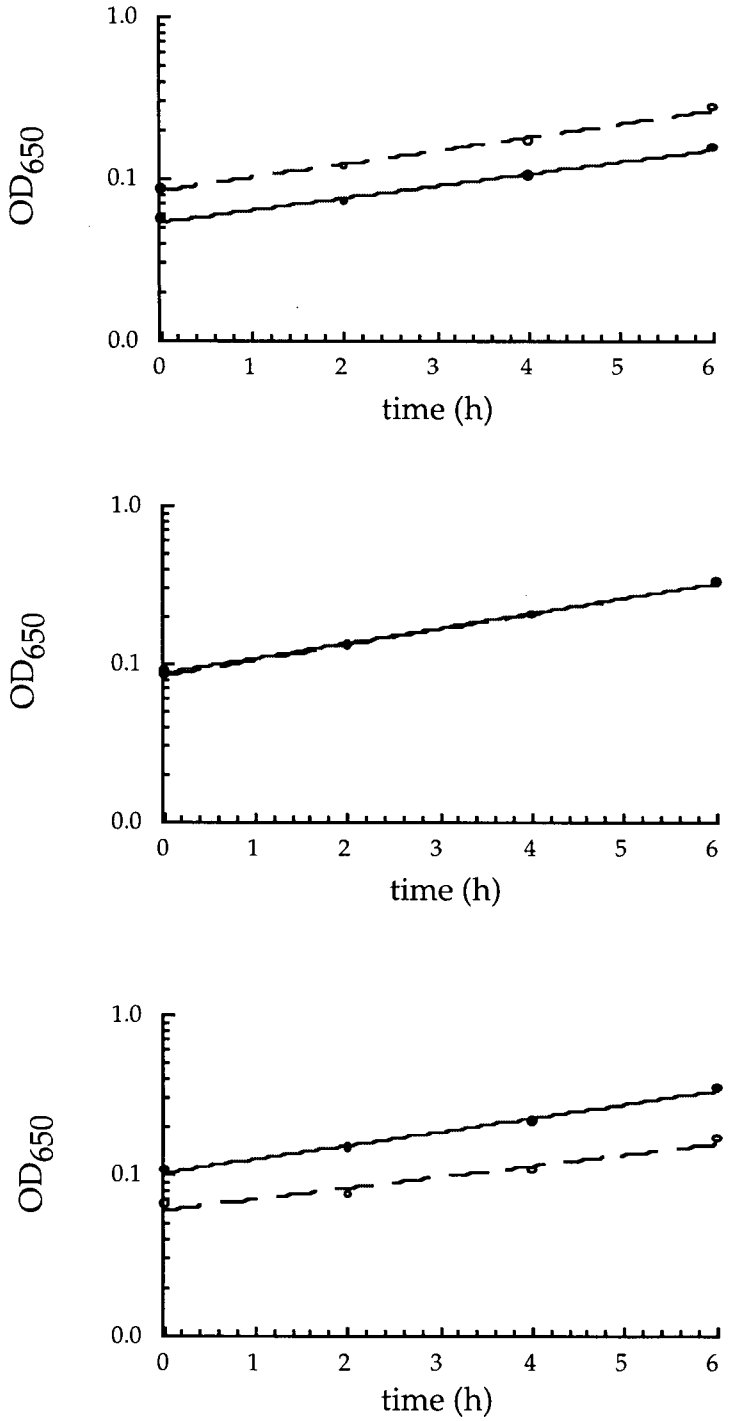

Figure 21. Growth curves for ΔLHII (solid line) and ΔStu (dashed line) over time for three replicate experiments. ΔStu (dashed line) and ΔLHII (solid line) were grown under anaerobic, photosynthetic growth conditions then transferred to highly aerated growth conditions to repress LHI synthesis.

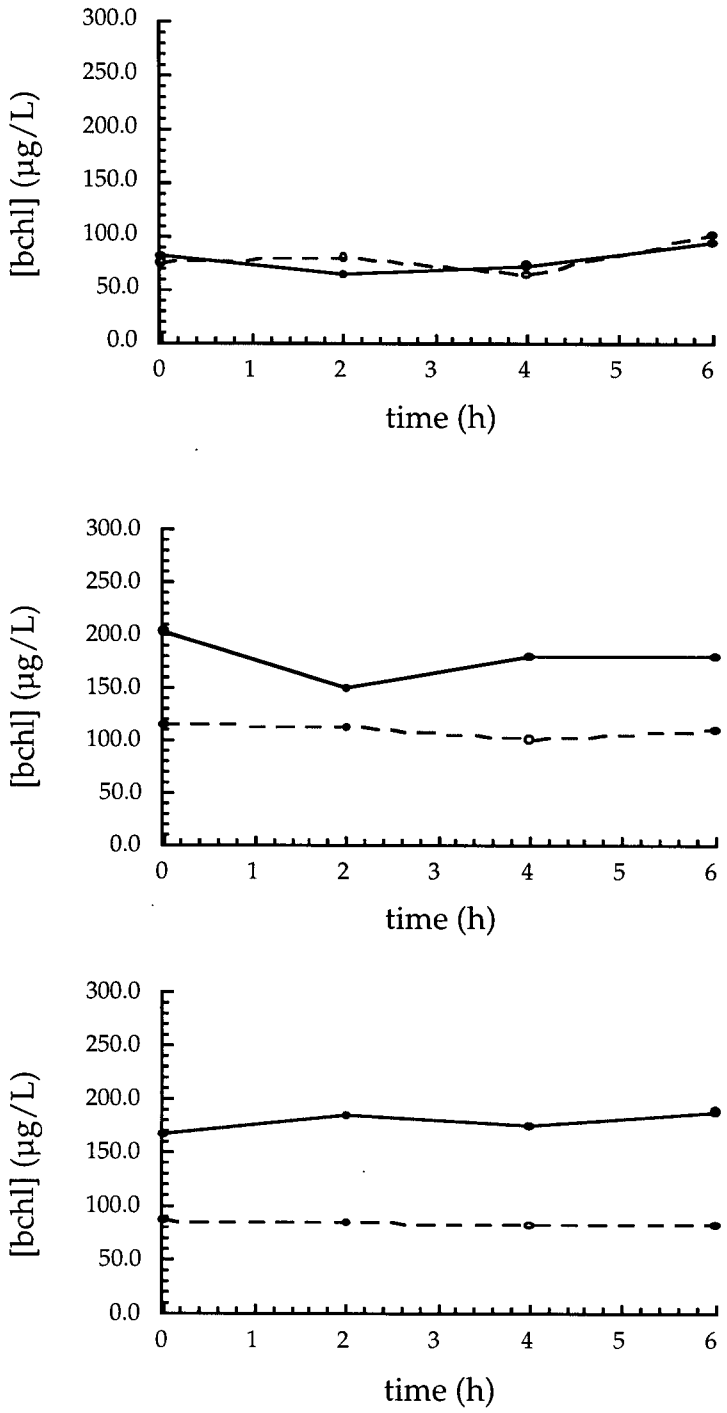

Figure 22. Concentration of bacteriochlorophyll in cultures of strain ΔLHII (solid line) and ΔStu (dashed line) over time. Cultures were grown as described for Fig. 21.

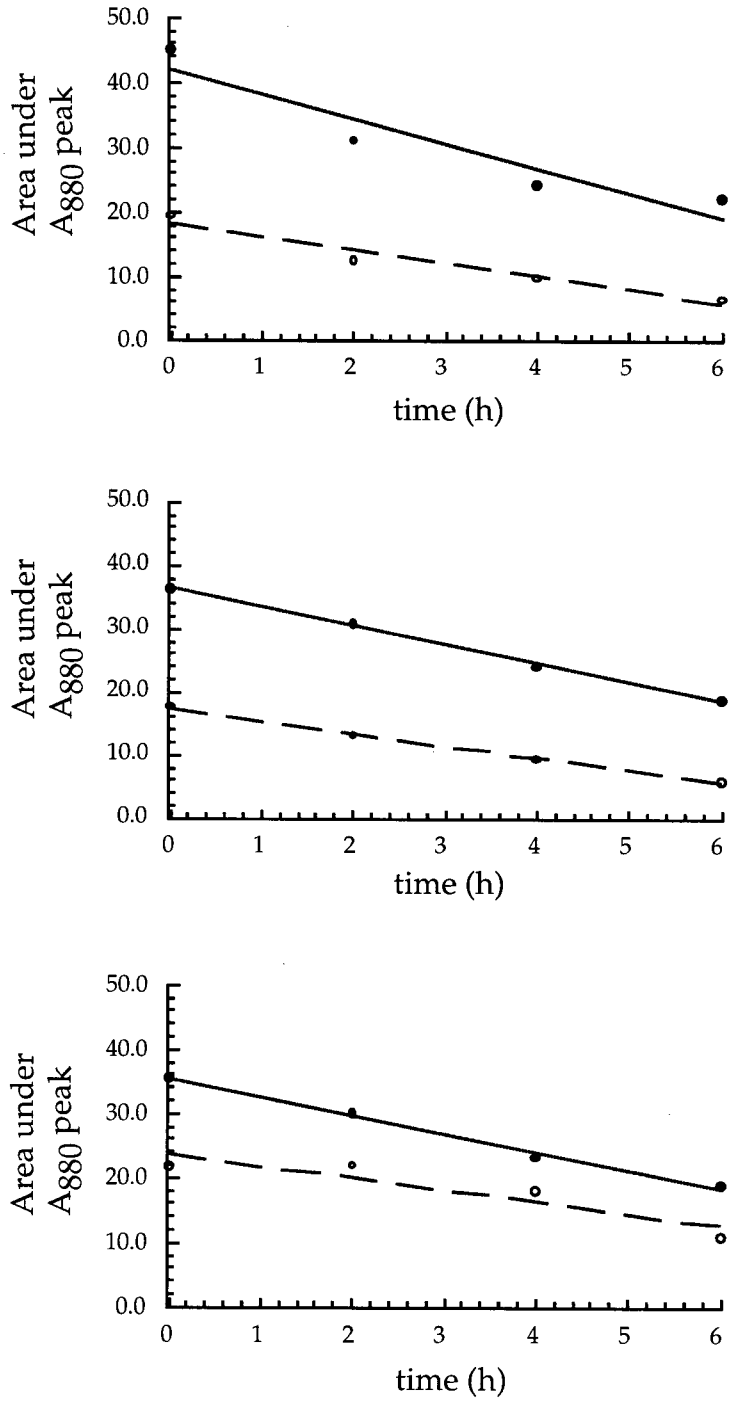

Figure 23. LHI complex decay in ΔLHII (solid line) and ΔStu (dashed line) over time for three replicate experiments. Cultures were grown as described for Figure 21.

the varied rates of LHI decay are due mainly to a difference in LHI stability rather than to a difference in dilution as a result of cell growth and division. Furthermore, the total amount of bchl was relatively constant over the first 6 hours of each experiment for both strains, as shown in Fig. 22. Thus, assembly of LHI complexes should have had little or no influence on the apparent LHI decay rates observed for both strains unless bchl synthesis was equally balanced by degradation. However, since LHI assembly was greater in ΔLHII in the assembly experiments (described above), formation of LHI in the decay experiments would have been greater in the ΔLHII strain than in the ΔStu strain. Table 5 summarizes the results of three experiments, showing that the ratio of the average ΔLHII:ΔStu slopes for LHI decay was 1.7. In contrast, the ΔLHII:ΔStu ratio was 2.8 in the induction experiments (Table 4). Thus, in conclusion, the major role of the ORF1696 protein is in the assembly of the LHI antenna complex in the *R. capsulatus* ICM.

Table 5. Growth rates and LHI decay rates expressed as the slopes taken from LHI decay graphs for ΔLHII and ΔStu grown under low aeration conditions.

Strain	Generation time (h)	Slope of the line from LHI decay graph	Ratio of ΔLHII:ΔStu LHI decay slopes
ΔLHII	3.3	-2.5	1.3
	3.2	-2.6	1.7
	3.0	-3.0	2.0
Average	3.2 +/- 0.2	-2.7 +/- 0.3	1.7 +/- 0.4
ΔStu	3.6	-1.9	
	3.2	-1.5	
	3.5	-1.5	
Average	3.4 +/- 0.2	-1.6 +/- 0.2	

3.3 TOPOLOGICAL ANALYSIS OF THE ORF1696 PROTEIN

3.3.1 Hydropathy and positive inside rule analyses of ORF1696

ORF1696 encodes 477 amino acid residues of which 346 residues have hydrophobic or neutral side-chains, suggesting that it is likely to be an integral membrane protein.

This sequence was subjected to three different topology analyses included as part of the TopPred II 1.1 software package (29), as a preliminary attempt to predict the number and approximate locations of transmembrane segments in the protein (Fig. 24). Green (1990) found that an accurate prediction of transmembrane domains can be made by using a consensus from comparisons of the results of analyses derived from more than one type of hydropathy scale (54), thus, the GES (42), GvH1 (141), and Kyte and Doolittle (77) scales were chosen to evaluate a consensus ORF1696 topology. The GES and GvH1 scales are related in that hydropathy values are assigned to each amino acid on the basis of the free energy of transfer of the amino acid sidechain from aqueous to non-aqueous solvent environments. For both scales, additional consideration is given to the potential of the sidechain groups to form hydrogen bond pairs in α-helices. The GvH1 scale also considers the frequency of the amino acids found in transmembrane segments compared to non-membranous segments in 24 bacterial genuine inner membrane proteins including the *Rhodopseudomonas viridis* reaction center L and M subunits (the topologies of which are known from X-ray crystallography), and thus is perhaps most appropriate for hydropathy predictions with ORF1696. The Kyte and Doolittle scale is based upon the water to vapor transfer free energies of amino acid sidechains along with

Figure 24. Hydropathy analyses of the ORF1696 protein. GES = Goldman, Engelman, and Steitz hydropathy scale, GvH1 = Gunnar von Heijne 1 hydropathy scale, KD = Kyte and Doolittle hydropathy scale. Vertical axes give hydropathy values (positive for hydrophobic regions) and horizontal axes give the amino acid number of ORF1696 residues. Lines marked as "certain" or "putative" indicate default average hydropathy cutoff values used for assigning stretches of amino acids as membrane spanning segments. The line at the bottom of the figure represents the primary amino acid sequence of ORF1696 with positively charged residues symbolized as black dots. The rectangles symbolize predicted membrane spanning segments. Filled and unfilled rectangles are strongly predicted and weakly predicted membrane spanning segments, respectively.

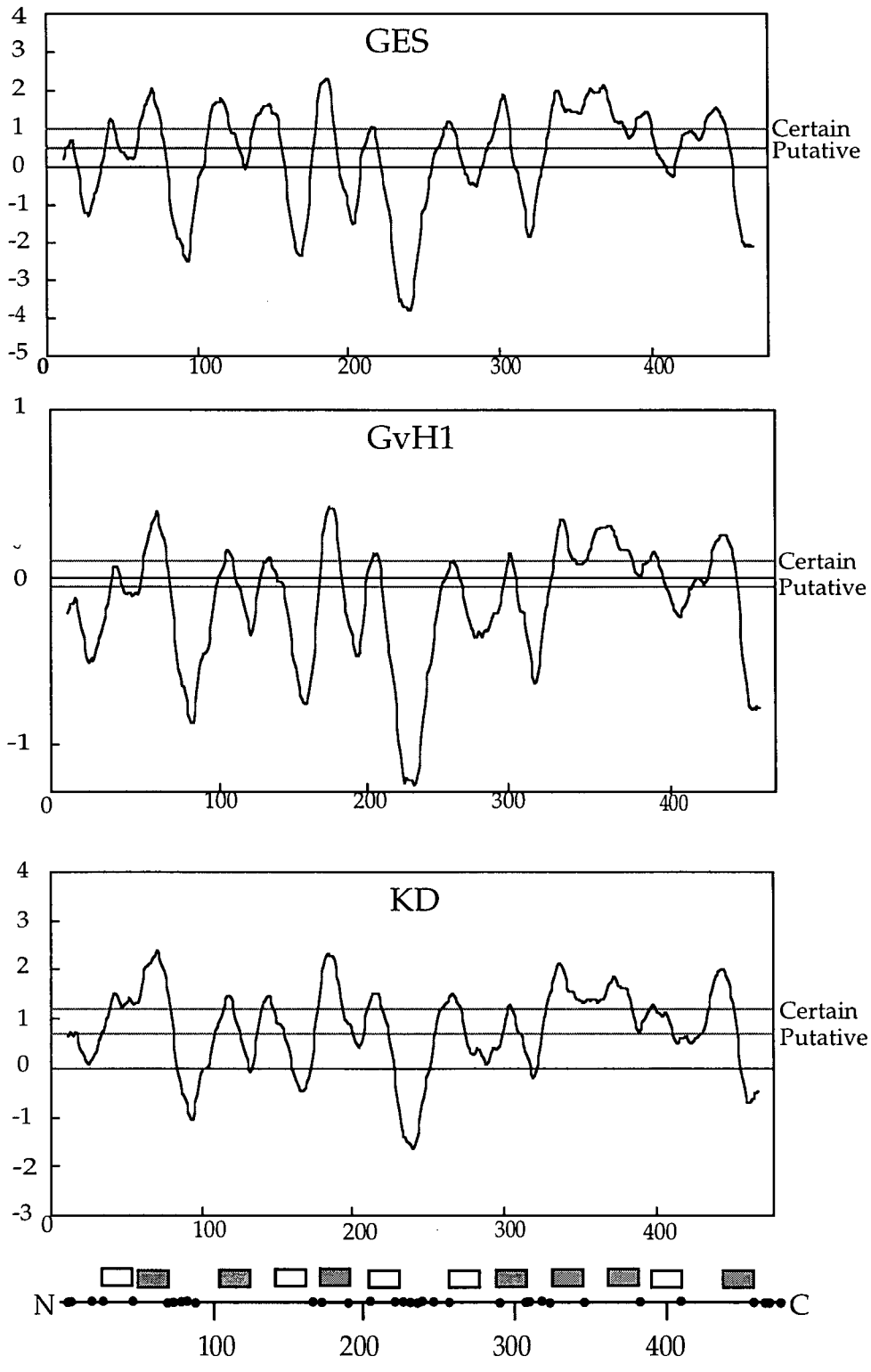
GES
Certain
Putative
GvH1
Certain
Putative
KD
Certain
Putative
N
C
100
200
300
400

their known distribution in the interior and exterior of soluble, globular proteins. These three hydropathy scales were used in TopPred analyses.

As illustrated in Fig. 24, hydropathy plots were generated using the different hydropathy scales applied to the ORF1696 primary amino acid sequence, and the number and locations of predicted membrane-spanning segments were obtained and are listed in Table 6. Twelve transmembrane segments were predicted to occur over nearly the same spans of amino acids by all of the hydropathy scales. Segments #2, #7, #11 and #12 were predicted to contain exactly the same amino acids by all of the scales used, and the rest of the predicted membrane-spanning segments differed by where they begin and end by only one or two residues. The #1, #4, #6, #7 and #11 predicted transmembrane segments were not as strongly indicated on the basis of their average hydropathies compared to predicted transmembrane segments #2, #3, #5, #8, #9, #10, and #12.

In summary of the TopPred analyses, the predictions made using the three different hydropathy scales indicate that the secondary structure of ORF1696 contains 12 transmembrane segments.

In order to construct a two-dimensional topological representation of the ORF1696 protein, the "positive-inside" rule (141) must be considered along with the location of predicted transmembrane domains. The "positive-inside" rule stipulates that positively charged amino acid residues (Arg and Lys) of bacterial inner membrane proteins are generally found to be concentrated in extramembranous domains localized to the cytoplasmic side of the inner membrane. The topological models of the ORF1696 protein generated by the TopPred II 1.1 program included the predicted transmembrane segments made by the hydropathy analyses and selected for the greatest positive charge bias toward the cytoplasmic extramembranous

Table 6. Membrane-spanning segments of the ORF1696 protein predicted by the TopPred II 1.1 program using the GES, GvH1 and Kyte and Doolittle hydropathy scales.

Number of membrane -spanning segment*	ORF1696 amino acid residues predicted to span the membrane bilayer		
	GES	GvH1	KD
1	33-53	33-53	32-52
2	60-80	60-80	60-80
3	106-126	107-127	107-127
4	138-158	134-154	134-154
5	177-197	174-194	173-193
6	207-227	204-224	204-224
7	256-276	256-276	256-276
8	293-313	294-314	294-314
9	329-349	328-348	327-347
10	359-379	359-379	363-383
11	388-408	388-408	388-408
12	433-453	433-453	433-453

*A "putative" membrane-spanning segment was predicted for amino acids 6-26 using the GES and KD hydropathy scales and was not predicted by the GvH1 scale. The membrane-spanning segments listed are predicted as "certain" by the TopPred II 1.1 software.

domains. Some minor adjustments were made to the beginnings and ends of transmembrane segments, for example segment #7 was predicted to contain Arg or Lys residues such that positively charged amino acids reside outside of, or at the interface of the cytoplasmic side of the phospholipid bilayer. In the absence of structural information for the ORF1696 protein, it is difficult to determine whether the positive charges of Arg and Lys sidechains would be cancelled out by neighbouring, negatively charged amino acid sidechains (Glu and Asp) or whether the charged residues would be buried within a protective layer of hydrophobic amino acids traversing the membrane in neighbouring a-helices. These types of

associations would reduce the energy requirements needed to transport positively charged residues into the hydrophobic interior of the phospholipid bilayer. Thus, the ORF1696 topology model presented is conservative. A consensus model was obtained (Fig. 25), which consists of twelve transmembrane domains and twenty out of twenty-six positively charged residues localized in cytoplasmic extramembranous domains. This model was used to identify regions of the ORF1696 protein which would be targets for the construction of *ORF1696'::pho'A* and *ORF1696'::lac'Z* translational in-frame fusions.

3.3.2 Analysis of ORF1696'::Pho'A fusions

Although the prediction of the topology of many bacterial inner membrane proteins by theoretical analyses is a useful tool for generating models (141), the theoretical topology of the ORF1696 protein was tested by the experimental method of construction and evaluation of gene fusions to *ORF1696* (136).

Gene fusions of the *E. coli phoA* gene were constructed by ligating *phoA* alleles, lacking the DNA sequences encoding the signal sequence of AP, with nested 3' deletions of the *ORF1696* gene generated either by using *Bal* 31 nuclease, with *ORF1696* sequences upstream of restriction sites, or by L-PCR. Alkaline phosphatase is active in the periplasm of *E. coli* because it can fold properly by forming two intramolecular disulfide bonds and bind Zn^{2+} ions. AP then dimerizes in the periplasm and becomes protease-resistant (2, 35). In the cytoplasm,

Figure 25. Model of the membrane topology of the ORF1696 protein. Amino acids are given in sequence using single letter code. Positive residues are highlighted by a "+" sign next to them. A phospholipid bilayer is symbolized by the two horizontal lines. Cylinders represent predicted membrane spanning segments. Periplasmically or cytoplasmically localized extramembranous domains are denoted "P" or "C" , respectively. Locations of the fusion joints for key ORF1696'::Pho'A and ORF1696'::Lac'Z fusion proteins are indicated by the amino acid number and a bold line.

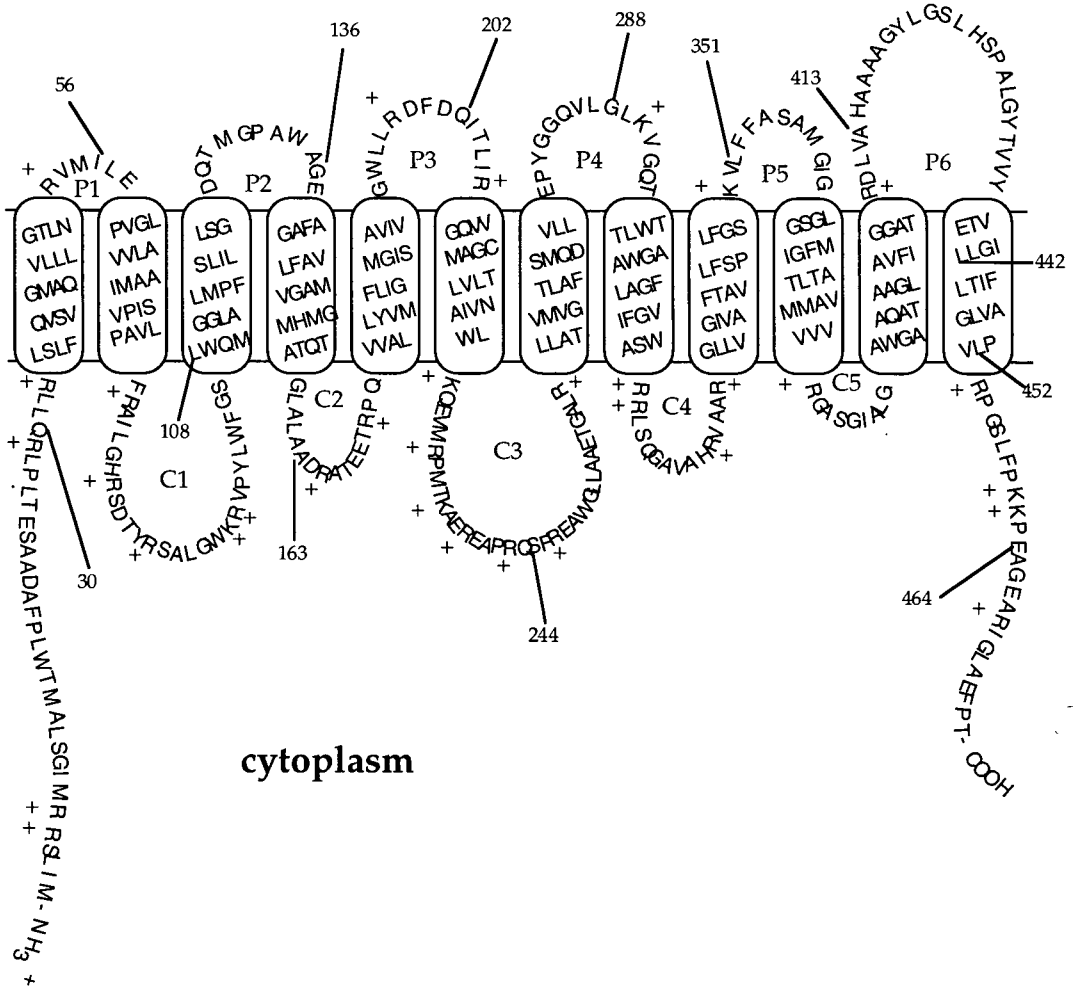
periplasm
cytoplasm
P1
P2
P3
P4
P5
P6
C1
C2
C3
C4
C5
56
136
202
288
351
413
442
452
30
108
163
244
464
NH3
COOH

reducing conditions prevent the formation of the disulfide bonds and alkaline phosphatase is relatively inactive and often degraded when located in this compartment (36). Thus, the logic behind using *phoA* as a gene fusion tool for studying membrane protein topology is that *phoA* fusions to regions of a membrane protein where the AP moiety is periplasmically localized should have relatively high AP activities and those where the AP moiety is localized to the cytoplasm should have low activities.

Previous studies have indicated that anomalous AP activities often arise in PhoA fusions which interrupt membrane spanning segments or which occur N-terminal to positively charged amino acids (Arg or Lys) in cytoplasmic extramembranous loops, both of which are important topological determinants of bacterial inner membrane proteins (20, 136). The interruption of a membrane spanning segment can reduce the efficiency of that segment's ability to act as a transport signal such that the PhoA portion of the fusion protein becomes aberrantly or inefficiently localized to one or the other cellular compartments. PhoA fusions which eliminate positively charged residues in cytoplasmic domains can result in anomolously high AP activities since these residues help anchor the cytoplasmic domains of bacterial membrane proteins (141).

Table 7 summarizes the *ORF1696'::pho'A* translational in-frame fusions in terms of the location of the fusion joint and the AP activities measured in *E. coli* cells. AP activity values of greater than 30 units were considered high, activities between 30 and 15 units were considered intermediate, and activities below 15 units were considered low. The AP activities measured range from a high value of 94.2 units for the N15-3 fusion (predicted to be periplasmic) to a low value of 0.7 units measured for the Hin1.0 fusion (predicted to be cytoplasmic). AP activities of theoretically predicted periplasmically located fusions were between 130-fold to approximately 3-fold higher than PhoA fusions to predicted cytoplasmically

localized domains of ORF1696, except for the AP activities of fusions in the P6 predicted periplasmic domain (amino acid # 410 to 435) compared to the C-terminal domain (amino acid # 454 to 477) fusions. ORF1696'::Pho'A fusions in these regions were found to have low or intermediate AP activities. Outside of this region there is a good correlation between the pattern of high and low AP activities and whether

Table 7. AP activities of*ORF1696'::pho'A* gene fusions.

ORF1696'::pho'A fusion	Position of fusion joint (number of amino acids from ORF1696 N-terminus)	AP activity (units)	Standard deviation
Nae1.5	464	20.0	1.3
N10-2	452	18.9	2.2
N10-1	442	9.1	0.8
N5-1	413	11.3	0.9
N20-1	367	78.1	5.1
N15-1	360	56.3	5.7
N15-3	351	94.2	1.8
N25-5	347	79.5	9.8
N30-1	344	79.5	5.6
N15-2	300	61.3	1.6
N20-4	293	55.9	1.0
N25-1	288	52.2	6.8
X3-5	275	22.8	0.6
Hin1.0	244	0.7	0.1
X20-2	214	3.0	0.1
B25-1	202	37.1	9.6
Bs2-2	163	3.5	0.0
B15-4	136	43.6	5.6
B20-2	129	20.5	3.3
B15-3	128	11.5	4.3
B20-1	126	35.5	0.2
Bs5-2	108	2.4	0.1
pCY165	56	35.3	0.8
Mun0.2	30	56.5	1.3

the PhoA moiety is predicted to be transported across the membrane as part of a periplasmic domain or whether it is predicted to be inactive in the cytoplasm, respectively (compare fusions Bs5-2, Bs2-2, and Hin1.0 with fusions CY165, B15-4, B25-2, and N25-2 in Table 7 and Fig. 25). This observation is based on the AP activities measured for ORF1696'::Pho'A fusions which occur outside of predicted transmembrane segments and in which the fusion joint is located C-terminally within a predicted extramembranous domain.

3.3.3 Stability of the ORF1696'::Pho'A fusion proteins

It has been proposed that Pho'A fusions to membrane proteins may yield AP activities that differ from one another because different amounts of PhoA are translated from the heterologous segment of the fusion mRNA, as opposed to the PhoA protein segment being located periplasmically or cytoplasmically (116). To evaluate the rates of synthesis of the ORF1696 moieties of the ORF1696'::Pho'A fusions in *E. coli*, I used ^{35}S-methionine pulse labeling to normalize the raw AP activities (see Table 7 for raw AP activities) (116).

A subset of the ORF1696'::Pho'A fusions was labelled with ^{35}S-methionine during a 2 min pulse, as described in Materials and Methods. The radiolabeled proteins were immunoprecipitated using an anti-AP rabbit polyclonal antibody preparation, separated by SDS-PAGE and the gels were exposed to a phosphor screen (Fig. 26). No full-length fusion proteins (based on predicted molecular masses) were seen using this technique, although protein bands corresponding to approximately 47 kDa and 40 kDa (see arrows pointing to these bands in Fig. 26) were present in each lane of samples from the different fusion strains. The 47 kDa protein is the

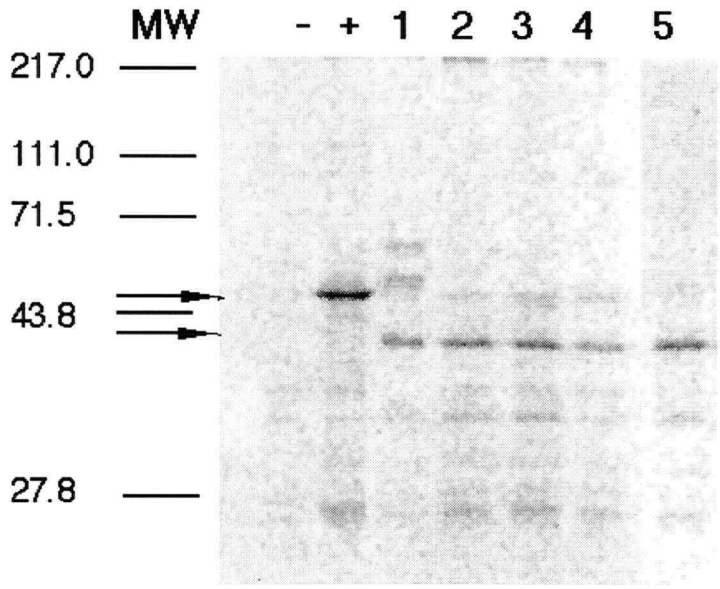

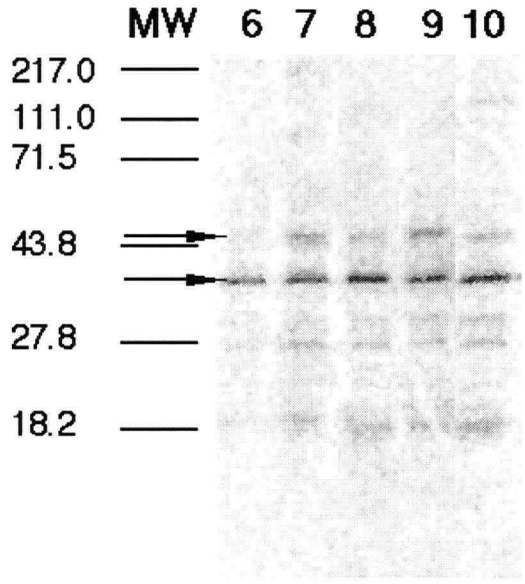

Figure 26. ^{35}S-methionine labeled ORF1696'::Pho'A fusion proteins isolated from *E. coli* CC118 observed after a two minute pulse.; Arrows point to common 47 kDa and 40 kDa degradation products present in each lane. MW = molecular mass in kilodaltons (kDa), "-" = *E. coli* CC118 (negative control), "+" = *E. coli* CC149 (positive control), 1 = Mun0.2, 2 = N15-3, 3 = N10-1, 4 = N25-2, 5 = N5-1, 6 = Bs2-2, 7 = Nae1.5, 8 = B25-2, 9 =Hin1.0, 10 = Bs5-2. This figure was made using the Adobe Photoshop software program.

same size as the AP band observed in the CC149 positive control lane (Fig. 26, lane "+"). The 40 kDa band does not appear in the negative or positive control lanes (Fig. 26, lanes "-" and "+", respectively) and is thus unique to the strains expected to produce ORF1696'::Pho'A fusion proteins. The inability to observe full-length fusion proteins indicates that ORF1696'::Pho'A hybrid proteins are unstable in *E. coli* CC118. Proteolytic cleavage of the fusion proteins at the fusion junction would yield a PhoA protein with a deduced molecular mass of approximately 50 kDa (25). The 47 kDa and 40 kDa bands are most likely PhoA remnant proteolytic degradation products of the full-length fusion proteins, and so the intensities of these bands were used to normalize the raw AP activities obtained for each pulse-labeled ORF1696'::Pho'A fusion strain (Table 8), employing the following equation, according to the method of Boyd *et al.* (20):

Table 8. AP activities for ORF1696'::Pho'A fusion proteins normalized to the rate of synthesis as determined by ^{35}S-methionine pulse-labeling experiments

ORF1696'::Pho'A fusion	Raw AP activity (units)	Raw AP activity (%)	Normalized AP activity (%)*
Mun 0.2	56.5	60.0	77.8
Bs5-2	2.4	2.5	1.0
B15-4	43.6	46.3	17.6
Bs2-2	3.5	3.7	2.6
B25-1	37.1	39.4	21.0
Hin1.0	0.7	0.7	0.6
N25-1	52.2	55.4	54.2
N15-3	94.2	100.0	100
N5-1	11.3	12.0	9.0
N10-1	9.1	9.7	22.0
Nae1.5	20.0	21.2	21.4

*% of normalized AP activity per pixel # for fusion N15-3. Values are averaged from two or three experiments.

AP Activity (units)/0.01 x $V_{(t)}$ x Specific Activity$_{(N15-3)}$ (units/pixel #) = Normalized activity (%)

where $V_{(t)}$ is the total sum pixel # of the 47 kDa and 40 kDa protein bands.

The normalized AP activities for each fusion reveal a similar trend when compared to the raw AP activities in Table 8 with some changes. Fusions B25-1 and B15-4 have lower AP activities when normalized for the rate of synthesis of the fusion proteins than was indicated by the raw AP activity. B25-1 and B15-4 were predicted to be periplasmic, and so the AP moiety must be poorly transported across the membrane for this fusion protein. Fusion N10-1 exhibited a higher normalized AP activity than was indicated by the raw AP activities, indicating that the AP moiety is more efficiently transported to the periplasm than would appear to be the case if the raw AP activity was considered alone. The N10-1 fusion joint was predicted to occur near the C-terminal end of the P6 periplasmic loop region, such that an ORF1696'::Pho'A fusion would be expected to have a high AP activity (Fig. 25). The N10-1 fusion protein appears to be synthesized at a low rate such that the low or intermediate AP activity value is only partly due to poor transport of the AP portion across the membrane to the periplasm. Fusion proteins B25-1 and B15-4 were synthesized relatively rapidly and thus yielded higher raw AP activities due to the presence of larger amounts of hybrid protein in the cells compared to other ORF1696'::Pho'A fusion proteins.

In summary, the pulse-labeling studies indicated that the rate of ORF1696'::Pho'A fusion protein synthesis varies. These experiments suggest that the topology model presented is valid, since the pattern of high *vs.* low normalized AP activities generally support the predictions made by the model, with the assumption that two of the fusion proteins yielded anomalous AP activities (B15-4 and B25-1).

Western blot analysis of PhoA fusion proteins can be done to assess fusion protein steady state levels by visualization of full-length PhoA fusion proteins (84), but the use of such studies do not give reliable measurements of PhoA fusion protein amounts for normalizing AP activity (116), since cytoplasmically located fusions are sometimes unstable; they cannot fold properly and the PhoA segments are degraded rapidly (116). The hybrid proteins detected on immunoblots often represent the fraction of the hybrid protein synthesized that is transported into the periplasm and become more stable due to proper folding. Because no full-length ORF1696'::Pho'A fusion proteins were visible on the phosphorimages of ^{35}S-methionine pulse labeled proteins from fusion strains, Western blot analysis of ORF1696'::Pho'A fusions was done to assess the stability of the fusion proteins transported to the periplasmic space.

A Western blot analysis of a subset of the ORF1696'::Pho'A fusion proteins is shown in Fig. 27. Several faint bands correlated well with the theoretical molecular masses of hybrid proteins and likely represent the full-length fusion proteins of Nae1.5, N10-1, N15-3, N25-2 and Mun0.2 (lanes 1-4 and 10, Fig. 27). It is possible that other fusion proteins are present on the blot but are obscured by degradation or aggregation products. Aggregation seemed to occur with fusions B25-1, Bs2-2, B15-4, Bs5-2, and Mun0.2, since there were bands of greater size than predicted by the fusion site. Fusion proteins predicted to have PhoA domains localized in the

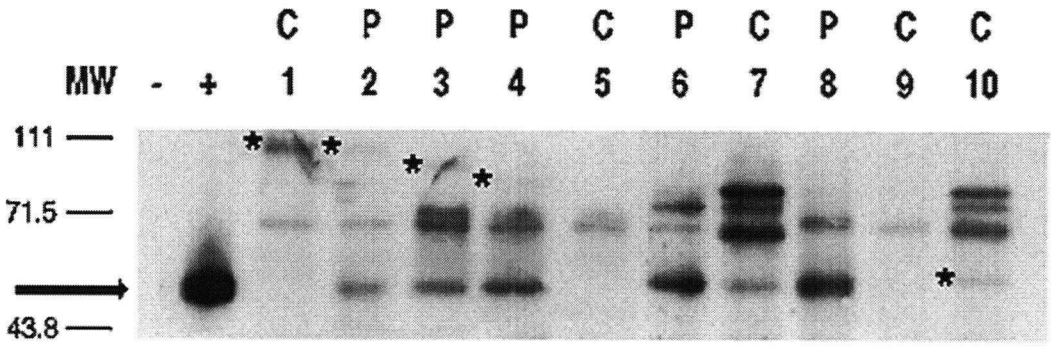

Figure 27. Western blot of ORF1696'::Pho'A fusion proteins in *E. coli* CC118. "C" and "P" above the lanes indicate the predicted cytoplasmic or periplasmic localization of the Pho'A moiety. Molecular masses (MW) are indicated in kDa. The arrow marks the position of the PhoA protein and stars (*) highlight bands having molecular masses similar to those predicted for the full-length fusion proteins. - = *E. coli* CC118, + = *E. coli* CC149, 1 = Nae1.5, 2 = N10-1, 3 = N15-3, 4 = N25-2, 5 = Hin1.0, 6 = B25-1, 7 = Bs2-2, 8 = B15-4, 9 = Bs5-2, 10 = Mun0.2.

periplasm show larger amounts of a presumed free PhoA degradation product (bands indicated by the arrow in Fig. 27 at about 47 kDa) than most of the cytoplasmic fusions (compare "P" lanes to "C" lanes in Fig. 27). This is probably due to the proper folding of AP in the periplasm making it more resistant to proteolytic degradation compared to AP in the cytoplasm where it remains in a proteolytically sensitive, loose conformation. Based on the intensity of the PhoA band (at 47 kDa) in each lane of the Western blot in Fig. 27, the amounts of the fusion proteins tested are consistent with the predicted periplasmic or cytoplasmic location, and thus the Western blot results support the predictions of the theoretical topology model.

3.3.4 Analysis of ORF1696'::Lac'Z fusions

The evaluation of the predicted ORF1696 topology by PhoA fusion analysis generally supported the model predicted by hydropathy analysis (with the exceptions of fusions B15-4 and Nae1.5), and so I investigated the model further by an alternative method. Fusion switching (89) was carried out to generate a set of data utilizing β-galactosidase (β-gal) activity measured for *ORF1696'::lac'Z* fusions located at the same positions along the ORF1696 amino acid sequence as the *ORF1696::pho'A* fusions. Since β-gal fusions are normally active only when joined to a cytoplasmic domain, fusions located at cytoplasmic regions will have relatively high activities compared to fusions located at periplasmic segments. This is because, when fused to a protein export signal, β-gal does not efficiently traverse the cytoplasmic membrane and is rendered enzymatically inactive (136). The *lacZ* allele of plasmid pSP72::*lacZ* (84) was substituted in place of the *pho'A* sequence in *ORF1696'::pho'A* fusion plasmids. ORF1696'::Lac'Z fusion activities are listed in Table 9 alongside the corresponding ORF1696'::Pho'A fusion raw and corrected activities. The β-gal activities were generally low for the predicted periplasmic fusions and relatively high for predicted cytoplasmically located fusions. This pattern is opposite to the AP

activity data and therefore generally supportive of the structural predictions made by the topology model for ORF1696 domain localization.

The pattern of AP and β-gal fusion activity along the primary amino acid sequence of ORF1696 is illustrated more clearly as a graph in Fig. 28. The β-gal fusions near the C-terminus exhibited activities which were high and were not consistent with the predicted fixed periplasmic location of domain P6 (Fig. 25). However, the ORF1696'::Lac'Z fusion at the N10-2 site (Table 9) was determined to have the highest β-gal activity of all the LacZ fusions constructed, arguing for a cytoplasmic localization of the C-terminus of ORF1696.

Table 9. β-galactosidase activity of ORF1696'::Lac'Z fusions.

Fusion joint	Position of fusion joint (# of amino acids from ORF1696 N-terminus)	Raw AP activity (units)	Corrected AP activity (%)	β-gal activity (Miller units)
CY165	56	35.0	ND	1.4
Bs5-2	108	2.4	0.6	12.4
B15-4	136	43.6	6.6	0.7
Bs2-2	163	3.5	2.6	17.0
B25-1	202	37.1	23.2	0.3
N25-1	288	52.2	38.3	0.7
N15-3	351	94.2	100.0	1.9
N5-1	413	11.3	10.6	15.8
N10-1	442	9.1	47.9	9.4
N10-2	452	18.9	ND	34.2

ND = not determined

3.3.5 Conclusions

The ORF1696 topology model presented in Fig. 25 is consistent with the results of the hydropathy analyses, application of the 'positive-inside' rule, and the

Figure 28. Histogram of alkaline phosphatase (AP) and β-galactosidase (β-gal) activities measured for ORF1696'::Pho'A and ORF1696'::Lac'Z fusions. The line at the top of the figure represents the primary amino acid sequence of ORF1696 with positive amino acid residues (Arg and Lys) highlighted using black dots. The amino acid number is given below the line. The rectangles above the line represent predicted membrane spanning segments. The shaded and unshaded rectangles represent transmembrane segments which are strongly and weakly indicated by the hydropathy analyses, respectively, based on their average hydropathies. The location of the fusion activity bars in the histogram correspond with their location along the ORF1696 amino acid sequence shown at the top.

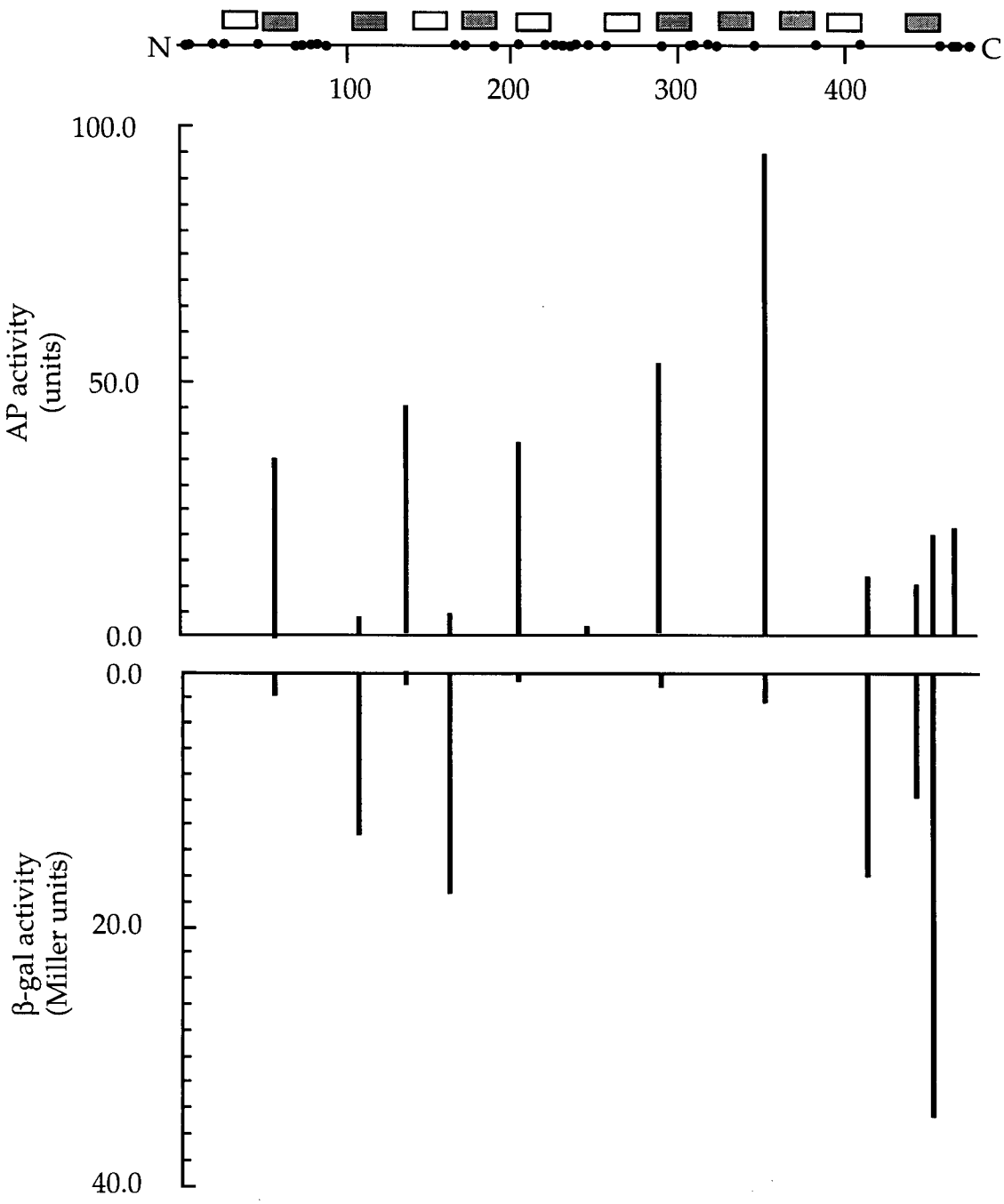
N
C
100
200
300
400
100.0
50.0
0.0
AP activity
(units)
0.0
20.0
40.0
β-gal activity
(Miller units)

AP and β-gal activities measured for ORF1696' fusion proteins. Apparently anomalous AP activities measured for fusions Mun0.2 and N10-1 were partially resolved by normalizing the raw AP activities to the rates of synthesis of the proteins by ^{35}S-methionine pulse labeling. The results of these pulse labeling experiments suggested a greater proportion of cytoplasmic localization of the AP moiety for the Mun0.2 fusion located near the end of the N-terminal domain of ORF1696 and, conversely, of periplasmic localization for the N10-1 fusion located near the end of the P6 domain. Normalization of the AP activity data indicated anomalous behaviour of fusions B15-4 and Nae1.5, suggesting that B15-4 is not transported efficiently to the periplasm despite the location of the fusion within the predicted P2 domain, whereas the Nae1.5 fusion appears to transport the AP moiety to the periplasm despite its location after three positive amino acid residues of the C-terminal domain. However, the B15-4 LacZ fusion exhibited a very low activity while Western blots indicated that a large amount of the B15-4 PhoA fusion protein was present in the periplasm of *E. coli* cells. These results suggest a periplasmic location for the B15-4 fusion in spite of the low AP fusion activity. It is more difficult to explain the apparent Nae1.5 AP fusion anomaly, although it seems likely this fusion would be cytoplasmically located based on the positive amino acid residues present in the C-terminus and the very high β-Gal activity measured for the preceding fusion, N10-2, which suggests that N10-2 is localized to the cytoplasm. It is possible that the C-terminal 13 amino acid residues of ORF1696 are required to stably maintain the C-terminus in the cytoplasm.

Attempts to obtain PhoA fusions in two of the predicted cytoplasmic loop domains (C4 and C5, Fig. 25), located in the C-terminal half of the ORF1696 protein were unsuccessful (data not shown). However, it is likely that the C4 domain resides in the cytoplasm in accordance with the 'positive inside' rule (141), since it contains four Arg residues as opposed to the one positive residue present in each of

the flanking predicted periplasmic loops (loops P4 and P5), consistent with the finding that the predicted membrane spanning segments flanking C4 are strongly indicated by different hydropathy algorithms (Fig. 24). PhoA fusion activities for P4 and P5 domains were quite high whereas LacZ fusion activities were low, confirming their periplasmic localization; this topological arrangement indicates a cytoplasmic location for the C4 domain. In agreement with this idea, the C5 domain is preceded N-terminally by a strongly predicted membrane spanning segment (Figs. 24 and 25) and the strongly indicated periplasmic domain, P5. The closest PhoA fusion C-terminal to C5 (N5-1, Table 6) exhibited a low AP activity and high β-gal activity (Table 9) which suggests that the PhoA domain is primarily located in the cytoplasm, even though it is preceded by a predicted membrane spanning segment. This membrane spanning segment is not indicated as strongly (Fig. 24) by the hydropathy algorithms applied in this study and may not act as an efficient translocation signal for the PhoA domain of the N5-1 fusion. The C5 domain contains one positively charged residue, is preceded by a strongly predicted transmembrane segment and the strongly indicated P5 domain, and so it seems likely that C5 would be located in the cytoplasm.

4 DISCUSSION

ORF1696 is an open reading frame that encodes 477 amino acids, which is located 3' of the *bchFNBHLM* genes and immediately 5' of the *puhA* gene within the photosynthesis gene cluster (PSGC) of *R. capsulatus* (3) (Fig. 4, Introduction). Two promoters service this region of the PSGC, one located upstream of the *bchF* gene and another located within *ORF1696* (10). Topological analyses of the ORF1696 protein show it to be very hydrophobic, and it is predicted to be an integral membrane protein with 12 transmembrane segments. The positions of the putative transmembrane regions along the ORF1696 primary amino acid sequence approximate the positions of the 12 transmembrane helices proposed in the PucC membrane topology model (29, 84). Therefore, the ORF1696 protein is likely to be located in the ICM, which contains the LHI antenna complex.

My results demonstrate that Km^r interposon mutations of the *ORF1696* gene in *R. capsulatus* strains ΔNae and ΔStu reduced the amount of the LHI complex, and were complemented in *trans* with a plasmid-borne copy of *ORF1696* (Fig. 11). Northern blot analysis demonstrated that an *ORF1696* Km^r disruption mutation had no effect on the levels of *pufBA* mRNA, and so the ORF1696 protein should not modulate transcription of the *puf* operon (10). I tested the possibility that the ORF1696 protein acts to regulate *pufB* gene expression at the level of transcription and/or translation by introducing a plasmid encoding a *pufB'::lac'Z* translational fusion into the strains ΔLHII and ΔStu, driven by the *puf* promoter (plasmid pXCA6::935, (1)). The β-galactosidase activities obtained confirmed that the ORF1696 protein does not affect transcription and indicated that it does not modulate translation of *puf* mRNA (Results, section 3.1.7). Therefore, restoration of the LHI complex in the complemented strains to near-normal levels indicates that a diffusible factor derived from the *ORF1696* gene enhances the assembly (see below)

of the LHI complex in the ICM. Thus, I conclude that *ORF1696* is expressed to produce a protein in *R. capsulatus* during low O_2 and phototrophic growth, which is an LHI complex assembly factor.

Several reasons might account for the partial restoration of the LHI complex observed in the complemented ΔNae and ΔStu strains. For example, the *ORF1696* gene may not be expressed as strongly from the pCY42 plasmid as it is from its natural chromosomal location. Alternatively, the truncated ORF1696 polypeptides synthesized from the Km^r disrupted genes on the chromosome might interfere with the activity of the plasmid-encoded complete ORF1696 protein, thus preventing full restoration of LHI.

The 50% reduction of the LHI complex level observed in the ΔNae mutant suggests that loss of as few as the 13 C-terminal amino acid residues of ORF1696 impairs its function. Since the 5' remnant of the Ble^r gene on the Km^r cartridge was fused translationally in-frame to the 3' codons of *ORF1696* in ΔNae, no ORF1696 amino acid residues were deleted *per se*. That is, 97 heterologous amino acids were added to Ala 464 of the N-terminal segment of ORF1696 at the disruption site, and the C-terminal 13 amino acid segment of ORF1696 (starting with Gly 465) was fused to the truncated Ble^r protein. Nevertheless, this disruption greatly interfered with the function of the transected ORF1696 protein (Fig. 11A). Insertion of the Km^r cartridge downstream of the P_{puhA} promoter in ΔNae might be thought to interfere with transcription of *puhA* and other ORFs downstream of *puhA* (152). However, transcription reading through, or originating from the Km^r gene promoter must contribute to the expression of *puhA* and genes located 3' of *puhA*, since the amount of the RC complex was not significantly affected in ΔNae. This can be seen in Figure 11A, where the 800 nm RC peak area of ΔNae is at most slightly reduced compared to that for ΔLHII (in which some contribution from the relatively large 875 nm LHI peak is evident). Since the level of the RC did not

appear to be affected by the ΔNae mutation, it is unlikely that transcription of *puhA* or ORFs located downstream of *puhA*, such as *ORF214*, was reduced. This is significant because disruptions of *puhA* and *ORF214* showed that the expression of these genes, like *ORF1696*, is required to obtain the wild type level of the LHI complex (152). However, it was proposed that the reductions in the amounts of the LHI complex resulting from *puhA* or *ORF214* mutations were derived indirectly (due to decreases in the amount of the RC) (152), whereas the results of this thesis show that ORF1696 has a direct, LHI-specific effect on the assembly of this antenna complex.

The ORF1696 N-terminal segments remaining in the mutants described here, as short as 31 amino acid residues in length in the ΔMun mutant, conceivably could contribute to a small amount of LHI assembly (Fig. 11A), or else LHI can assemble, albeit inefficiently, in the complete absence of ORF1696 activity. Therefore, although ORF1696 is a major factor in LHI complex assembly, there could be additional assembly factors or else LHI forms spontaneously to a limited degree *in vivo*, as has been observed *in vitro* (87).

The lower level of the LHI complex in ΔStu::Ω , compared to ΔStu and ΔMun, is attributed to a combination of the direct effect of the disruption of *ORF1696* and the indirect effect of the low level of the RC (see Fig. 13B). The RC and LHI complexes are closely associated in the ICM, which likely provides mutual stabilization as a result of protein-protein interactions (106, 143, 152, unpublished observations). In fact, the amounts of the RC complex in these strains correspond to the order ΔStu > ΔMun > ΔStu::Ω (Fig. 11B). Thus, the Ω cartridge insertion in ΔStu::Ω and the ΔMun Km^r cartridge insertion have different degrees of polar effects on transcription of *puhA* and genes located 3' of *puhA*, such as *ORF214*, which have been observed to reduce RC and LHI levels when mutated (152). This conclusion is supported by the results of the complementation experiments on these

strains (Figs. 11A and B). Although a Rho protein has not been described in *R. capsulatus*, a *rho* gene was recently cloned and characterized in the closely related *R. sphaeroides* (52). A *rho*-dependent transcription terminator may exist between the *Mun* I and the nearest *Stu* I site within the *ORF1696* sequence, and give rise to the polar effect on *puhA* gene expression observed in ΔMun but not in ΔStu or ΔNae. Although the insertion of the Km^r cartridge at the *Mun* I site might be thought to disrupt or interfere with an upstream *cis*-active element required to enhance optimal trancription initiation from the P_{puhA} promoter, located downstream of nucleotide 1066 in the *ORF1696* coding sequence, this seems unlikely. It was reported that a *puhA::lacZ* translational fusion lacking the first 1066 nucleotides of *ORF1696* showed little change in the O_2 regulation of β-galactosidase activity in *R. capsulatus* cells, compared to a fusion in which sequences 5' of the *Mun* I site in *ORF1696* were included (10). My results indicate that transcription initiated at the *bchF* promoter is required for normal expression of *puhA*, *ORF214* and perhaps other genes located 3' of *ORF214*. Thus the *bch-puhA* superoperon extends beyond the *puhA* gene (10, 13, 152).

It is difficult to account for the appearance of the broad, heterogeneous region of absorption extending from approximately 750-790 nm in the ΔMun and ΔStu::Ω spectra, which accompanied the reduction in the 800 nm RC peak (Fig. 13A and 14). This region of absorption does not appear to be caused by the accumulation of bchl biosynthetic intermediates or degradation products in ΔMun cells (Fig. 15). This absorption could indicate bchl molecules associated with RC L and M polypeptides due to a combination of the depletion of the H subunit, reduced expression of genes 3' of *puhA* and the absence of a full-length ORF1696 protein. *R. capsulatus* strains which do not produce RC complexes because of interposon disruption or translational in-frame deletion of the *puhA* gene have no H protein but still have small amounts of L and M proteins present in purified ICM preparations (152).

Gm^r cartridge disruptions of the *ORF428* gene in any of the genetic backgrounds tested did not conclusively suggest a role for this gene in photocomplex assembly although *trans*-complementation of the mutant strains would help resolve this issue. In the SB1003 wild type background there appeared to be a greater decrease in the LHII 800 nm peak relative to the decrease in the 850 nm peak (see Fig. 18, Results). The 800 nm peak is due to the absorption of light by the monomeric bchl molecule of LHII, and a crystal structure of LHII from *Rp. acidophila* reveals this bchl to be arranged parallel to the plane of the membrane (91). One explanation for the greater decrease of this peak is that the binding site for the monomeric bchl exhibits a higher degree of specificity for the phytol containing bchl *a* and tolerates less well the presence of a bchl *a* molecule having a geranyl-geraniol tail (bchl a_{gg}). This explanation assumes a polar effect of the *ORF428*::Gm^r disruption on expression of *bchP*. The LHII 850 nm peak is due to a bchl *a* dimer which is arranged perpendicularly to the plane of the membrane. It is likely that the B850 binding site differs from that of the monomeric bchl significantly, and may be more able to accomodate bchl a_{gg} molecules. Binding of bchl a_{gg} may also explain the red-shift from 858 nm to 861 nm of the LHII B850 peak in the SB1003*ORF428*::Gm^r mutant (Fig. 18).

The comparisons of the kinetics of LHI assembly and decay in strains ΔLHII and ΔStu show that ORF1696 functions as a LHI assembly catalyst (Figs. 19 to 23, Tables 4 and 5). It is conceivable that ORF1696 can function reversibly to promote loss or disassembly of the LHI complex, as indicated by the LHI decay kinetics (Fig. 23, Table 5), although because of the small differences in decay between ΔLHII and ΔStu, additional experiments would be necessary to test this possibility. ORF1696 is the first protein demonstrated to function *in vivo* for pigment-protein complex assembly in *R. capsulatus*. However, it seems that ORF1696 is not the only factor involved in LH assembly.

Although the differences between the ΔLHII and ΔStu kinetics for LHI accumulation are significant (Fig. 20 and Table 4), none of the chromosomal disruptions of *ORF1696* resulted in the complete loss of LHI under steady-state conditions (Fig. 11). This partial phenotype resulting from mutation of *ORF1696* raises questions as to how many factors may be involved in maintaining the LHI complex at normal steady-state levels. The *ORF428* was at one time considered to encode an alternative assembly protein because it has 24% sequence identity to *ORF1696* , but Km^r disruptions of *ORF428* had little or no direct effect on the levels of pigment-protein complexes (19). My results from the Gm^r disruption of *ORF428* in various genetic backgrounds indicate a marginal, if any, role in LHI assembly.

In contrast to the LHI depleted phenotypes of *ORF1696* disruptions, a complete loss of the LHII complex results from deletion of *pucC*, a gene in the *puc* operon that encodes a protein with 47% amino acid identity with ORF1696 (83) (Fig. 29). Therefore, despite the primary sequence similarity, a functional difference between PucC and ORF1696 is that the PucC protein is essential for LHII complex formation whereas ORF1696 is a major factor in LHI complex formation. Although the exact step at which ORF1696 exerts its role in assembly of the LHI complex, whether by interacting with the subunit polypeptides or with pigments, is unknown, I propose below two non-exclusive models for ORF1696 function.

First, translocation of the LHI α and β polypeptides into the ICM has been hypothesized to involve a relatively large, integral membrane protein, such as ORF1696, in concert with a proton motive force (39). The addition of the *E. coli* chaperonin protein DnaK promoted synthesis of the LHI α and β polypeptides in a *R. capsulatus* cell-free translation system, and depletion of the *R. capsulatus* GroEL protein from this system decreased the amounts of the LHI polypeptides inserted into membranes isolated from chemotrophically grown wild type cells (94). *In vivo*, these cytoplasmic chaperonins (or homologues) may bind to and escort the LHI

polypeptides to the ICM, where the membrane-bound translocation apparatus (which may consist of ORF1696 alone or as part of a larger complex) promotes stable insertion of LHI α and β into the membrane. This process would be followed by, or coincide with, the binding of bchl and carotenoid pigment molecules to the membrane-spanning portions of the LHI α and β polypeptides to yield the mature LHI holocomplex.

Second, another function that ORF1696 might provide for assembly of LHI is in the insertion of bchl. This model suggests that bchl is delivered to the nascent LHI polypeptides by ORF1696. It was suggested that the PufQ protein carries bchl precursors (11), and it was shown that a heterologously expressed PufQ binds the bchl precursor molecule protochlorophyllide *in vitro* (47). The gene product of *pufQ* was proposed to be a factor in LHI assembly in *R. sphaeroides* (53). However strains ΔStu and ΔNae harboring plasmid pJAJ9, which has the entire *pufQ* gene included as part of the *puf* operon promoter region, showed no increase in the area of the LHI peak in spectra of cells grown under low aeration conditions compared to cells of the same strains lacking pJAJ9 (82). Thus, the function of PufQ is uncertain, although it is conceivable that ORF1696 acts as an intermediary, transferring bchl molecules from a PufQ-bchl complex to the LHI apoproteins, to enhance formation of the mature LHI holocomplex. Regardless of the function of PufQ, I suggest that ORF1696 is involved in the transfer of bchl to help assemble the LHI complex in the ICM.

Amino acid sequence comparisons between the *R. capsulatus* ORF1696 and PucC proteins, and homologues found in other purple non-sulfur bacteria reveal the presence of several His residues, including a conserved amino acid sequence, that contains an invariant histidine residue at position 152 of the *R. capsulatus* ORF1696, which could participate in binding of bchl (see Figure 16 (Results) and 29 (Discussion)). The conserved His-152 is situated as part of transmembrane segment

Figure 29. Alignment of ORF1696 and PucC homologs. Identical amino acids are boxed. The amino acid number is given on the far right of each sequence. *R.* = *Rhodobacter, Rs.* = *Rhodospirillum,* and *Rv.* = *Rhodovulum* . Accession nos. are Z11165, B61213, P23462, U81968, Q02443,

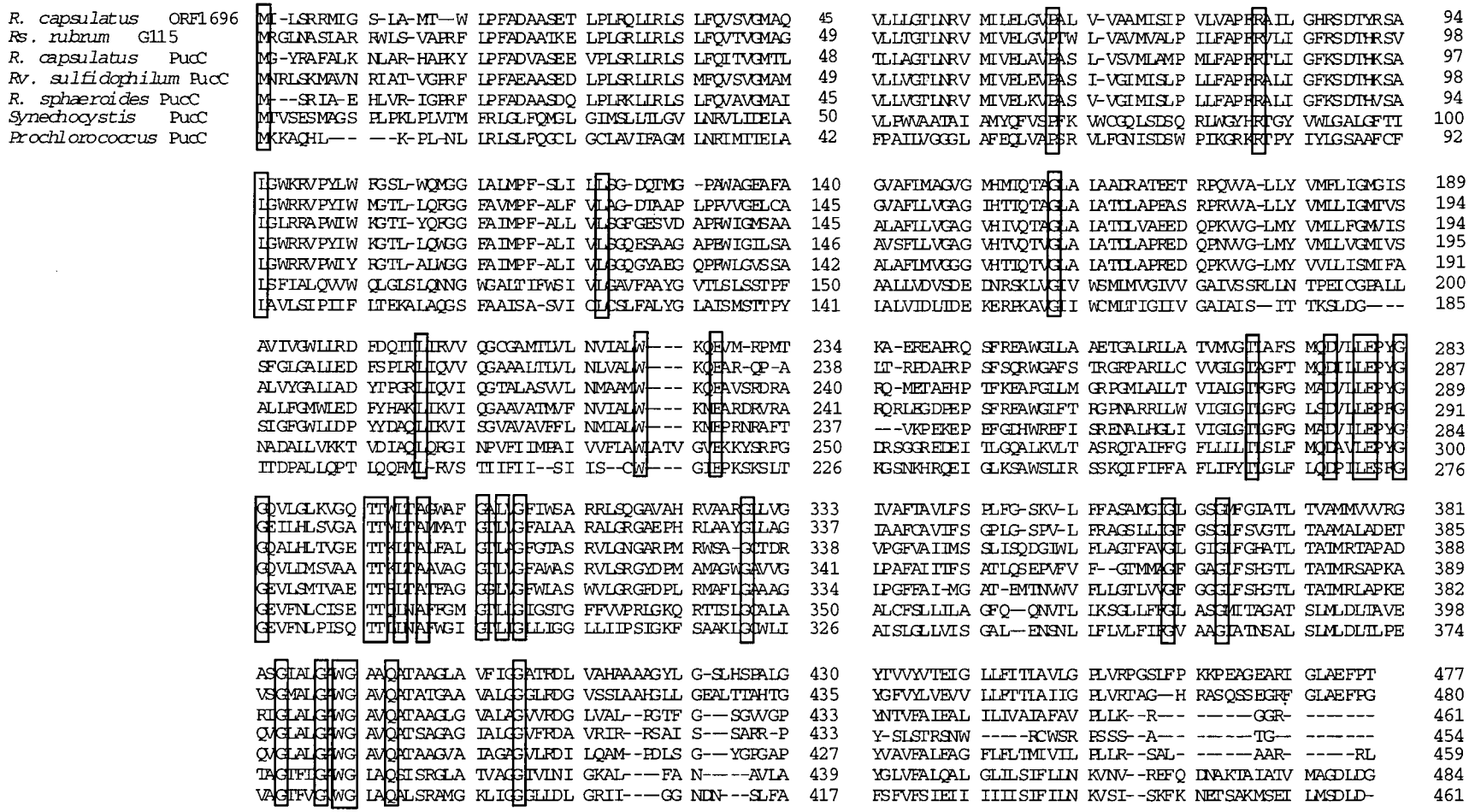
R. capsulatus ORF1696
Rs. rubrum G115
R. capsulatus PucC
Rv. sulfidophilum PucC
R. sphaeroides PucC
Synechocystis PucC
Prochlorococcus PucC

#4 in the ORF1696 topology model (see Fig. 25). Although substitution of the His-152 residue with either Asn or Phe by site-directed mutagenesis indicated that the His-152 residue does not play a major role in the functioning of the ORF1696 protein, these results do not negate the possibility that ORF1696 transfers bchl molecules to the LHI complex or that other amino acid residues in the protein may be involved in that process. Other candidates for the transient binding of bchl include other His residues that are less conserved among the ORF1696/PucC homologs (for example His-86, His-323, His-414, and His-425). His-86 is of interest because it is preceded by the consensus bchl binding sequence Ala-x-x-x-His found in other bchl binding proteins (Results, Fig. 16). His-323 is conserved in ORF1696 and in the *Rs. rubrum* G115 protein, but not in the PucC homologs and is preceded by the consensus sequence Gly-x-x-x-His. His-414 and His-425 appear less likely to bind bchl based on the sequences preceding them which are Asp-x-x-x-His and Leu-x-x-x-His, respectively, although it would be important to mutate these residues in any case to rule them out as potential bchl binding sites in ORF1696.

Homologs of *ORF1696* have been found in the purple non-sulfur bacteria *Rhodopseudomonas viridis*(150), *Rhodospirillum rubrum* (16) and *R. sphaeroides* (10, 38), and are similarly located 5' to the *puhA* gene. Furthermore, the closely related *pucC* gene is conserved amongst purple bacteria that contain the LHII complex. The cyanobacterium *Synechocystis* sp. PCC6803 (66) and the organism *Prochlorococcus marinus* (60) contain ORF1696/PucC homologs with 24% and 25% amino acid sequence identity (to ORF1696), respectively, in alignments (see Fig. 29). Since cyanobacteria and *Prochlorococcus* do not contain purple bacterial LH complexes, the presence of an ORF1696 homolog in these organisms could provide a hint about the function of this class of proteins. There are great differences in the amino acid sequences of purple bacterial and cyanobacterial LH complexes (78). In

contrast, the chlorophyll *a* (chl *a*) and bchl *a* molecules differ only in that chl *a* has a vinyl functional group bound to pyrrole ring I where bchl *a* has an acetyl group at this position and pyrrole ring II of chl *a* is unsaturated while the same ring of bchl *a* is saturated (81). Thus, the primary amino acid sequence conservation in ORF1696-like proteins may be due to a common function in bchl (chl) binding for LH complex assembly in these otherwise diverse photosynthetic organisms. It will be interesting to see if proteins expressed from these ORFs play a role in LH complex assembly as does the ORF1696 protein in *R. capsulatus*.

The membrane topology of ORF1696 was evaluated to provide a two-dimensional structural representation of the protein, which could have potential applications in the identification of antigenic sites for the generation of anti-ORF1696 antibodies, and to provide insight into structure-function relationships (Fig. 25, Results). Hydropathy analyses and application of the 'positive-inside rule' were used to generate a membrane topology model of the ORF1696 protein that consists of 12 transmembrane segments, seven extramembranous cytoplasmic domains enriched for the positively charged amino acids Arg and Lys, and six periplasmic domains. Extramembranous domains consist of 10 (C5) to 35 (C3) amino acid residues and the N- and C-termini are located in the cytoplasm. Expression of enzymatic fusions in the *phoA* strain *E. coli* CC118 helped to verify the predictions made by the hydropathy analyses. The assay of PhoA fusions to heterologous proteins expressed in *E. coli* to assess their membrane topology has been applied in several studies (40, 84, 88, 137), and the validity of this approach was verified by comparing the topology of the *R. sphaeroides* RC L polypeptide, predicted by a series of PhoA fusions to the L protein, to the topology determined by X-ray crystallography (4, 160). The correct membrane topology of the L subunit was obtained by assaying *pufL'::pho'A* fusions in both *E. coli* and *R. sphaeroides* (160),

and so I assume that ORF1696 fusions would similarly insert into the *E. coli* cytoplasmic membrane as they do in *R. capsulatus*.

ORF1696'::Pho'A fusions to periplasmic domains P1 through P5 have relatively high AP activities while fusions to the C1 through C3 domains yield low activities. The ORF1696'::Lac'Z fusions to these regions confirm the results of the PhoA fusion studies. As for domains C4 and C5 for which no enzymatic fusions were obtained, arguments were made based on the "positive-inside" rule, the enzymatic activity of fusions in neighbouring extramembranous domains, and the hydropathy of flanking transmembrane segments (section 3.3.5), which suggested that these regions are likely localized to the cytoplasm.

The low AP activity measured for PhoA fusion N10-1 seemed to correlate with a relatively low level of fusion protein synthesis (Fig. 26 and Table 8, Results) since the normalized AP activity for this fusions was increased relative to other ORF1696'::Pho'A proteins. The four positively charged residues located near the C-terminus of the ORF1696 protein (Arg-454, Lys-461, Lys-462, and Arg-469) probably help to anchor the C-terminal domain in the cytoplasm, and thus seem to be important topological determinants. Since these residues are replaced by the AP and β-gal moieties in fusions N5-1, N10-1, N10-2 and partially in Nae1.5, alternative conformations may result which could give rise to different topologies for these fusions and which might lead to anomalous enzyme activities (Table 7, Results). For this reason, it is proposed that domain P6 is periplasmically localized and there is a requirement for topological determinants in the C-terminal domain, including positively charged amino acids, which help establish the native topology of the region extending from Asp 410 to Tyr 435 (P6). The need for C-terminal amino acid sequences in NodC'::Pho'A and PucC'::Pho'A fusions was observed, and confirmed that caution should be exercised in interpreting AP activities as the sole method upon which to base the topology of a membrane protein (7, 84).

Both the raw and normalized AP activities measured for the Mun0.2 fusion were relatively high indicating that the PhoA moiety is efficiently transported to the periplasm. The Mun0.2 fusion protein includes the first 30 amino acids of ORF1696 of which three are positively charged and strongly predicted transmembrane segments C-terminal to the fusion joint have been eliminated. Thus, significant topological determinants are not present in this fusion product which might participate in orienting the N-terminal portion of the ORF1696 protein in the cytoplasmic membrane in the correct fashion. A "putative" transmembrane segment was predicted to occur from amino acid 6 to 26 by the GvH1 hydropathy algorithm which was not detected by the GES or KD algorithms applied in the study. It is possible that this portion of the ORF1696 protein, in isolation from the rest of the protein, can act as a transmembrane segment or as a signal sequence which promotes transport of the PhoA portion of the Mun0.2 fusion protein into the periplasm. As a transmembrane segment, amino acids 6 to 26 separate the two positively charged residues, Arg-5 and Arg-6, from a single positive residue, Arg-29 (Fig. 1C). Thus, in accordance with the "positive-inside rule", the N-terminus of the Mun0.2 fusion product would be oriented toward the cytoplasm and the PhoA moiety located in the periplasm where it would contribute to the high AP activities measured for this fusion. Alternatively, if the N-terminus of ORF1696 were to be placed on the periplasmic side of the cytoplasmic membrane. It would place five positively charged amino acids in the periplasm compared with five positive residues in the C1 domain. There is no positive charge bias created in favor of a periplasmic location for the N-terminus. The single positive charge in domain P1, location of transmembrane segment #1, and greater numbers of positively charged amino acids in the N-terminal and C1 domains (compared to P1) argue for a cytoplasmic location for the approximately 32 amino acids of the ORF1696 N-

terminal domain based on the methods and tools available to predict membrane protein topology.

^{35}S-methionine pulse-labeling (Fig. 26, Results) and Western blotting of ORF1696'::Pho'A fusion proteins (Fig. 27) indicated that all of these full-length fusion proteins were degraded rapidly. The presence of a protein of 47 kDa, which comigrated with the AP band in the *phoR* strain CC149 lane in the pulse-labeled phosphorimages and the Western blots, suggests that the fusion joint region is susceptible to proteolytic attack. For those fusion proteins predicted to have the AP moiety localized to the cytoplasm (Nae1.5, Hin1.0, Bs2-2, Bs5-2, Mun0.2), the Western blots showed that the 47 kDa AP protein was not present or present at very low levels compared to periplasmic fusions (Fig. 27, Results). The intensity of the 47 kDa AP protein for cytoplasmic and periplasmic PucC'::Pho'A fusions exhibited a similar trend in Western blots (84). Because AP is unable to form disulfide bonds in the cytoplasm, required to obtain a stable protease-resistant conformation (35), it is assumed that the unfolded protein is degraded by cytoplasmic protease enzymes.

The PucC protein of *R. capsulatus* consists of 461 amino acids of which 47% show sequence identity with ORF1696 (10). PucC and ORF1696 function similarly to one another in that both participate in the formation of LH complexes (84, 155). A model of the membrane topology of PucC was proposed to have 12 transmembrane segments with the N- and C-termini located in the cytoplasm, which closely resembles the model presented for ORF1696 (84) (Fig. 30).

The testing of the predicted PucC topology model with most fusions of truncated *pucC* alleles to *phoA* and *lacZ* revealed a clear correlation between the high and low activities measured and the expected localization of the reporter enzyme moieties to periplasmic or cytoplasmic sides of the cytoplasmic membrane. However, the results of the enzyme fusion analyses in the last periplasmic loop were not as clear as in the more N-terminal portions of the protein. This is

Figure 30. Membrane topology models of ORF1696 (top) and PucC (84) (bottom). Details of the models are given in the description of Fig. 25 (Results) except that positively charged amino acids are circled in the PucC model.

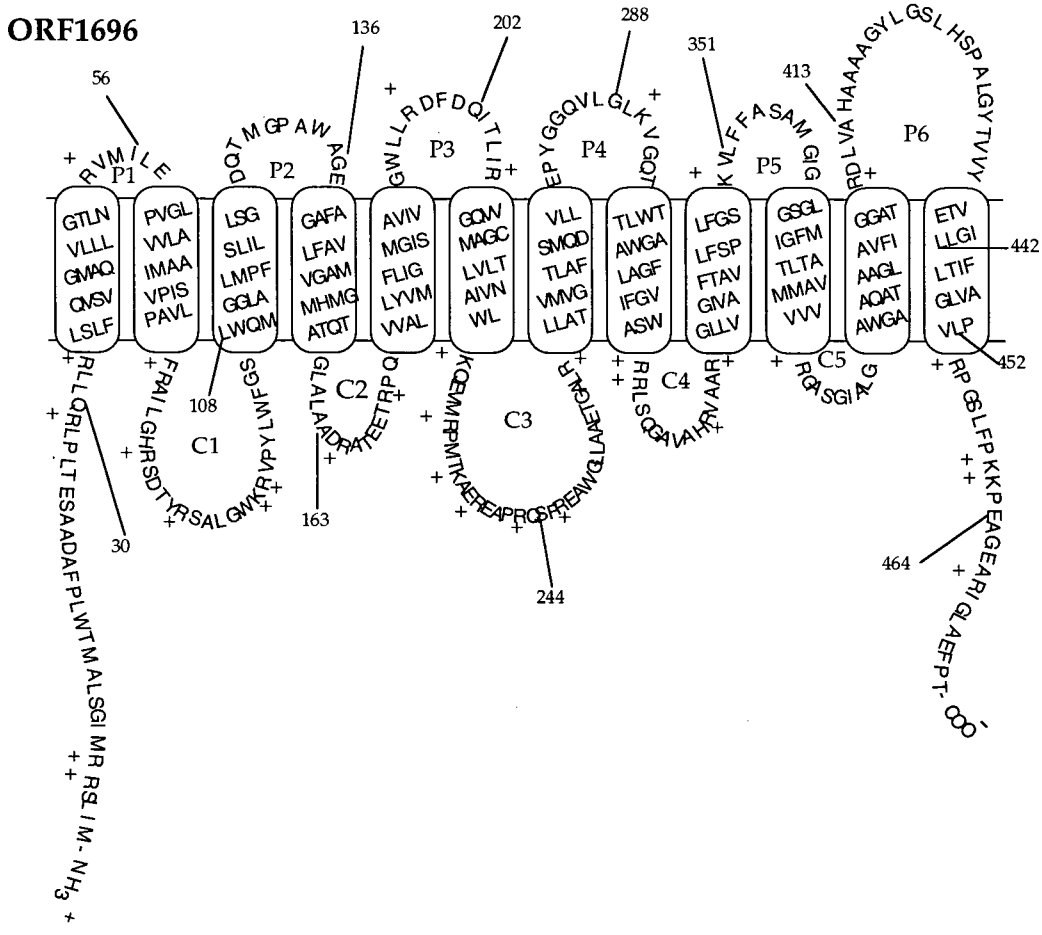
ORF1696
P1
P2
P3
P4
P5
P6
C1
C2
C3
C4
C5
56
136
202
288
351
413
442
452
30
108
163
244
464

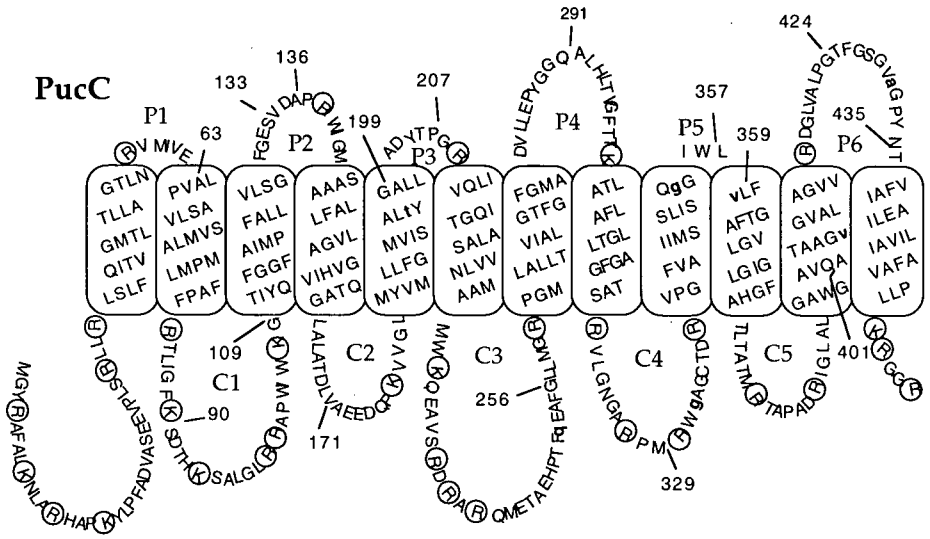
PucC
P1
P2
P3
P4
P5
P6
C1
C2
C3
C4
C5
63
133
136
199
207
291
357
359
424
435
109
171
256
329
401

interesting because apparent anomalies were also observed for enzyme fusions in the C-terminal region of ORF1696. This similarity suggests that the C-terminal domain of this family of proteins is somewhat flexible in its topology, and perhaps this is related to a function that is important for LH complex assembly. (Furthermore, the spectral results obtained with the ΔNae mutant suggested that the C-terminal 13 amino acids of ORF1696 are important for function (Fig. 11A)).

As discussed above, one function in which the ORF1696 protein might participate is in the translocation of the LHI α and β polypeptides into the cytoplasmic membrane. The unstable topology of Pho'A and β-gal fusions in the C-terminal region of both ORF1696 and PucC suggests that these proteins may be able to assume more than one topology in that region. In the topology models, the P6 domain consists of primarily hydrophobic amino acids with the only charged amino acids, Arg-409 and Asp-410 (Arg-416 and Asp-417 in PucC), located at the beginning of this periplasmic loop (Fig. 30) (84). Perhaps the relatively extensive hydrophobic character of this portion of ORF1696 and PucC allows for some movement of the penultimate transmembrane segment (#11), such that some of the amino acids making up the P6 domain migrate into and out of the membrane. A mobile, conformationally variable region such as this could be envisioned to participate in the translocation of the LHI α and β polypeptides, pulling them through the membrane to assist proper integration of transmembrane a-helices of these proteins. It would be interesting to evaluate if there is any charge complementarity between this region and the N- and C-termini of the LH proteins.

The specificity of the ORF1696 protein and PucC for assembly of the LHI and LHII complexes, respectively, can be addressed at low resolution by comparison of the topology models (84). The most obvious differences between the two models is in the number and content of amino acids in the three proposed extramembranous domains P3, P5 and the C-terminus. The P3 domain of PucC is predicted to consist

of seven amino acid residues, one of which is positively charged (Arg-209) and one of which is negatively charged (Asp-204), while P3 of ORF1696 is predicted to have fourteen amino acids of which two are positively charged (Arg-198 and Arg-207), and two of which are negatively charged (Asp-199 and Asp-201). Differences between the two proteins are more profound in the P5 domain, which consists of three amino acids in PucC and twelve amino acids in ORF1696 including one positively charged residue (Lys-349). The C-terminal regions of both proteins are enriched for positively charged residues (Lys-457, Arg-458, and Arg-461 for PucC and Arg-454, Lys-461, Lys-462, and Arg-468 for ORF1696) but in PucC consists of only five amino acids whereas there are twenty-three amino acids comprising the C-terminal region of ORF1696. Furthermore, there are three negatively charged residues present as part of the ORF1696 C-terminal domain (Glu-463, Glu-466, and Glu-473). The C-terminus and P5 domains of ORF1696 are likely to be bulkier, globular domains compared to the same regions of PucC because of the greater number of amino acids in these regions of ORF1696. These differences might contribute to the specificity of these two proteins for the LHI or LHII α and/or β polypeptides.

The relative similarity in both topology and amino acid sequence of ORF1696 and PucC in the N-terminal halves of the proteins, in contrast to the greater dissimilarities found nearer the C-termini (see Figs. 29 and 30), suggest the possibility that two functional domains exist in these proteins. The N-terminal half could be more important for the transient binding of bchl molecules that are transferred and more firmly bound to the LH α and β polypeptides during membrane insertion. This hypothetical bchl binding domain might be demarked in each protein by the C3 region, a cytoplasmically localized portion of the proteins enriched for charged residues, from the C-terminal domain which bestows specificity for either the LHI or LHII complex polypeptides and their translocation across the cytoplasmic membrane. This model of ORF1696 and PucC function

predicts that these proteins give rise to a subunit form of an LH complex ($\alpha 1\beta 1$) with two bchl molecules delivered in succession to the LH polypeptides. The LHII complex contains the 850 nm bchl dimer (like the LHI B870 dimer) and also a 800 nm bchl monomer. The alignment of PucC homologues in Fig. 29 reveals a possible site for bchl binding at amino acid number 376 (corresponding to Gly-X-X-X-His). Perhaps the monomer bchl molecule of the LHII complex is transferred to the α and β polypeptides from this region of PucC. The $\alpha 1\beta 1$ pigment-protein complexes would then interact to form the mature LHI and LHII holocomplexes: a 16 $\alpha 1\beta 1$ or 9 $\alpha 1\beta 1\gamma 1$ member oligomeric ring, respectively. The ring of LHI surrounding the RC complex is formed by a mechanism assisted by other proteins in the cell or occurs spontaneously, as has been observed *in vitro* (87).

In summary, the *ORF1696* gene product can act in *trans* to restore LHI complex levels in *R. capsulatus* strains containing a Km^r cartridge disruption of the chromosomal copy of *ORF1696*. The Km^r cartridge disruption present in strain ΔMun has a polar effect on the expression of downstream genes, including *puhA*, which may be due to Rho-dependent transcription termination. A broad region of absorption over 750 to 790 nm observed for this strain after spectral analysis is likely due to bchl *a* molecules associating aberrantly with proteins.

The ORF1696 protein is a major factor in LHI complex assembly and does not affect the transcription or translation of the *puf* operon, which gives rise to the LHI α and β polypeptides. The amino acid residue, His-152, does not play a role in the function of ORF1696. It does not appear that *ORF428* factors greatly in maintaining levels of the photocomplexes, although this requires confirmation by *trans* complementation of *ORF428*::Gm^r mutations.

The membrane topology model predicted for ORF1696 consists of 12 transmembrane segments, with six periplasmic and seven cytoplasmic regions which include the N- and C-terminal domains. The ORF1696 and PucC topology

models closely resemble one another, although there are several differences which might account for their specificities for the LHI and LHII complexes, respectively. Several ORF1696/PucC homologs have been identified from a variety of photosynthetic prokaryotes providing impetus for further study to establish that they function analogously to ORF1696 in photocomplex assembly.

5 REFERENCES

1. Adams, C. W., M. E. Forrest, S. N. Cohen and J. T. Beatty. 1989. Structural and functional analysis of transcriptional control of the *Rhodobacter capsulatus puf* operon. J. Bacteriol. **171:**473-482.

2. Akiyama, Y. and K. Ito. 1993. Folding and assembly of bacterial alkaline phosphatase *in vitro* and *in vivo*. J. Biol. Chem. **268:**8146-8150.

3. Alberti, M., D. E. Burke, and J. E. Hearst. 1995. Structure and sequence of the photosynthetic gene cluster., 1083-1106. *In* R. E. Blankenship, M. T. Madigan, and C. E. Bauer (eds.), Anoxygenic photosynthetic bacteria. Kluwer Academic Publishers, Dordrecht, The Netherlands.

4. Allen, J. P., G. Feher, T. O. Yeates, H. Komiya and D. C. Rees. 1987. Structure of the reaction center from *Rhodobacter sphaeroides* R-26: the protein subunits. Proc. Natl. Acad. Sci. USA **84:**6162-6166.

5. Babst, M., H. Albrecht, I. Wegmann, R. Brunisholz and H. Zuber. 1991. Single amino acid substitutions in the B870 α and β light-harvesting polypeptides of *Rhodobacter capsulatus*: Structural and spectral effects. Eur. J. Biochem. **202:**277-284.

6. Barany, F. 1985. Single-stranded hexameric linkers: a system for in-phase insertion mutagenesis and protein engineering. Gene **37:**111-123.

7. Barny, M.-A., E. Schoonejans, A. Economou, A. W. B. Johnston, and J. A. Downie. 1996. The C-terminal domain of the *Rhizobium leguminosarum* chitin synthase NodC is important for function and determines the orientation of the N-terminal region in the inner membrane. Mol. Microbiol. **19:**443-453.

8. Barz, W. P. and D. Oesterhelt. 1994. Photosynthetic deficiency of a *pufX* deletion mutant of *Rhodobacter sphaeroides* is suppressed by point mutations in the light-harvesting complex genes *pufB* and *pufA*. Biochemistry **33:**9741-9752.

9. Bauer, C. E. 1995. Regulation of Photosynthesis Gene Expression, 1221-1234. *In* R. E. Blankenship, M. T. Madigan, and C. E. Bauer (eds.), Anoxygenic Photosynthetic Bacteria. Kluwer Academic Publishers, Dordrecht, The Netherlands.

10. Bauer, C. E., J. Buggy, Z. Yang and B. L. Marrs. 1991. The superoperonal organization of genes for pigment biosynthesis and reaction center proteins is a conserved feature in *R. capsulatus*: analysis of overlapping *bchB* and *puhA* transcripts. Mol. Gen. Genet. **228:**438-444.

11. Bauer, C. E. and B. L. Marrs. 1988. *Rhodobacter capsulatus puf* operon encodes a regulatory protein (PufQ) for bacteriochlorophyll biosynthesis. Proc. Natl. Acad. Sci. USA **85:**7074-7078.

12. Beatty, J. T. Personal communication.

13. Beatty, J. T. 1995. Organization of photosynthesis gene transcripts, 1209-1219. *In* R.E. Blankenship, M. T. Madigan, and C.E. Bauer (eds.), Anoxygenic photosynthetic bacteria. Kluwer Academic Publishers, Dordrecht, The Netherlands.

14. Beatty, J. T. and H. Gest. 1981. Generation of succinyl-coenzyme A in photosynthetic bacteria. Arch Microbiol **129:**335-340.

15. Belasco, J. G., J. T. Beatty, C. W. Adams, A. von Gabain and S. N. Cohen. 1985. Differential expression of photosynthesis genes in *R. capsulatus* results from segmental differences in stability within the polycistronic *rxcA* transcript. Cell **40:**171-181.

16. Bérard, J. and G. Gingras. 1991. The *puh* structural gene coding for the H subunit of the *Rhodospirillum rubrum* photoreaction center. Biochem. Cell. Biol. **69:**122-131.

17. Bibb, M. J. and S. N. Cohen. 1982. Gene expression in *Streptomyces*: construction and application of promoter-probe plasmid vectors in *Streptomyces lividans*. Mol. Gen. Genet. **187:**265-277.

18. Bingle, W., H. D. Kurtz and J. Smit. 1993. An "all-purpose" cellulase reporter for gene fusion studies and applications to the paracrystalline surface (S)-layer protein of *Caulobacter crescentus*. Can. J. Microbiol. **39:**70-80.

19. Bollivar, D. W., J. Y. Suzuki, J. T. Beatty, J. M. Dobrowski and C. E. Bauer. 1994. Directed mutational analysis of bacteriochlorophyll *a* biosynthesis in *Rhodobacter capsulatus*. J. Mol. Biol. **237:**622-640.

20. Boyd, D., B. Traxler and J. Beckwith. 1993. Analysis of the topology of a membrane protein by using a minimum number of alkaline phosphatase fusions. J. Bacteriol. **175:**553-556.

21. Brand, M., A. F. Garcia, N. Pucheu, A. Meryandini, N. Kerber, M. H. Tadros, and G. Drews. 1995. Phosphorylation of the light-harvesting polypeptide LHIα of *Rhodobacter capsulatus* at serine after membrane insertion under chemotrophic and phototrophic growth conditions. Biochim. Biophys. Acta **1231:**169-175.

22. Brent, R. and M. Ptashne. 1980. The *lexA* gene product represses its own promoter. Proc. Natl. Acad. Sci. USA **77:**1932-1936.

23. Buggy, J. and C. E. Bauer. 1995. Cloning and characterization of *senC*, a gene involved in both aerobic respiration and photosynthesis gene expression in *Rhodobacter capsulatus*. J. Bacteriol. **177:**6958-6965.

24. Buggy, J. J., M. W. Sganga, and C. E. Bauer. 1994. Characterization of a light-responding *trans*-activator responsible for differentially controlling reaction center and light-harvesting I gene expression in *Rhodobacter capsulatus*. J. Bacteriol. **176:**6936-6943.

25. Chang, C. N., W-J. Kuang, and E. Y. Chen. 1986. Nucleotide sequence of the alkaline phosphatase gene of *Escherichia coli*. Gene **44:**121-125.

26. Chen, C.-Y. A., J. T. Beatty, S. N. Cohen and J. G. Belasco. 1988. An intercistronic stem-loop structure functions as an mRNA decay terminator necessary but insufficient for *puf* mRNA stability. Cell **52:**609-619.

27. Cheng, S., C. Fockler, W. M. Barnes, and R. Higuchi. 1994. Effective amplification of long targets from cloned inserts and human genomic DNA. Proc. Natl. Acad. Sci. USA **91:**5695-5699.

28. Clark, W. G., E. Davidson and B. L. Marrs. 1984. Variation of levels of mRNA coding for antenna and reaction center polypeptides in *Rhodopseudomonas capsulata* in response to changes in oxygen concentration. J. Bacteriol. **157:**945-948.

29. Claros, M. G. and G. von Heijne. 1995. TopPred II, version 1.1: Prediction of transmembrane segments in integral membrane proteins, and the putative topologies. CABIOS **10:**685-686.

30. Cogdell, R. J., P. K. Fyfe, S. J. Barrett, S. M. Prince, A. A. Freer, N. W. Isaacs, P. McGlynn and C. N. Hunter. 1996. The purple bacterial photosynthetic unit. Photosyn. Res. **48:**55-63.

31. Cortez, N., A. F. Garcia, M. H. Tadros, N. Gad'on, E. Schiltz, and G. Drews. 1992. Redox-controlled, *in vivo* and *in vitro* phosphorylation of the α subunit of the light-harvesting I complex in *Rhodobacter capsulatus*. Arch. Microbiol. **158:**315-319.

32. Davis, C. M., P. S. Parkes-Loach, C. K. Cook, K. A. Meadows, M. Bandilla, H. Scheer, and P. A. Loach. 1996. Comparison of the structural requirements for bacteriochlorophyll binding in the core light-harvesting complexes of *Rhodospirillum rubrum* and *Rhodobacter sphaeroides* using reconstitution methodology with bacteriochlorophyll analogs. Biochemistry **35:**3072-3084.

33. Davis, C. M., P. L. Bustamante, J. B. Todd, P. S. Parkes-Loach, P. McGlynn, J. D. Olsen, L. McMaster, C. N. Hunter, and P. A. Loach. 1997. Evaluation of structure-function relationships in the core light-harvesting complex of photosynthetic bacteria by reconstitution with mutant polypeptides. Biochemistry **36:**3671-3679.

34. Deisenhofer, J., K. M. O. Epp, R. Huber and H. Michel. 1985. Structure of the protein subunits in the photosynthetic reaction centre of *Rhodopseudomonas viridis* at 3Å resolution. Nature (London) **318:**618-624.

35. Derman, A. I. and J. Beckwith. 1991. *Escherichia coli* alkaline phosphatase fails to acquire disulfide bonds when retained in the cytoplasm. J. Bacteriol. **173:**7719-7722.

36. Derman, A. I. and J. Beckwith. 1995. *Escherichia coli* alkaline phosphatase localized to the cytoplasm slowly acquires enzymatic activity in cells whose growth has been suspended: a caution for gene fusion studies. J. Bacteriol. **177:**3764-3770.

37. Ditta, G., T. Schmidhauser, E. Yakobsen, P. Lu, X.-W. Liang, D. R. Finlay, D. Guiney and D. R. Helinski. 1985. Plasmids related to the broad host range vector, pRK290, useful for gene cloning and for monitoring gene expression. Plasmid **13:**149-153.

38. Donohue, T. J., J. H. Hoger and S. Kaplan. 1986. Cloning and expression of the *Rhodobacter sphaeroides* reaction center H gene. J. Bacteriol. **168:**953-961.

39. Drews, G. and J. R. Golecki. 1995. Structure, molecular organization, and biosynthesis of membranes of purple bacteria, 231-257. *In* R.E. Blankenship, M. T. Madigan, and C. E. Bauer. (eds.), Anoxygenic photosynthetic bacteria. Kluwer Academic Publishers, Dordrecht, The Netherlands.

40. Eitinger, T. and B. Friedrich. 1994. A topological model for the high-affinity nickel transporter of *Alcaligenes eutrophus*. Mol. Microbiol. **12:**1025-1032.

41. Ellis, R. J. and S. M. van der Vies. 1991. Molecular chaperones. Annu. Rev. Biochem. **60:**321-347.

42. Engelman, D. M., T. A. Steitz and A. Goldman. 1986. Identifying nonpolar transbilayer helices in amino acid sequences of membrane proteins. Ann. Rev. Biophys. Biophys. Chem. **15:**321-353.

43. Eraso, J. M. and S. Kaplan. 1995. Oxygen-sensitive synthesis of the photosynthetic membranes of *Rhodobacter sphaeroides*: a mutant histidine kinase. J. Bacteriol. **177:**2695-2706.

44. Eraso, J. M. and S. Kaplan. 1994. *prrA*, a putative response regulator involved in oxygen regulation of photosynthesis gene expression in *Rhodobacter sphaeroides*. J. Bacteriol. **176:**32-43.

45. Ermler, U., G. Fritzsch, S. K. Buchanan and H. Michel. 1994. Structure of the photosynthetic reaction centre from *Rhodobacter sphaeroides* at 2.65 Å resolution: cofactors and protein-cofactor interactions. Structure **2:**925-936.

46. Feick, R. and G. Drews. 1978. Isolation and characterization of light harvesting bacteriochlorophyll-protein complexes from *Rhodobacter capsulatus*. Biochim. Biophys. Acta **501:**499-513.

47. Fidai, S., S. B. Hinchigeri and W. R. Richards. 1994. Association of protochlorophyllide with the PufQ protein of *Rhodobacter capsulatus*. Biochem. Biophys. Res. Comm. **200:**1679-1684.

48. Foloppe, N., M. Ferrand, J. Breton and J. C. Smith. 1995. Structural model of the photosynthetic reaction center of *Rhodobacter capsulatus*. Proteins **22:**226-244.

49. Fonstein, M. and R. Hearst. 1993. Chromosomal structure of *Rhodobacter capsulatus* strain SB1003: cosmid encyclopedia and high-resolution physical and genetic map. Proc. Natl. Acad. Sci. USA **90:**2522-2526.

50. Gest, H. 1966. Comparative biochemistry of photosynthetic processes. Nature (London) **209:**879-882.

51. Gest, H. 1993. History of concepts of the comparative biochemistry of oxygenic and anoxygenic photsyntheses. Photosyn. Res. **35:**87-96.

52. Gomelsky, M. and S. Kaplan. 1996. The *Rhodobacter sphaeroides* 2.4.1 *rho* gene: expression and genetic analysis of structure and function. J. Bacteriol. **178:**1946-1954.

53. Gong, L., J. K. Lee and S. Kaplan. 1994. The *Q* gene of *Rhodobacter sphaeroides*: its role in *puf* operon expression and spectral complex assembly. J. Bacteriol. **176:**2946-2961.

54. Green, B. R. 1990. Structure prediction methods for membrane proteins: comparison with the X-ray structure of the *R. viridis* photosynthetic reaction center, *In* J. J. Villafranca (ed.), Current research in protein chemistry. Academic Press, New York.

55. Gromet-Elhanan, Z. 1995. The Proton-Translocating F_0F_1 ATP Synthase-ATPase Complex, 807-830. *In* R. E. Blankenship, M. T. Madigan, and C. E. Bauer, (eds.), Anoxygenic Photosynthetic Bacteria. Kluwer Academic Publishers, Dordrecht, The Netherlands.

56. Hanahan, D. 1983. Studies on transformation of *Escherichia coli* with plasmids. J. Mol. Biol. **166:**557.

57. Harmer, A. Personal communication.

58. Heck, C., R. Rothfuchs, A. Jager, R. Rauhut, and G. Klug. 1996. Effect of the *pufQ-pufB* intercistronic region on *puf* mRNA stability in *Rhodobacter capsulatus*. Mol. Microbiol. **20:**1165-1178.

59. Heller, B. A. and P. A. Loach. 1990. Isolation and characterization of a subunit form of the B875 light-harvesting complex from *Rhodobacter capsulatus*. Photochem. Photobiol. **51:**621-627.

60. Hess, W. Personal communication.

61. Holt, J. G. 1979. The Shorter Bergey's Manual of Determinative Bacteriology. The Williams and Wilkins Co., Baltimore.

62. Inoue, K., J. K. Kouadio, C. S. Mosley, and C. E. Bauer. 1995. Isolation and *in vitro* phosphorylation of sensory transduction components controlling anaerobic induction of light harvesting and reaction center gene expression in *Rhodobacter capsulatus*. Biochemistry **34:**391-396.

63. Johnson, J. A., W. K. R. Wong and J. T. Beatty. 1986. Expression of cellulase genes in *Rhodobacter capsulatus* by use of plasmid expression vectors. J. Bacteriol. **167:**604-610.

64. Jones, M. R., G. J. S. Fowler, L. C. D. Gibson, G. G. Grief, J. D. Olsen, W. Crielaard and C. N. Hunter. 1992. Mutants of *Rhodobacter sphaeroides* lacking one or more pigment-protein complexes and complementation with reaction-centre, LH1, and LH2 genes. Mol. Microbiol. **6:**1173-1184.

65. Joshi, H. M. and F. R. Tabita. 1996. A global two component signal transduction system that integrates the control of photosynthesis, carbon dioxide assimilation, and nitrogen fixation. Proc. Natl. Acad. Sci. USA **93:**14515-14520.

66. Kaneko, T., S. Sato, H. Kotani, A. Tanaka, E. Asamizu, Y. Nakamura, N. Miyajima, M. Hirosawa, M. Sugiura, S. Sasamoto, T. Kimura, T. Hosouchi, A. Matsuno, A. Muraki, N. Nakazaki, K. Naruo, S. Okumura, S. Shimpo, C. Takeuchi, T. Wada, and A. Watanabe. 1996. Sequence analysis of the genome of the unicellular Cyanobacterium *Synechocystis* sp. strain PCC6803. II. Sequence determination of the entire genome and assignment of potential protein-coding regions (supplement). DNA Res. **3:**185-209.

67. Klug, G. 1991. A DNA sequence upstream of the *puf* operon of *Rhodobacter capsulatus* is involved in its oxygen-dependent regulation and functions as a protein binding site. Mol. Gen. Genet. **226:**167-176.

68. Klug, G. 1991. Endonucleolytic degradation of *puf* mRNA in *Rhodobacter capsulatus* is influenced by oxygen. Proc. Natl. Acad. Sci. USA **88:**1765-1769.

69. Klug, G. 1995. Post-transcriptional control of photosynthesis gene expression, 1235-1244. *In* R. E. Blankenship, M. T. Madigan and C. E. Bauer (eds.), Anoxygenic Photosynthetic Bacteria. Kluwer Academic Publishers, Dordrecht, The Netherlands.

70. Klug, G., S. Jock, and R. Rothfuchs. 1992. The rate of decay of *Rhodobacter capsulatus*-specific *puf* mRNA segments is differentially affected by RNase E activity in *Escherichia coli*. Gene **121:**95-102.

71. Klug, G. 1993. The role of mRNA degradation in the regulated expression of bacterial photosynthesis genes. Mol. Microbiol. **9:**1-7.

72. Klug, G., C. W. Adams, J. Belasco, B. Doerge and S. N. Cohen. 1987. Biological effects of segmental alterations in mRNA stability: effects of deletion of the intercistronic hairpin loop region of the *Rhodobacter capsulatus puf* operon. EMBO J. **6:**3515-3520.

73. Klug, G., R. Liebetanz and G. Drews. 1986. The influence of bacteriochlorophyll biosynthesis on formation of pigment-binding proteins and assembly of pigment protein complexes in *Rhodopseudomonas capsulata*. Arch. Microbiol. **146:** 284-291.

74. Klug, G. and S. N. Cohen. 1990. Combined actions of multiple hairpin loop structures and sites of rate-limiting endonucleolytic cleavage determine differential degradation rates of individual segments within polycistronic *puf* operon mRNA. J. Bacteriol. **172:**5140-5146.

75. Klug, G. and S. Jock. 1991. A base pair transition in a DNA sequence with dyad symmetry upstream of the *puf* promoter affects transcription of the *puc* operon in *Rhodobacter capsulatus*. J. Bacteriol. **173:**6038-6045.

76. Kunkel, T. A., J. D. Roberts, and R. A. Zakour. 1987. Rapid and efficient site-specific mutagenesis without phenotypic selection. Meth. Enzymol. **154:**367-382.

77. Kyte, J. and R. F. Doolittle. 1982. A simple method for displaying the hydropathic character of a protein. J. Mol. Biol. **157:**105-132.

78. La Roche, J., G. W. van der Staay, F. Partensky, A. Ducret, R. Aebersold, R. Li, S. S. Golden, R. G. Hiller, P. M. Wrench, A. W. Larkum, and B. R. Green. 1996. Independent evolution of the prochlorophyte and green plant chlorophyll a/b light-harvesting proteins. Proc. Natl. Acad. Sci. USA **93:**15244-15248.

79. Lancaster, C. R. D., U. Ermler and H. Michel. 1995. The structures of photosynthetic reaction centers from purple bacteria as revealed by X-ray crystallography, pp. 503-526, *In* R. E. Blankenship, M. T. Madigan and C. E. Bauer (eds.), Anoxygenic photosynthetic bacteria. Kluwer Academic Publishers, Dordrecht, The Netherlands.

80. Langer, T., C. Lu, H. Echols, H. Flanagan, M. K. Hayer, and F. U. Hartl. 1992. Successive action of DnaK, DnaJ, and GroEL along the pathway of chaperone-mediated protein folding. Nature (London) **356:**683-689.

81. Lawlor, D. W. 1993. Photosynthesis: molecular, physiological, and environmental processes. Longman Scientific and Technical, Burnt Mill.

82. LeBlanc, H. 1995. Directed Mutagenesis and Gene Fusion Analysis of the *Rhodobacter capsulatus puc* Operon. Ph.D thesis, University of British Columbia, Vancouver.

83. LeBlanc, H. N. and J. T. Beatty. 1993. *Rhodobacter capsulatus puc* operon: promoter location, transcript sizes and effects of deletions on photosynthetic growth. J. Gen. Microbiol. **139:**101-109.

84. LeBlanc, H. N. and J. T. Beatty. 1996. Topological analysis of the *Rhodobacter capsulatus* PucC protein and effects of C-terminal deletions on light-harvesting complex II. J. Bacteriol. **178:**4801-4806.

85. Lilburn, T. G., R. C. Prince and J. T. Beatty. 1995. Mutation of the Ser2 codon of the light-harvesting B870 a polypeptide of *Rhodobacter capsulatus* partially suppresses the *pufX* phenotype. J. Bacteriol. **177:**4593-4600.

86. Loach, P. A., P. S. Parkes-Loach, C. M. Davis and B. A. Heller. 1994. Probing protein structural requirements for formation of the core light-harvesting complex of photosynthetic bacteria using hybrid reconstitution methodology. Photosynth. Res. **40:**231-245.

87. Loach, P. A. and P. S. Parkes-Loach. 1995. Structure-function relationships in core light-harvesting complexes (LHI) as determined by characterization of the structural subunit and by reconstitution experiments, 437-471. *In* R. E. Blankenship, M. T. Madigan and C. E. Bauer. (eds.), Anoxygenic Photosynthetic Bacteria. Kluwer Academic Publishers, Dordrecht, The Netherlands.

88. Lois, A. F., G. S. Ditta, and D. R. Helinski. 1993. The oxygen sensor FixL of *Rhizobium meliloti* is a membrane protein containing four possible transmembrane segments. J. Bacteriol. **175:**1103-1109.

89. Manoil, C. 1991. Analysis of membrane protein topology using alkaline phosphatase and β-galactosidase, 61-75. Methods in Cell Biology. Academic Press, Inc., San Diego.

90. Manoil, C. and J. Beckwith. 1986. A genetic approach to analyzing membrane protein topology. Science **233:**1403-1408.

91. McDermott, G., S. M. Prince, A. A. Freer, A. M. Hawthornthwaite-Lawless, M. Z. Papiz, R. J. Cogdell and N. W. Isaacs. 1995. Crystal structure of an integral membrane light-harvesting complex from photosynthetic bacteria. Nature (London) **374:**517-521.

92. McGlynn, P., W. H. J. Westerhuis, M. R. Jones, and C. N. Hunter. 1996. Consequences for the organization of reaction center-light harvesting antenna 1 (LH1) core complexes of *Rhodobacter sphaeroides* arising from deletion of amino acid residues from the C terminus of the LH1 a polypeptide. J. Biol. Chem. **271:**3285-3292.

93. Meadows, K. A., K. Iida, P. A. Recchia, B. A. Heller, B. Antonio, M. Nango, and P. A. Loach. 1995. Enzymatic and chemical cleavage of the core light-harvesting polypeptides of photosynthetic bacteria: toward the determination of the minimal polypeptide size and structure required for subunit and light-harvesting complex formation. Biochemistry **34:**1559-1574.

94. Meryandini, A. and G. Drews. 1996. Import and assembly of the α and β-polypeptides of the light-harvesting complex I (B870) in the membrane system of *Rhodobacter capsulatus* investigated in an *in vitro* translation system. Photosynth. Res. **47:**21-31.

95. Messing, J. 1983. New M13 vectors for cloning. Meth. Enzymol. **101:**20-78.

96. Miller, J. F., S. B. Hinchigeri, P. S. Parkes-Loach, P. M. Callahan, J. R. Sprinkle, J. R. Riccobono, and P. A. Loach. 1987. Isolation and characterization of a subunit form of the light-harvesting complex of *Rhodospirillum rubrum*. Biochemistry **26:**5055-5062.

97. Miller, J. H. 1992. A Short Course in Bacterial Genetics: A Laboratory Manual and Handbook for *Escherichia coli* and Related Bacteria. Cold Spring Harbor Laboratory Press, Plainview, New York.

98. Mosley, C. S., J. Y. Suzuki, and C. E. Bauer. 1994. Identification and molecular genetic characterization of a sensor kinase responsible for coordinately regulating light harvesting and reaction center gene expression in response to anaerobiosis. J. Bacteriol. **176:**7566-7573.

99. Narro, M. L., C. W. Adams, and S. N. Cohen. 1990. Isolation and characterization of *Rhodobacter capsulatus* mutants defective in oxygen regulation of the *puf* operon. J. Bacteriol. **172:**4549-4554.

100. Nickel, C. M., J. Vanderkerckhove, P. Beyer, and M. H. Tadros. 1997. Molecular analysis of the *Rhodobacter capsulatus* chaperone *dnaKJ* operon: purification and characterization of DnaK. Gene **192:**251-259.

101. Okamura, M. Y. and G. Feher. 1995. Proton-Coupled Electron Transfer Reactions of Q_B in Reaction Centers from Photosynthetic Bacteria, 577-594. *In* R. E. Blankenship, M. T. Madigan and C. E. Bauer (eds.), Anoxygenic Photosynthetic Bacteria. Kluwer Academic Publishers, Dordrecht, The Netherlands.

102. Oling, F., Ė. J. Boekema, I. O. de Zarate, R. Visschers, R. van Grondelle, W. Keegstra, A. Brisson, and R. Picorel 1996. Two-dimensional crystals of LH2 light-harvesting complexes from *Ectothiorhodospira sp.* and *Rhodobacter capsulatus* investigated by electron microscopy. Biochim. Biophys. Acta **1273:**44-50.

103. Papiz, M. Z., S. M. Prince, A. M. Hawthornthwaitelawless, G. Mcdermott, A. A. Freer, N. W. Isaacs, and R. J. Cogdell. 1996. A model for the photosynthetic apparatus of purple bacteria. Trends Plant Sci. **1:**198-206.

104. Parkes-Loach, P. S., T. J. Michalski, W. J. Bass, U. Smith, and P. A. Loach. 1990. Probing the bacteriochlorophyll binding site by reconstitution of the light-harvesting complex of *Rhodospirillum rubrum* with bacteriochlorophyll *a* analogues. Biochemistry **29:**2951-2960.

105. Parkes-Loach, P. S., J. R. Sprinkle, and P. A. Loach. 1988. Reconstitution of the B873 light-harvesting complex of *Rhodospirillum rubrum* from the separately isolated α- and β-polypeptides and bacteriochlorophyll *a*. Biochemistry **27:**2718-2727.

106. Peters, J. and G. Drews. 1983. Chemical cross-linking studies of the light-harvesting pigment-protein complex B800-850 of *Rhodopseudomonas capsulata*. Eur. J. Cell Biol. **29:**115-120.

107. Peters, J., J. Takemoto and G. Drews. 1983. Spatial relationships between the photochemical reaction center and the light-harvesting complexes in the membrane of *Rhodopseudomonas capsulata*. Biochemistry **22:**5660-5667.

108. Phillips-Jones, M. K. and C. N. Hunter. 1994. Cloning and nucleotide sequence of *regA*, a putative response regulator gene of *Rhodobacter sphaeroides*. FEMS Microbiol. Lett. **116:**269-276.

109. Prentki, P. and H. M. Krisch. 1984. *In vitro* insertional mutagenesis with a selectable DNA fragment. Gene **29:**303-313.

110. Rees, D. C., H. Komiya, T. O. Yeates, J. P. Allen, and G. Feher. 1989. The bacterial photosynthetic reaction center as a model for membrane proteins. Annu. Rev. Biochem. **58:**607-633.

111. Richter, P., M. Brand, and G. Drews. 1992. Characterization of LHI^- and LHI^+ *Rhodobacter capsulatus pufA* mutants. J. Bacteriol. **174:**3030-3041.

112. Richter, P., N. Cortez and G. Drews. 1991. Possible role of the highly conserved amino acids Trp-8 and Pro-13 in the N-terminal segment of the pigment-binding polypeptide LHI α of *Rhodobacter capsulatus*. FEBS Lett. **285:**80-84.

113. Richter, P. and G. Drews. 1991. Incorporation of light-harvesting complex I α and β polypeptides into the intracytoplasmic membrane of *Rhodobacter capsulatus*. J. Bacteriol. **173:**5336-5345.

114. Ruttiman, C., M. Cotoras, J. Zaldivar and R. Vicuna. 1985. DNA polymerases from the extremely thermophilic bacterium *Thermus thermophilus* HB-8. Eur. J. Biochem. **149:**41-46.

115. Sambrook, J., E.F. Fritsch, and T. Maniatis. 1989. Molecular Cloning: A Laboratory Manual. Cold Spring Harbor Laboratory Press, Cold Spring Harbor, New York.

116. San Millan, J. L., D. Boyd, R. Dalbey, W. Wickner and J. Beckwith. 1989. Use of *phoA* fusions to study the topology of the *Escherichia coli* inner membrane protein leader peptidase. J. Bacteriol. **171:**5536-5541.

117. Schumacher, A. and G. Drews. 1979. Effects of light-intensity on membrane differentiation in *Rhodopseudomonas capsulata*. Biochim. Biophys. Acta **547:**417-428.

118. Schumacher, A. and G. Drews. 1978. The formation of bacteriochlorophyll-protein complexes of the photosynthetic apparatus of *Rhodopseudomonas capsulata* during early stages of development. Biochim. Biophys. Acta **501:**183-194.

119. Scolnik, P. A., D. Zannoni and B. L. Marrs. 1980. Spectral and functional comparisons between the carotenoids of the two antenna complexes of *Rhodopseudomonas capsulata*. Biochim. Biophys. Acta **593:**230-240.

120. Sganga, M. W. and C. E. Bauer. 1992. Regulatory factors controlling photosynthetic reaction center and light-harvesting gene expression in *Rhodobacter capsulatus*. Cell **68:**945-954.

121. Shimada, H., K. Iba and K-I. Takamiya. 1992. Blue-light irradiation reduces the expression of *puf* and *puc* operons of *Rhodobacter sphaeroides* under semi-aerobic conditions. Plant Cell Physiol. **33:**471-475.

122. Shimada, H., H. Ohta, T. Masuda, Y. Shioi and K. Takamiya. 1993. A putative transcription factor binding to the upstream region of the *puf* operon in *Rhodobacter sphaeroides*. FEBS Lett. **328:**41-44.

123. Shimada, H., T. Wada, H. Handa, H. Ohta, H. Mizoguchi, K. Nishimura, T. Masuda, Y. Shioi, and K-I. Takamiya. 1996. A transcription factor with a leucine-zipper motif involved in light-dependent inhibition of expression of the *puf* operon in the photosynthetic bacterium *Rhodobacter sphaeroides*. Plant Cell Physiol. **37:**515-522.

124. Shimada, K. 1995. Aerobic Anoxygenic Phototrophs, 105-122. *In* R. E. Blankenship, M. T. Madigan, and Bauer, C. E. (eds.), Anoxygenic Photosynthetic Bacteria. Kluwer Academic Publishers, Dordrecht.

125. Simon, R., U. Priefer and A. Pühler. 1983. A broad host range mobilization system for *in vivo* genetic engineering: transposon mutagenesis in Gram-negative bacteria. Bio/Technology **1:**37-45.

126. Steenburgen, C. L. M. and H. J. Korthals. 1982. Distribution of phototrophic microorganisms in the anaerobic and microaerophilic strata of Lake Vechten (The Netherlands). Pigment analysis and role in primary production. Limnol. Oceanogr. **27:**883-895.

127. Stiehle, H., N. Cortez, G. Klug and G. Drews. 1990. A negatively charged N terminus in the α polypeptide inhibits formation of light-harvesting complex I in *Rhodobacter capsulatus*. J. Bacteriol. **172:**7131-7137.

128. Stowell, M. H. B., T. M. McPhillips, D. C. Rees, S. M. Soltis, E. Abresch, and G. Feher. 1997. Light-induced structural changes in photosynthetic reaction center-implications for mechanism of electron-proton transfer. Science **276:**812-816.

129. Tadros, M. H., F. Suter, G. Drews, and H. Zuber. 1983. The complete amino acid sequence of the large bacteriochlorophyll-binding polypeptide from light-harvesting complex II (B800-850) from *Rhodopseudomonas capsulata*. Eur. J. Biochem. **129:**533-536.

130. Tadros, M. H., R. Frank, and G. Drews. 1985. The complete amino acid sequence of the small bacteriochlorophyll-binding polypeptide B800-850β from light-harvesting complex B800-850 of *Rhodopseudomonas capsulata*. FEBS Lett. **183:**91-94.

131. Tadros, M. H., G. Frank, H. Zuber and G. Drews. 1985. The complete amino acid sequence of the large bacteriochlorophyll-binding polypeptide B870α from the light-harvesting complex B870 of *Rhodopseudomonas capsulata*. FEBS Lett. **190:**41-44.

132. Tadros, M. H., F. Suter, G. Drews and H. Zuber. 1984. Isolation and complete amino acid sequence of the small polypeptide from light-harvesting pigment protein complex I (B870) of *Rhodopseudomonas capsulata*. Eur. J. Biochem. **138:**209-212.

133. Taylor, D. P., S. N. Cohen, W. G. Clark and B. L. Marrs. 1983. Alignment of genetic and restriction maps of the photosynthesis region of the *Rhodopseudomonas capsulata* chromosome by a conjugation-mediated marker rescue technique. J. Bacteriol. **154:**580-590.

134. Tichy, H. V., B. Oberlé, H. Stiehle, E. Schiltz and G. Drews. 1989. Genes downstream from *pucB* and *pucA* are essential for formation of the B800-850 complex of *Rhodobacter capsulatus*. J. Bacteriol. **171:**4914-4922.

135. Towbin, H., T. Staehelin, and J. Gordon. 1979. Electrophoretic transfer of proteins from polyacrylamide gels to nitrocellulose sheets: Procedure and some applications. Proc. Natl. Acad. Sci. USA **76:**4350.

136. Traxler, B., D. Boyd and J. Beckwith. 1993. The topological analysis of integral cytoplasmic membrane proteins. J. Membr. Biol. **132:**1-11.

137. Varcamonti, M., R. Marasco, M. De Felice, and M. Sacco. 1997. Membrane topology analysis of the *Bacillus subtilis* BofA protein involved in pro-σ^K processing. Microbiology **143:**1053-1058.

138. Varga, A. R. and S. Kaplan. 1993. Synthesis and stability of reaction center polypeptides and implications for reaction center assembly in *Rhodobacter sphaeroides*. J. Biol. Chem. **268:**19842-19850.

139. Varga, A. R. and S. Kaplan. 1989. Construction, expression, and localization of a CycA::PhoA fusion protein in *Rhodobacter sphaeroides* and *Escherichia coli*. J. Bacteriol. **171:**5830-5839.

140. Vlcek, C., Paces, V., Maltsev, N., Paces, J., Haselkorn, R., and M. Fonstein. 1997. Sequence of a 189 kb segment of the chromosome of *Rhodobacter capsulatus* SB1003. Proc. Natl. Acad. Sci. USA **94**:9384-9388.

141. von Heijne, G. 1986. The distribution of positively charged residues in bacterial inner membrane proteins correlates with the trans-membrane topology. EMBO J. **5:**3021-3027.

142. von Heijne, G. 1992. Membrane protein structure prediction: hydrophobicity analysis and the positive-inside rule. J. Mol. Biol. **225:**487-494.

143. Walz, T. and R. Ghosh. 1997. Two-dimensional crystallization of the light-harvesting I-reaction centre photounit from *Rhodospirillum rubrum*. J. Mol. Biol. **265:**107-111.

144. Weaver, P. F., J. D. Wall and H. Gest. 1975. Characterization of *Rhodopseudomonas capsulata*. Arch. Microbiol. **105:**207-216.

145. Wei, C.-F., G. A. Alianell, G. H. Bencen, and H. B. Gray, Jr. 1983. Isolation and comparison of two molecular species of the BAL 31 nuclease from *Altermonas espejiani* with distinct kinetic properties. J. Biol. Chem. **258:**13506-13512.

146. Wellington, C. L., C. E. Bauer and J. T. Beatty. 1992. Photosynthesis gene superoperons in purple nonsulfur bacteria: the tip of the iceberg? Can. J. Microbiol. **38:**20-27.

147. Wellington, C. L. and J. T. Beatty. 1991. Overlapping mRNA transcripts of photosynthesis gene operons in *Rhodobacter capsulatus*. J. Bacteriol. **173:**1432-1443.

148. Wellington, C. L., A. K. P. Taggart and J. T. Beatty. 1991. Functional significance of overlapping transcripts of *crtEF, bchCA,* and *puf* photosynthesis gene operons in *Rhodobacter capsulatus*. J. Bacteriol. **173:**2954-2961.

149. Welte, W., T. Wacker, M. Leis, W. Kreutz, J. Shiowaza, N. Gad'on, and G. Drews. 1985. Crystallization of the photosynthetic light-harvesting pigment-protein complex B800-850 of *Rhodopseudomonas capsulata*. FEBS Lett. **182:**260-264.

150. Wiessner, C. 1990. Molekularbiologische Analyse der Gene des photosynthetischen Apparates von *Rhodopseudomonas viridis*. Ph.D thesis, Johann Wolfgang Goethe-Universitat, Frankfurt.

151. Wong, D. H.-K. 1994. Directed mutational analysis of the *Rhodobacter capsulatus puhA* gene and downstream open reading frames. M.Sc., The University of British Columbia, Vancouver.

152. Wong, D. K.-H., W. J. Collins, A. Harmer, T. G. Lilburn and J. T. Beatty. 1996. Directed mutagenesis of the *Rhodobacter capsulatus puhA* gene and *orf214*: pleiotropic effects on photosynthesis reaction center and light-harvesting 1 complexes. J. Bacteriol. **178:**2334-2342.

153. Yen, H. C., N. T. Hu and B. L. Marrs. 1979. Characterization of the gene transfer agent made by an overproducer mutant of *Rhodopseudomonas capsulata*. J. Mol. Biol. **131:**157-168.

154. Yen, H. C. and B. Marrs. 1976. Map of genes for carotenoid and bacteriochlorophyll biosynthesis in *Rhodopseudomonas capsulata*. J. Bacteriol. **126:**619-629.

155. Young, C. S. and J. T. Beatty. 1997. Complementation and kinetic analyses of *Rhodobacter capsulatus ORF1696* mutants indicate that the ORF1696 protein catalyzes light-harvesting complex I assembly. (submitted)

156. Youvan, D. C., J. T. Elder, D. E. Sandlin, K. Zsebo, D. P. Alder, N. J. Panopoulos, B. L. Marrs, and J. E. Hearst. 1982. R-prime site-directed transposon Tn7 mutagenesis of the photosynthetic apparatus in *Rhodopseudomonas capsulata*. J. Mol. Biol. **162:**17-41.

157. Youvan, D. C., E. J. Bylina, M. Alberti, H. Begusch and J. E. Hearst. 1984. Nucleotide and deduced polypeptide sequences of the photosynthetic reaction-center, B870 antenna and flanking polypeptides from *R. capsulata*. Cell. **37:**949-957.

158. Youvan, D. C., S. Ismail and E. J. Bylina. 1985. Chromosomal deletion and plasmid complementation of the photosynthetic reaction center and light harvesting genes from *Rhodopseudomonas capsulata*. Gene **38:**19-30.

159. Youvan, D. C. and S. Ismail. 1985. Light harvesting II (B800-850 complex) structural genes from *Rhodopseudomonas capsulata*. Proc. Natl. Acad. Sci. USA **82:**58-62.

160. Yun, C.-H., S. R. Van Doren, A. R. Crofts and R. B. Gennis. 1991. The use of gene fusions to examine the membrane topology of the L-subunit of the photosynthetic reaction center and of the cytochrome *b* subunit of the bc_1 complex from *Rhodobacter sphaeroides*. J. Biol. Chem. **266:**10967-10973.

161. Yurkova, N. and J. T. Beatty. 1996. Photosynthesis-independent regulation of bacteriochlorophyll synthesis by light intensity in *Rhodobacter capsulatus*. FEMS Microbiol. Lett. **145:**221-225.

162. Zannoni, D. 1995. Aerobic and Anaerobic Electron Transport Chains in Anoxygenic Phototrophic Bacteria, 949-971. *In* R. E. Blankenship, M. T. Madigan and C. E. Bauer (eds.), Anoxygenic Photosynthetic Bacteria. Kluwer Academic Publishers, Dordrecht, The Netherlands.

163. Zhu, Y. S., D. N. Cook, F. Leach, G. A. Armstrong, M. Alberti and J. E. Hearst. 1986. Oxygen-regulated mRNAs for light-harvesting and reaction center complexes and for bacteriochlorophyll and carotenoid biosynthesis in *Rhodobacter capsulatus* during the shift from anaerobic to aerobic growth. J. Bacteriol. **168:**1180-1188.

164. Zhu, Y. S. and J. E. Hearst. 1986. Regulation of expression of genes for light-harvesting antenna proteins LH-I and LH-II; reaction center polypeptides RC-L, RC-M, biosynthesis in *Rhodobacter capsulatus* by light and oxygen. Proc. Natl. Acad. Sci., USA **83**:7613-7617.

165. Zsebo, K. M. and J. E. Hearst. 1984. Genetic-physical mapping of a photosynthetic gene cluster from *R. capsulata*. Cell **37**:937-947.

166. Zuber, H. 1990. Considerations on the structural principles of the antenna complexes of phototrophic bacteria, 161-180. *In* G. Drews and E. A. Dawes (eds.), Molecular biology of membrane-bound complexes in phototrophic bacteria. Plenum Press, New York.